General Disclaimer

One or more of the Following Statements may affect this Document

- This document has been reproduced from the best copy furnished by the organizational source. It is being released in the interest of making available as much information as possible.

- This document may contain data, which exceeds the sheet parameters. It was furnished in this condition by the organizational source and is the best copy available.

- This document may contain tone-on-tone or color graphs, charts and/or pictures, which have been reproduced in black and white.

- This document is paginated as submitted by the original source.

- Portions of this document are not fully legible due to the historical nature of some of the material. However, it is the best reproduction available from the original submission.

MSC-05537
NASA CR-
141911

SKYLAB PROGRAM

EARTH RESOURCES EXPERIMENT PACKAGE

GROUND TRUTH DATA
FOR TEST SITES (SL-3)

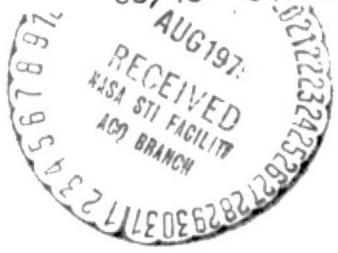

CONTRACT NAS8-24000
AMENDMENT JSC-14S

National Aeronautics and Space Administration

LYNDON B. JOHNSON SPACE CENTER

Houston, Texas

MARCH 29, 1974

MSC-05537

GROUND TRUTH DATA

FOR TEST SITES (SL-3)

Approved by:

Richard A. Moke
Manager, System Analysis and
Integration Office, JSC/HC

Contract NAS8-24000
Amendment JSC-14S

Skylab Program
Lyndon B. Johnson Space Center

GROUND TRUTH DATA
FOR TEST SITES (SL-3)

MARCH 29, 1974

Contract NAS8-24000
Amendment JSC-14S

Approved by:

W. W. Bollendonk
EREP Program Manager

R. L. Hulstrom
Technical Director

W. O. Nobles
Section Chief
Science Section

FOREWORD

This document is submitted by Martin Marietta Corporation in accordance with the requirements of Annex I to Exhibit A, Statement of Work, Part I, Data Requirements List (DRL), of Contract NAS8-24000, Amendment JSC-14S, Line Item 296, and was performed under WBS-02216.

The work was performed by R. L. Hulstrom and any inquiries should be addressed to him at (303) 794-5211, Ext. 3808. After June 30, 1974, inquiries should be addressed to NASA JSC, Earth Resources Program Office, Mail Code HA.

FOREWORD

This document is submitted by Martin Marietta Corporation in accordance with the requirements of Annex I to Exhibit A, Statement of Work, Part I, Data Requirements List (DRL), of Contract NAS8-24000, Amendment JSC-14S, Line Item 296, and was performed under WBS-02216.

The work was performed by R. L. Hulstrom and any inquiries should be addressed to him at (303) 794-5211, Ext. 3808. After June 30, 1974, inquiries should be addressed to NASA JSC, Earth Resources Program Office, Mail Code HA.

CONTENTS

Page

APPENDIX

Figure

Figure (Cont'd)

Figure (Cont'd) Page

Figure (Cont'd) Page

Figure (Cont'd) Page

1. INTRODUCTION

During the SL-3 Skylab mission, field measurements were performed simultaneous with Skylab overpasses in order to provide comparative calibration and performance evaluation measurements for the EREP sensors. Wavelength regions addressed were the solar radiation region from 400 to 1300 nanometers (nm) and the thermal radiation region from 8 to 14 micrometer (μm) region. Similar measurements and analyses were also performed for the SL-2 missions, "Ground Truth Data for Test Sites (SL-2), Report No. MSC-05531, August 15, 1973, NAS8-24000, Amendment JSC-14S.

Sites employed for the thermal radiation brightness temperature measurements consisted of "warm" and "cold" water lakes. These were: (1) Rio Grande Reservoir, Colorado - "cold" water, (2) Theodore Roosevelt Reservoir, Arizona - "warm" water, and (3) the Great Salt Lake, Utah - "warm" water. In general, the measurements and observations taken at these sites consisted of: (1) general conditions (observer); (2) near surface meteorology-temperature, pressure, wind, etc.; (3) temperature and humidity altitude profile - up to 13,500/15,500 feet above sea level; and (4) thermal brightness temperature for the 8-14 μm region taken from a helicopter platform.

Sites employed for the solar radiation region consisted of dry lake bed/desert areas having fairly uniform reflectance and arid climates. These sites were: (1) The Great Salt Lake Desert, Utah, and (2) Katherine Playa, New Mexico. Measurements consisted of, (1) direct solar radiation, (2) total solar radiation, (3) diffuse solar radiation, (4) reflected solar radiation, and (5) near surface meteorology. The measurements of direct solar radiation were subsequently analyzed for atmospheric optical depth; the total and reflected solar radiation were analyzed for target reflectifity. These analyses were then used in conjunc-

tion with a radiative transfer computer program in order to calculate the amount and spectral distribution of solar radiation at the apertures of the EREP sensors.

The purpose of this report is to present the measurements made, how they were made, calibrations and analyses performed, techniques used, and results obtained. It is not within the scope or intention of this report to interpret the measurements, calculations, results, etc., in terms of the detailed physical nature of the targets, the atmosphere, etc.

2. THERMAL INFRARED CALIBRATION MEASUREMENTS AND ANALYSES

2.1 Instrumentation and Techniques - The thermal brightness temperature, from 8 to 14 μm broadband, of the lake waters were measured with a Barnes Precision Thermal Radiometer, Model PRT-5. The PRT-5 was flown in a helicopter and manually operated. The uniformity of the entire body of water was established by having the helicopter fly at an elevation of approximately 500 feet above the water while traversing the entire lake. The operator then recorded the measured brightness temperatures, real time, on a large scale topographic map of the area. The PRT-5 has a sensitivity range of -20° C to +75° C, a F.O.V. of 2°, an accuracy of .5° C, and a stability of .1%. The calibration of this instrument was performed by a secondary standard calibration laboratory at Martin Marietta Aerospace, Denver, Colorado, see Appendix for details. In addition to the low altitude measurements of brightness temperature, the helicopter was flown at various altitude intervals up to 13,500/15,500 feet above sea level in order to provide an assessment of the possible influence of the atmospheric column between the helicopter and the lake, and a partial assessment of the atmospheric influence between Skylab-EREP and the lake.

The altitude profiles of atmospheric temperature and humidity were measured by dropping a radiosonde (attached to a parachute) from the above mentioned altitude (13,500 to 15,500 feet above sea level). The radiosonde data was telemetered to a ground receiving station (403 MHz) and recorded. The radiosonde, manufactured by Colspan Environmental Systems Company uses a coated bead thermistor for the temperature measurement, and a standard (ML-476) carbon element hygristor for the humidity measurement. From the raw radiosonde data to the reported data, a temperature error of $\pm$ .3 °C exists and a $\pm$ 5.5% humidity error exists. In addition, an altitude position error of $\pm$ 32 feet for temperature and $\pm$ 19 feet for humidity exists because of the sensors response time vs. parachute descent rate. The calibration and data analyses techniques used for this system and data are given in the Appendix.

The near surface meteorology measurements consisting of dry/wet bulb temperature, wind, and surface pressure, were taken with a sling psychromter (1 °F accuracy), a cup anemometer ($\pm$ 2 m.p.h. accuracy), and an aneroid barometer ($\pm$ .1 inch accuracy) respectively.

2.2 Measurements and Analyses

2.2.1 *RIO GRANDE RESERVOIR, COLORADO, 03 AUGUST 1973*

Site Coordinates:	37° 43' 45" N. Latitude 107° 17' 30" W. Longitude
EREP Pass:	Track 34, Pass No. 12, Rev. 1170/1171
Time of Overpass:	215:18:03:10 GMT

2.2.1.1 General Conditions - Poor weather conditions existed. There was a 90% cloud cover with light rain. Ground observers reported that EREP sensors could probably not view the lake.

2.2.1.2 Near Surface Meteorology - Dry bulb temperature = 15.5°C; wet bulb temperature = 9.75°C; surface pressure (from standard tables*) - 543.0 M.M. of Hg; wind - calm.

2.2.1.3 Temperature and Humidity Profile - Due to the poor weather conditions, radiosonde measurements of temperature and humidity were not reduced.

2.2.1.4 Brightness Temperature - Poor weather conditions did not permit helicopter platform measurements of the lake water brightness temperature; instead, measurements were made from a boat using the previously mentioned PRT-5. Eight different positions on the lake were measured and found to be at a brightness temperature of 14 ± 1°C. These measurements were made between the hours of 1025 to 1155 M.S.T.

* U.S. Standard Atmosphere Supplements, 1966
45° N latitude, July Model.

2.2.2 *RIO GRANDE RESERVOIR, COLORADO, 08 AUGUST 1973*

Site Coordinates:	37° 43' 45" N. Latitude 107° 17' 30" W. Longitude
EREP Pass:	Track 34, Pass No. 16, Rev. 1241/1242
Time of Overpass:	220:16:02:47 GMT

2.2.2.1 General Conditions - Clear

2.2.2.2 Near Surface Meteorology - Dry bulb temperature = 13.9°C; wet bulb temperature = 8.3°C; surface pressure (measured) = 541.0 M.M. of Hg; wind - 2.4 m.p.h./N.E.

2.2.2.3 Temperature and Humidity Profile - The temperature profile is shown in Figure 1 and listed in Table 1. The corresponding humidity profile is shown in Figure 2 and listed in Table 2.

2.2.2.4 Brightness Temperature - The lake water brightness temperature was measured at several locations above the lake and at several positions from a helicopter platform. The results are shown in Figure 3.

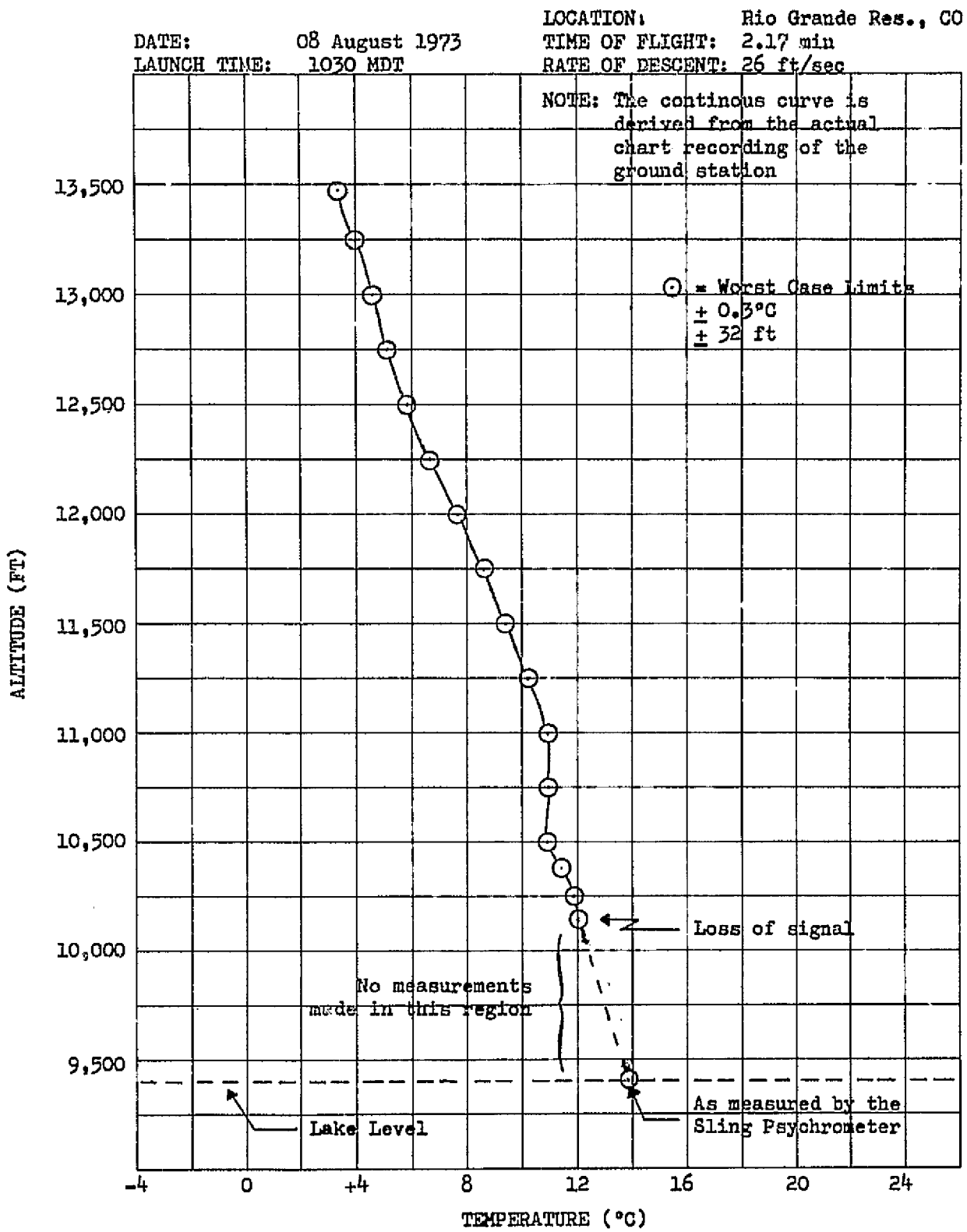

Fig. 1: Radiosonde Temperature Profile Plot For Rio Grande Reservoir, CO., 08 August 1973.

RADIOSONDE EVALUATION DATA

NUMBER OF ¼" FROM DROP	RAW DATA FROM ST.CH.	TIME FROM DROP	ALTITUDE REF: 13500'	ALTITUDE (A.S.L.)	TEMP OR HUM FROM TABLE	COMMENTS
1.00	5- 3.3	2.5 sec	- 65 ft	13435 ft	3.4 °C	
3.85	5- 7.2	9.62	250	13250	4.0	
7.70	5- 10.7	19.29	500	13000	4.6	
11.54	5- 13.8	28.85	750	12750	5.1	
15.38	5- 18.0	38.46	1000	12500	5.8	
19.23	5- 23.5	48.08	1250	12250	6.7	
23.08	5- 29.5	57.69	1500	12000	7.7	
26.92	5- 34.7	67.31	1750	11750	8.6	
30.77	5- 39.2	76.92	2000	11500	9.4	
34.61	5- 44.8	86.60	2250	11250	10.3	
38.46	5- 48.0	96.15	2500	11000	10.9	
42.31	5- 48.0	105.77	2750	10750	10.9	
46.15	5- 48.0	115.38	3000	10500	10.9	
48.075	6- 1.0	120.19	3125	10375	11.4	
50.00	6- 3.7	125.00	3250	10250	11.9	
52.00	6- 4.5	130.00	3380	10120	12.0	

TEMPERATURE X HUMIDITY ____ LOCATION Rio Grande Reservoir, CO

DATE 08-08-73

NOTES: 1) Recorder travels at 2.5 sec/ ¼" Div
2) Ballonsonde drop - descent rate = 26 ft/ sec
3) Data ceased transmitting at 10120 ft A.S.L. (720 ft above reservoir)

Table 1: Radiosonde Temperature Profile Listing for Rio Grande Reservoir, CO., 08 August 1973.

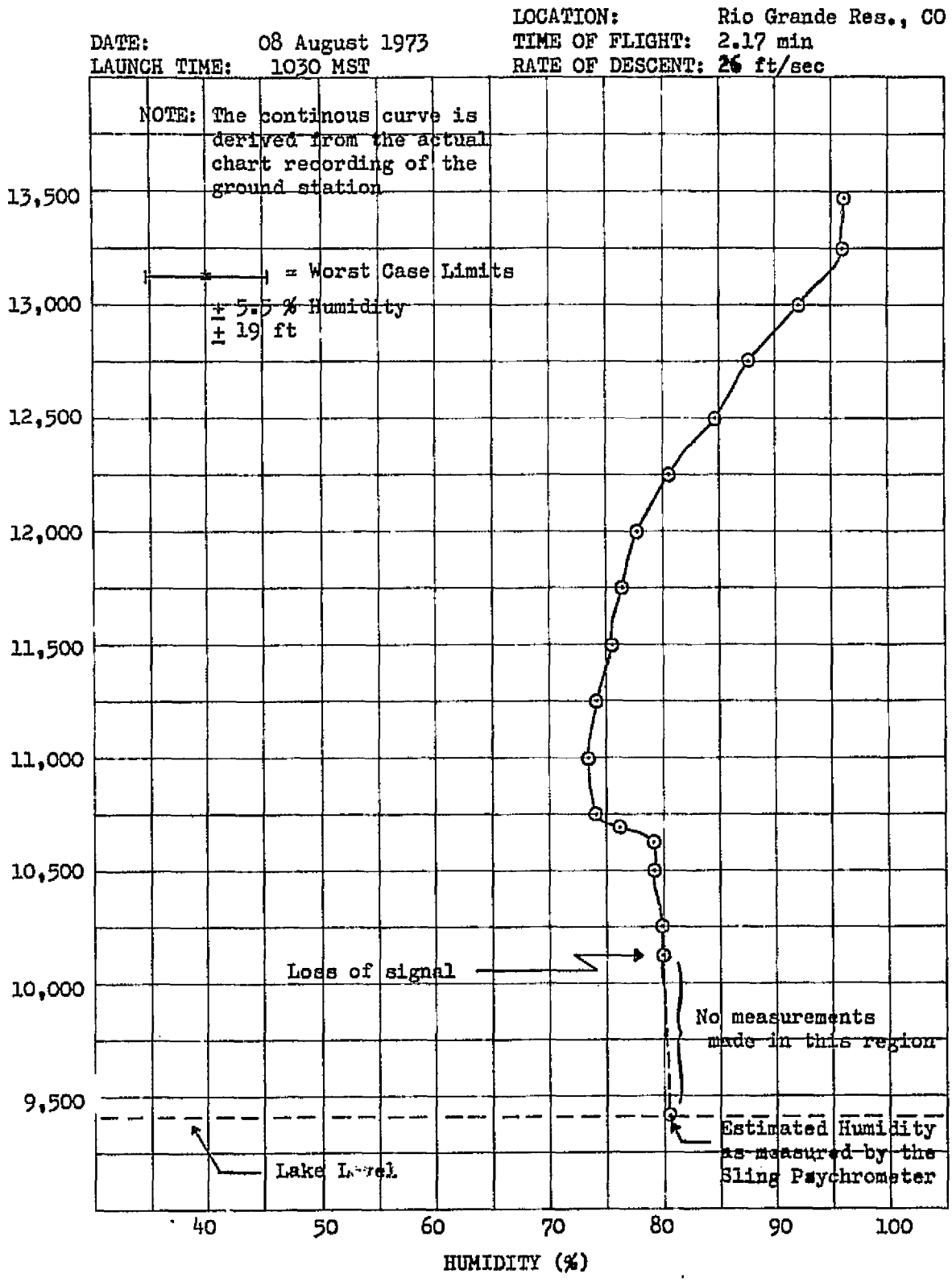

Fig. 2: Radiosonde Humidity Profile Plot for Rio Grande Reservoir, CO., 08 August 1973.

RADIOSONDE EVALUATION DATA

NUMBER OF ¼" FROM DROP	RAW DATA FROM ST.CH.	TIME FROM DROP	ALTITUDE REF: 13500'	ALTITUDE (A.S.L.)	TEMP OR HUM FROM TABLE	COMMENTS
1.00	4- 49.2	2.5 sec	- 65 ft	13465 ft	96 %	
3.85	4- 48.8	9.62	250	13250	96	
7.70	4- 44.0	19.29	500	13000	92.2	
11.54	4- 35.0	28.85	750	12750	87.7	
15.38	4- 28.0	38.46	1000	12500	84.7	
19.23	4- 18.0	48.08	1250	12250	80.5	
23.08	4- 7.2	57.69	1500	12000	77.7	
26.40	4- 1.0	66.00	1716	11784	76.2	
30.77	3- 45.4	76.92	2000	11500	75.5	
34.61	3- 40.8	86.60	2250	11250	74.2	
38.46	3- 36.8	96.15	2500	11000	73.5	
42.31	3- 41.0	105.77	2750	10750	74.2	
43.25	3- 49.0	108.13	2811	10688	76	
44.23	4- 12.0	110.58	2875	10625	79	
46.15	4- 12.8	115.38	3000	10500	79	
50.00	4- 15.3	125.00	3250	10250	79.7	
52.00	4- 15.3	130.00	3380	10120	79.7	

TEMPERATURE ___ HUMIDITY X LOCATION Rio Grande Reservoir, CO

DATE 08-08-73

NOTES: 1) Recorder travels at 2.5 sec / ¼" Div
2) Ballonsonde drop - descent rate = 26 ft / sec
3) Data ceased transmitting at 10120 ft A.S.L. (720 ft above reservoir)

Table 2: Radiosonde Humidity Profile Listing for
Rio Grande Reservoir, CO., 08 August 1973.

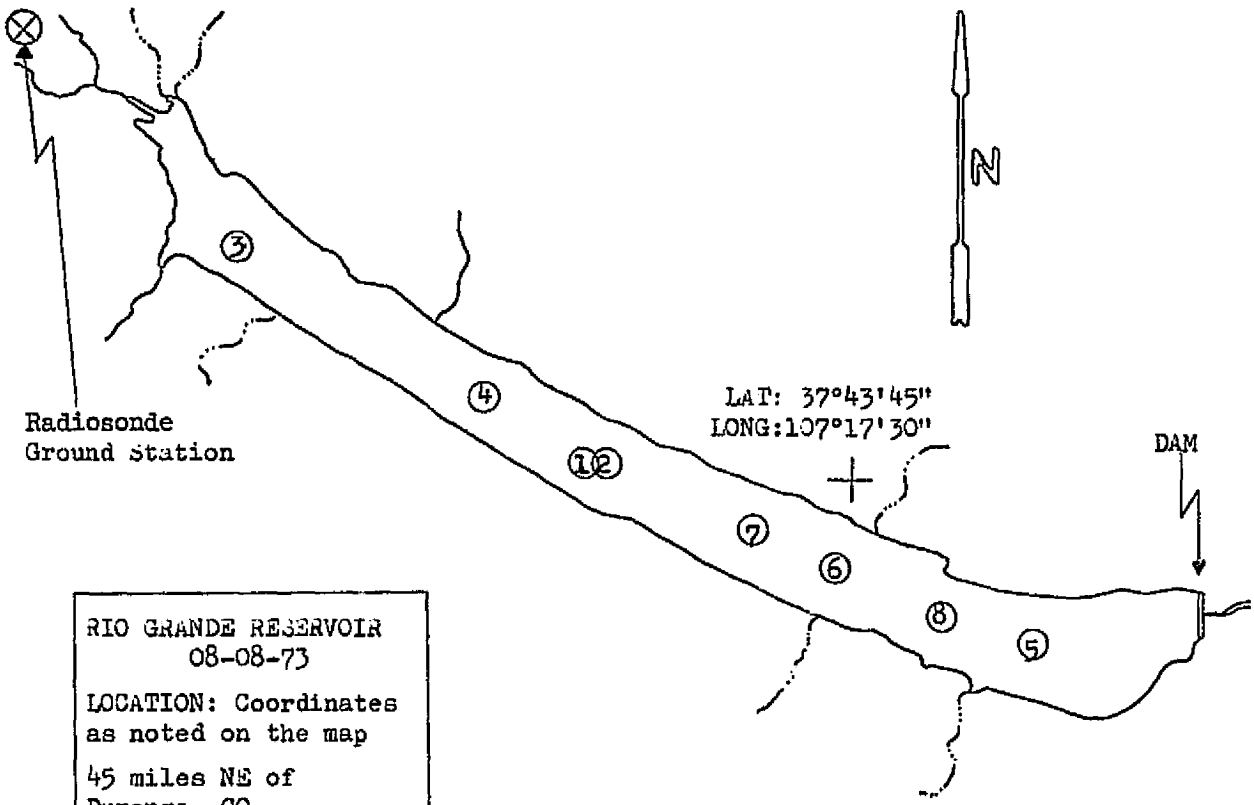

RIO GRANDE RESERVOIR
08-08-73

LOCATION: Coordinates as noted on the map

45 miles NE of Durango, CO

SCALE: 1:48,000

ELEVATION: 9400 FT A.S.L.

WATER TEMPERATURE AND BRIGHTNESS TEMPERATURE

A.S.L. ELEVATION	TIME (MDT)	SURFACE TEMP. (°C)	BRIGHTNESS TEMP. (°C)	LAKE POSITION	COMMENTS
13000 ft	0953		13.5	1	
13300	0955		13.5	2	
9600	1010		13-14	3	
9600	1012		13.5	4	
9900	1015		14.9	5	
10400	1017		13.5	6	
10900	1020		13.5	7	
11400	1021		13.5	8	

Fig. 3: Rio Grande Reservoir, CO., Water Brightness Temperature and Lake Location Map.

2.2.3 *THEODORE ROOSEVELT, ARIZONA, 11 AUGUST 1973*

Site Coordinates:	33° 34' 00" N. Latitude 110° 00' 00" W. Longitude
EREP Pass:	Track 06, Pass No. 18, Rev. 1284/1285
Time of Overpass:	223:15:29:15 GMT

2.2.3.1 General Conditions - Clear

2.2.3.2 Near Surface Meteorology - These measurements were inadvertently omitted from the field data collection activities.

2.2.3.3 Temperature and Humidity Profile - The temperature profile is shown in Figure 4 and listed in Table 3. The corresponding humidity profile is shown in Figure 5 and listed in Table 4.

2.2.3.4 Brightness Temperature - The lake water brightness temperature was measured at several elevations above the lake and at several positions from a helicopter. The results are shown in Figure 6.

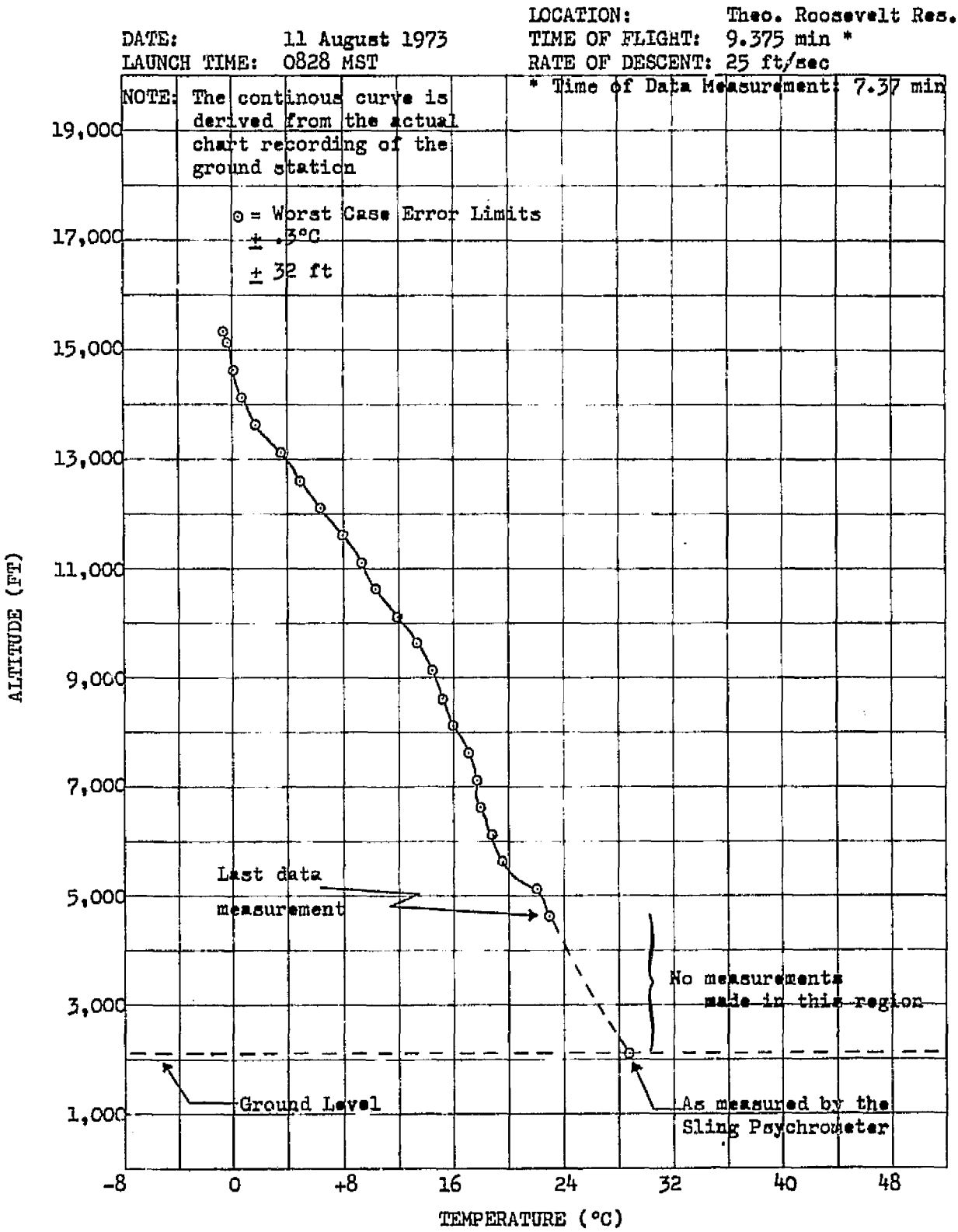

Fig. 4: Radiosonde Temperature Profile Plot for Theodore Roosevelt Res. AZ., 11 August 1973.

RADIOSONDE EVALUATION DATA

NUMBER OF ¼" FROM DROP	RAW DATA FROM ST.CH.	TIME FROM DROP	ALTITUDE REF: 15600'	ALTITUDE (A.S.L.)	TEMP OR HUM FROM TABLE	COMMENTS
4	4- 28.9	10 sec	250 ft	15350 ft	- 0.6 °C	
8	4- 31.0	20	500	15100	- 0.2	
16	4- 33.2	40	1000	14600	+ 0.1	
24	4- 36.7	60	1500	14100	0.7	
32	4- 43.1	80	2000	13600	1.7	
40	5- 3.7	100	2500	13100	3.5	
48	5- 12.4	120	3000	12600	4.9	
56	5- 21.6	140	3500	12100	6.4	
64	5- 30.7	160	4000	11600	7.9	
72	5- 38.6	180	4500	11100	9.3	
80	5- 44.5	200	5000	10600	10.3	
88	6- 4.0	220	5500	10100	11.9	
96	6- 11.4	240	6000	9600	13.3	
104	6- 17.5	260	6500	9100	14.4	
112	6- 21.9	280	7000	8600	15.2	
120	6- 26.0	300	7500	8100	16.0	
128	6- 32.2	320	8000	7600	17.1	
136	6- 35.0	340	8500	7100	17.2	
144	6- 35.9	360	9000	6600	17.9	
152	6- 41.3	380	9500	6100	18.9	
160	6- 44.8	400	10000	5600	19.6	
168	7- 7.0	420	10500	5100	22.1	scale change
176	7- 11.1	440	11000	4600	23.0	

TEMPERATURE X HUMIDITY ___ LOCATION Theodore Roosevelt Reservoir, AZ

DATE 08-11-73

NOTES: 1) Recorder travels at 2.5 sec / ¼" Div
2) Descent rate: 25 ft / sec
3) Rocketsonde lost to sight during descent and ground station inadvertently turned off when sonde reached 2500 ft above terrain

Table 3: Radiosonde Temperature Profile Listing for Theodore Roosevelt Res. AZ., 11 August 1973.

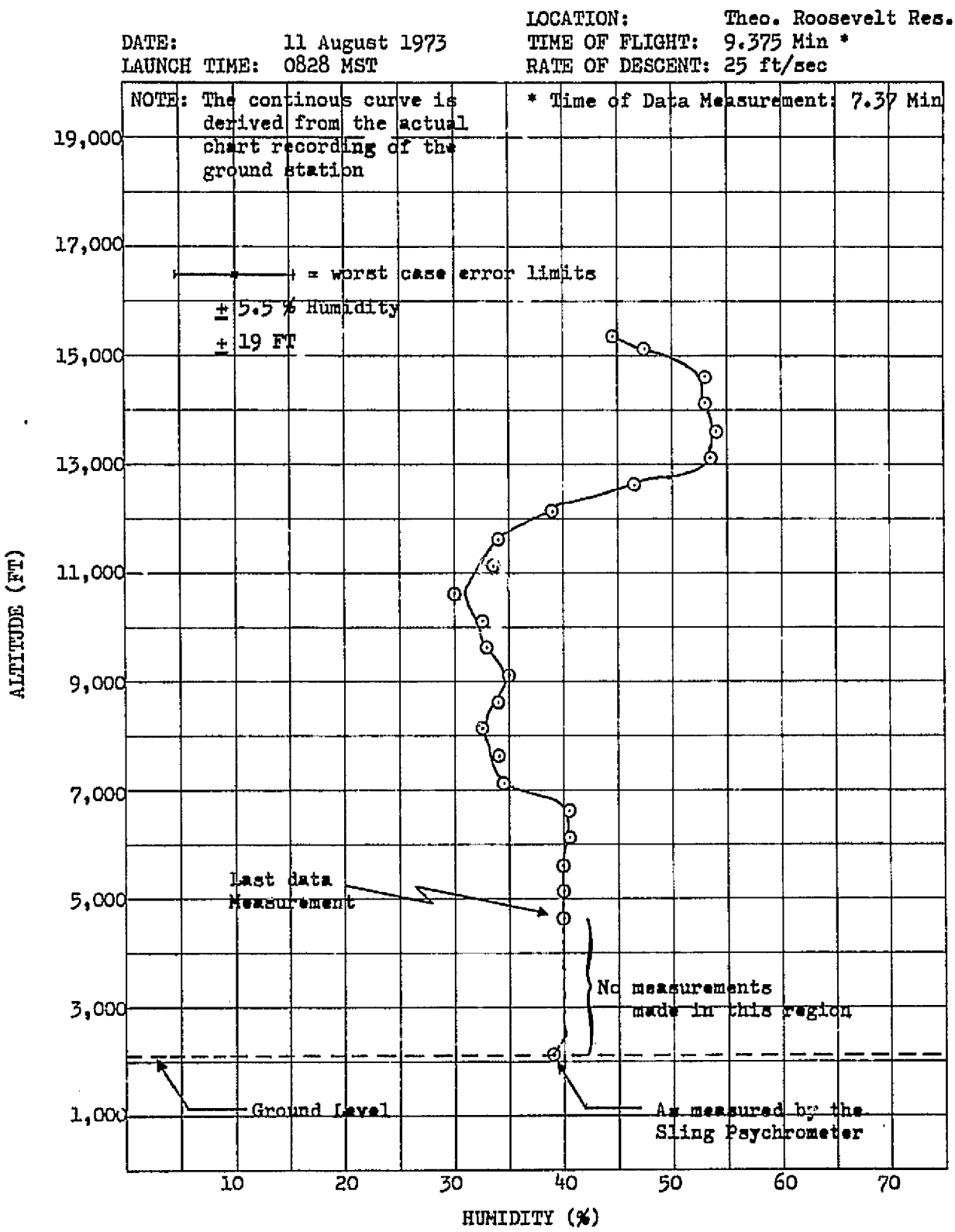

Fig. 5: Radiosonde Humidity Profile Plot for Theodore Roosevelt Res. AZ., 11 August 1973.

ORIGINAL PAGE IS
OF POOR QUALITY

RADIOSONDE EVALUATION DATA

NUMBER OF ¼" FROM DROP	RAW DATA FROM ST.CH.	TIME FROM DROP	ALTITUDE REF: 15600'	ALTITUDE (A.S.L.)	TEMP OR HUM FROM TABLE	COMMENTS
4	1- 36.2	10 sec	250 ft	15350 ft	44.5 %	
8	1- 42.0	20	500	15100	47.5	
16	2- 8.0	40	1000	14600	53	
24	2- 8.0	60	1500	14100	53	
32	2- 10.6	80	2000	13600	54	
40	2- 9.0	100	2500	13100	53.5	
48	1- 39.4	120	3000	12600	46.5	
56	1- 29.2	140	3500	12100	39	
64	1- 23.3	160	4000	11600	34	
72	1- 22.2	180	4500	11100	33.5	
80	1- 18.5	200	5000	10600	30	
88	1- 21.5	220	5500	10100	32.5	
96	1- 21.8	240	6000	9600	33	
104	1- 23.4	260	6500	9100	35	
112	1- 23.0	280	7000	8600	34	
120	1- 21.4	300	7500	8100	32.5	
128	1- 23.0	320	8000	7600	34	
136	1- 23.3	340	8500	7100	34.5	
144	1- 29.0	360	9000	6600	40.5	
152	1- 29.3	380	9500	6100	40.5	
160	1- 28.7	400	10000	5600	40	
168	1- 28.5	420	10500	5100	40	
176	1- 28.2	440	11000	4600	40	

TEMPERATURE ____ HUMIDITY X LOCATION Theodore Roosevelt Reservoir, AZ

DATE 08-11-73

NOTES: 1) Recorder travels at 2.5 sec / ¼" Div
2) Descent rate: 25 ft / sec
3) Rocketsonde lost to sight during descent and ground station inadvertently turned off when sonde reached 2500 ft above terrain.

Table 4: Radiosonde Humidity Profile Listing for Theodore Roosevelt Res. AZ., 11 August 1973.

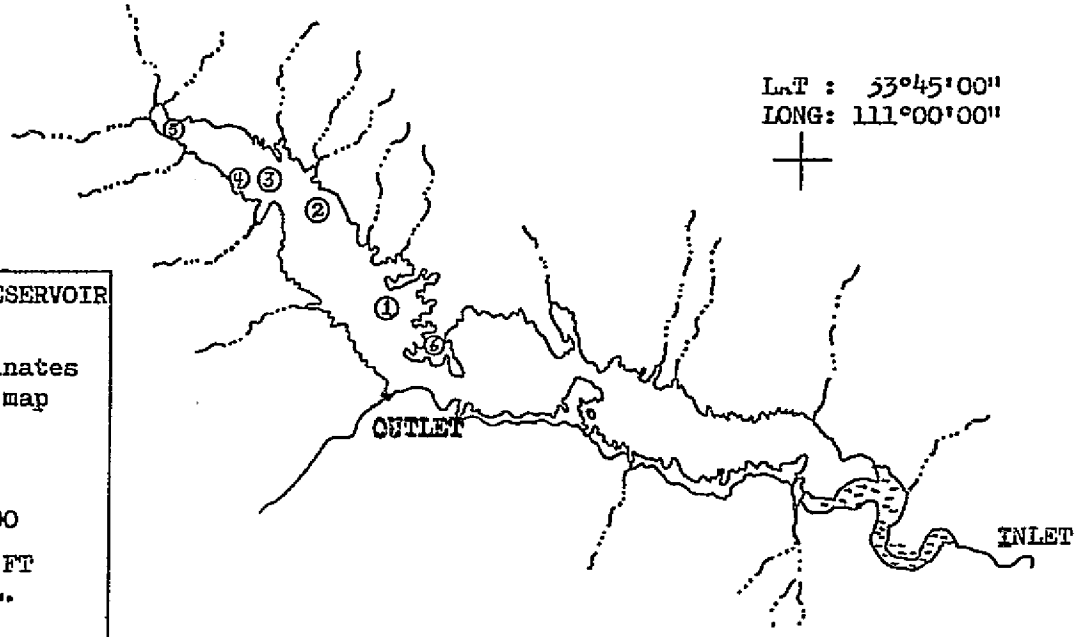

TH. ROOSEVELT RESERVOIR
08-11-73

LOCATION: Coordinates as noted on the map

27 miles ENE of Phoenix, AZ

SCALE: 1:250,000

ELEVATION: 2194 FT A.S.L.

WATER TEMPERATURE AND BRIGHTNESS TEMPERATURE

A.S.L. ELEVATION	TIME (MST)	SURFACE TEMP. (°C)	BRIGHTNESS TEMP. (°C)	LAKE POSITION	COMMENTS
2400-3100ft	0750 - 0752		27		Above lake
			30 - 35	6	Land areas
6100	0800		26	1	
	0803		26	2	
10000	0810		24	3	
11800	0812		24.5	4	
				5	This area always 1.5 to 2°C warmer than rest of lake

Fig. 6: Theodore Roosevelt Res., AZ., Water Brightness Temperature and Lake Location Map.

2.2.4 *GREAT SALT LAKE, UTAH, 13 SEPTEMBER 1973*

Site Coordinates:	14° 15' 00° N. Latitude 112° 45' 00° W. Longitude
EREP Pass:	Track 59A, Pass No. 39, Rev. 1763/1764
Time of Overpass:	256:19:34:29 GMT See Figures 7 and 8 for geographic details

2.2.4.1 General Conditions - Clear.

2.2.4.2 Near Surface Meteorology - Dry bulb temperature = 22.2°C; wet bulb temperature = 17.2°C; surface pressure = 652.8 M.M. of Hg; wind - 10 m.p.h./100° azimuth.

2.2.4.3 Temperature and Humidity Profile - The temperature profile is shown in Figure 9 and is listed in Table 5. The humidity profile is shown in Figure 10 and is listed in Table 6.

2.2.4.4 Brightness Temperature - The brightness temperature was measured on both sides of the causeway (shown in Figure 8) because of possible non-uniformities resulting from the causeway. These measurements were made at various altitudes from a helicopter and are listed in Table 7. In addition, brightness and contact probe measurements were made of the water near the shore and brightness temperatures of the sand were also made (see Figure 8).

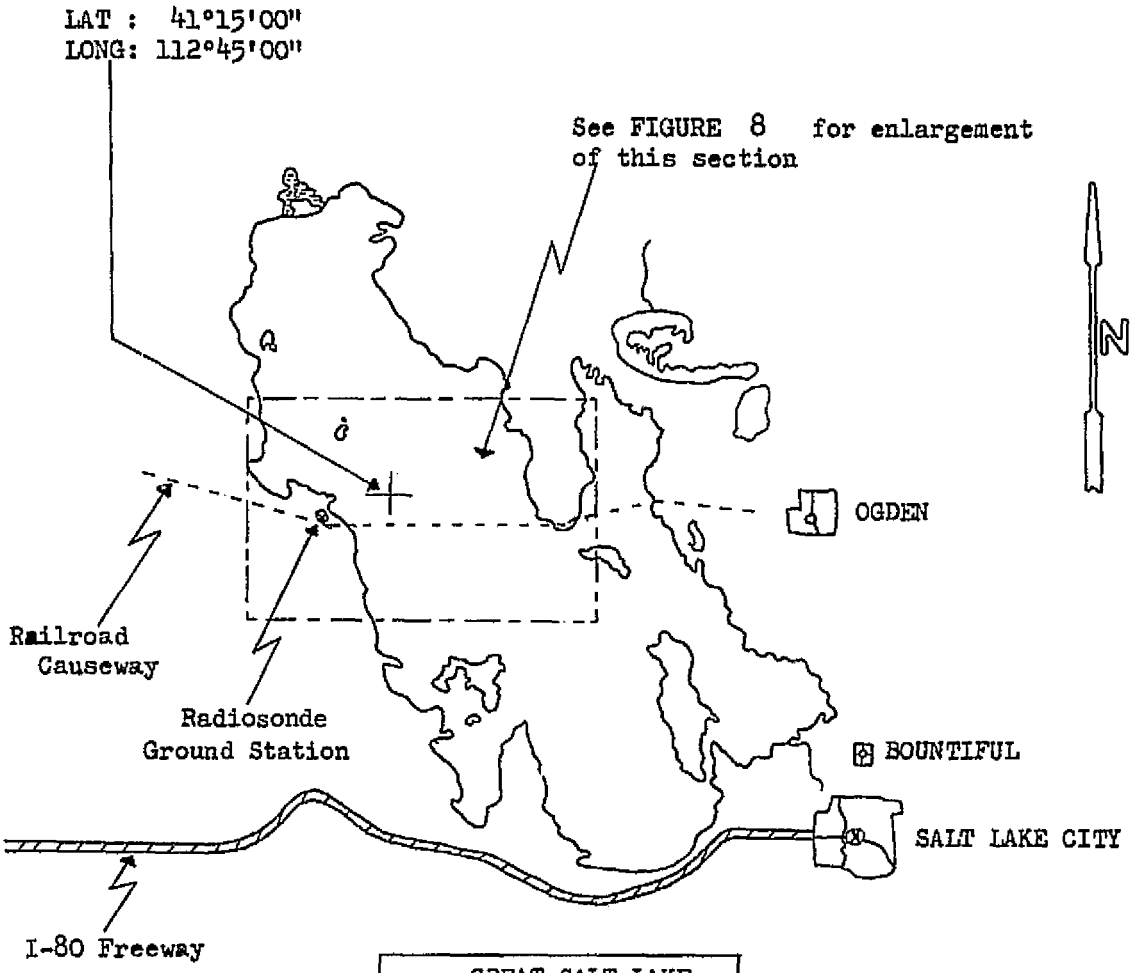

Fig. 7: Great Salt Lake, UT., Location Map and General Area of Measurements.

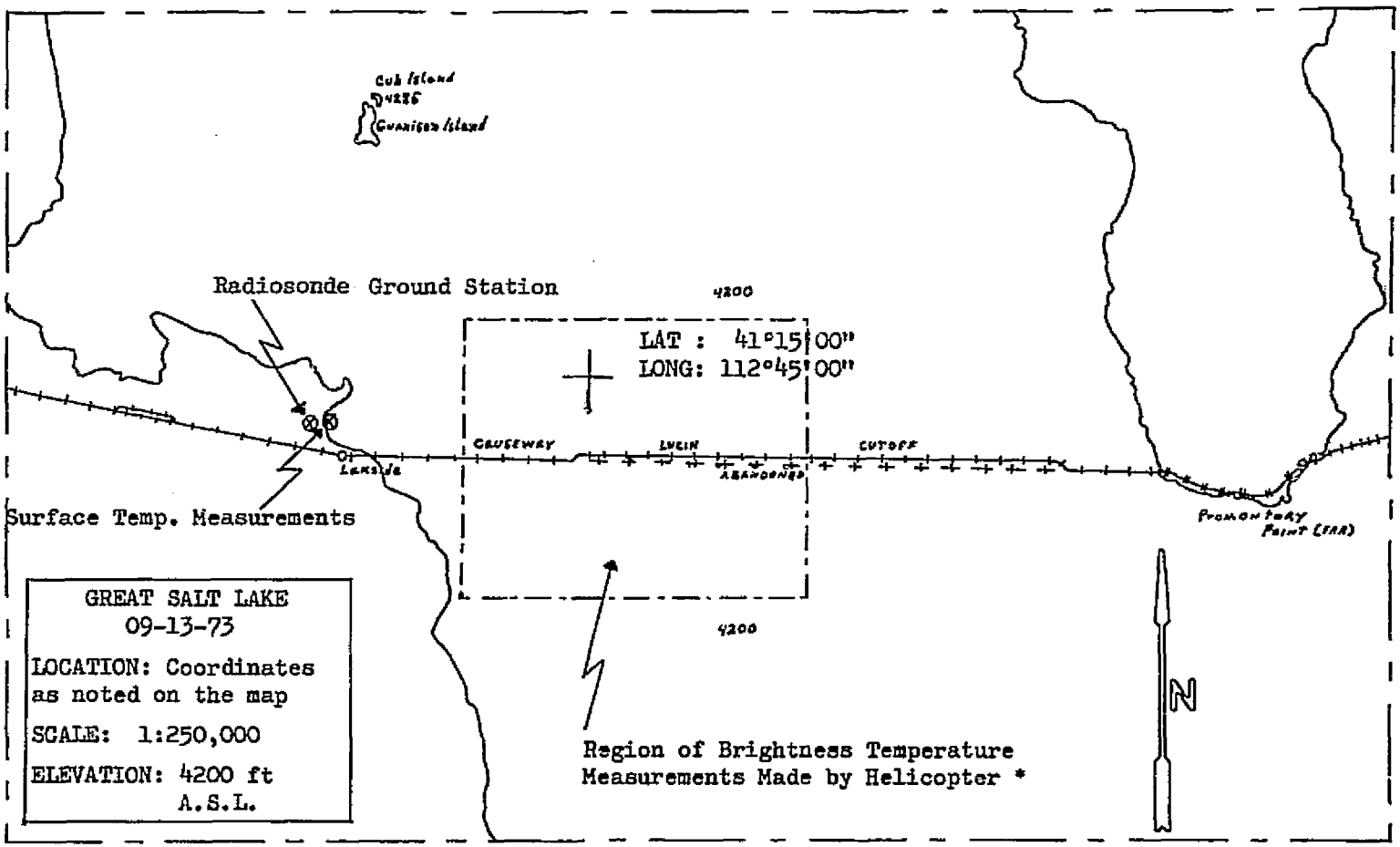

* Water Temperature and Brightness Temperature Distribution Values Found in Table 7

Fig. 8: Great Salt Lake, UT., Detailed Map of Measurement Area.

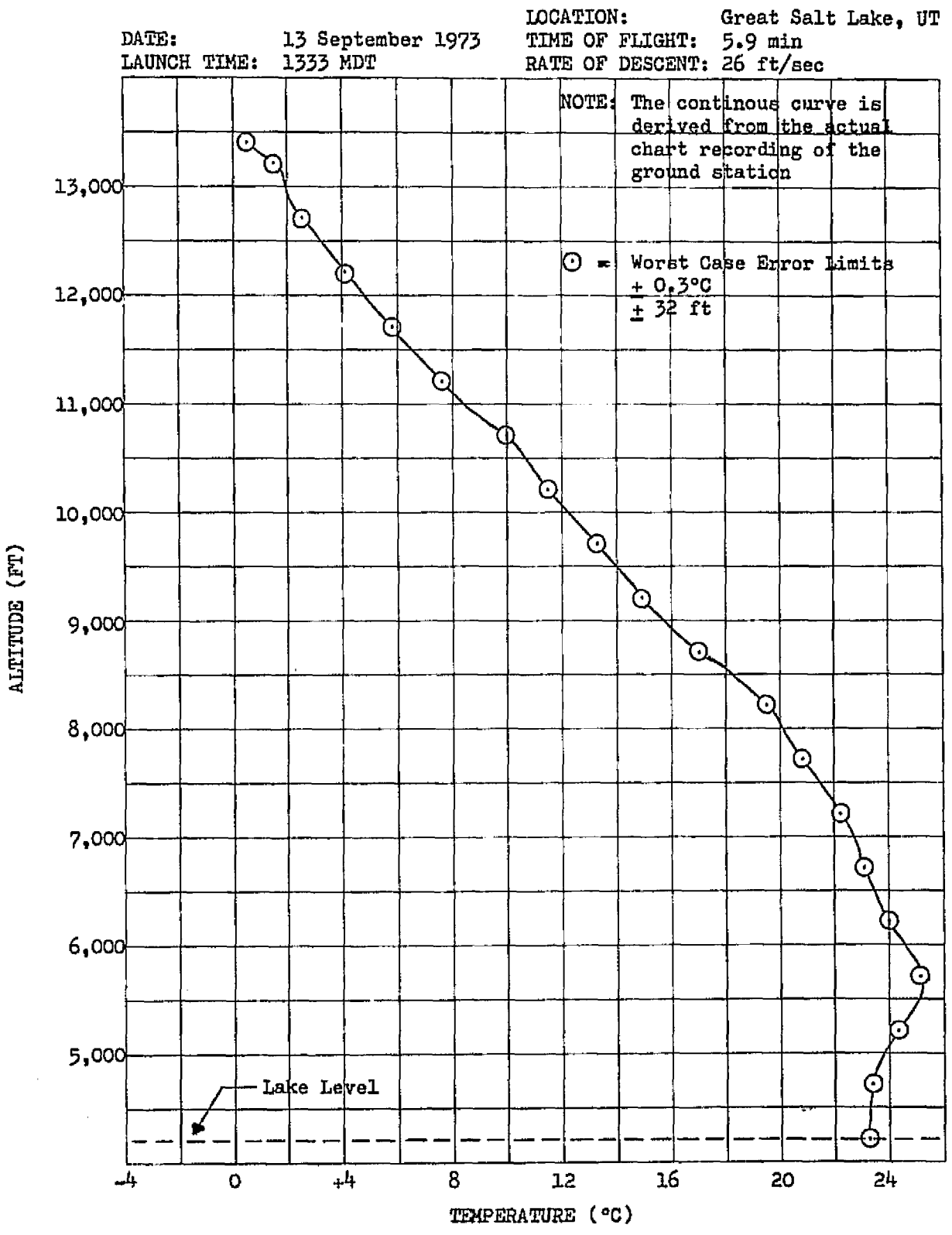

Fig. 9: Radiosonde Temperature Profile Plot for Great Salt Lake, UT., 13 September 1973.

RADIOSONDE EVALUATION DATA

NUMBER OF ¼" FROM LANDING	RAW DATA FROM ST.CH.	TIME FROM LANDING	ALTITUDE REF: 0'	ALTITUDE (A.S.L.)	TEMP OR HUM FROM TABLE	COMMENTS
0	6- 24.0	0 sec	000ft	4200 ft	23.3 °C	Temps. de-
7.70	6- 24.5	19.29	+ 500	4700	23.4	rived from
15.38	6- 28.4	38.46	1000	5200	24.3	table below
23.08	6- 31.6	57.69	1500	5700	25.1	
30.77	6- 27.0	76.92	2000	6200	24.0	
38.46	6- 23.0	96.15	2500	6700	23.1	
46.15	6- 19.0	115.38	3000	7200	22.2	
53.85	6- 12.8	134.62	3500	7700	20.8	
61.54	6- 6.5	153.85	4000	8200	19.5	
69.23	5- 44.5	173.08	4500	8700	17.0	
76.92	5- 34.3	192.31	5000	9200	14.9	
84.62	5- 26.0	211.54	5500	9700	13.3	
92.30	5- 16.5	230.77	6000	10200	11.5	
100.00	5- 8.3	250.00	6500	10700	10.0	
107.69	4- 44.4	269.23	7000	11200	7.6	
115.38	4- 34.2	288.46	7500	11700	5.8	
123.08	4- 25.0	307.69	8000	12200	4.1	
130.77	4- 15.5	326.92	8500	12700	2.5	
138.46	4- 9.6	346.15	9000	13200	1.5	
141.54	4- 3.8	353.85	9200	13400	0.5	

* RAW DATA	X	Y	I	D.P.	TEMP. (°C)	
6- 24.0	674.0	712.5	7	12.5	23.3	Cc/Xc=
6- 24.5	674.5	713.0	7	13.0	23.4	712.5/624.0=
6- 28.4	678.4	717.2	7	17.2	24.3	1.1418
6- 31.6	681.6	720.5	7	20.5	25.1	
6- 27.0	677.0	715.7	7	15.7	24.0	
6- 23.0	673.0	711.4	7	11.4	23.1	
6- 19.0	669.0	707.2	7	7.2	22.2	
6- 12.8	662.8	700.6	7	0.6	20.8	
6- 6.5	656.5	694.0	6	44.0	19.5	
5- 44.5	644.5	681.3	6	31.3	17.0	
5- 34.3	634.3	670.5	6	20.5	14.9	
5- 26.0	626.0	661.8	6	11.8	13.3	
5- 16.5	616.5	651.7	6	1.7	11.5	
5- 8.3	608.3	643.0	5	43.0	10.0	
4- 44.4	594.4	628.4	5	28.4	7.6	
4- 34.2	584.2	617.6	5	17.6	5.8	
4- 25.0	575.0	607.8	5	7.8	4.1	
4- 15.5	565.5	597.8	4	47.8	2.5	
4- 9.6	559.6	591.6	4	41.6	1.5	
4- 3.8	553.8	585.4	4	35.4	0.5	

TEMPERATURE X HUMIDITY ___ LOCATION Great Salt Lake, UT

DATE 09-13-73

NOTES: 1) Recorder travels at 2.5 sec / ¼" Div
2) Descent rate: 26 ft/sec
*3) Field calibration was incorrect, therfore a correction factor must be applied and this was supplied by vendor of Rocketsonde.
$X=[400+50(R-1)]+D.P. \Rightarrow Y=(Cc/Xc)X \Rightarrow Data'=(Y-350)/50 \Rightarrow I + Re$;
where: R=Range; D.P.=Data Point; Cc=Correct Calib. (R=7, D.P.=12.5 ⇒712.5); Xc=X at incorrect calib. D.P.; Data'=Corrected Data Point; I⇒Integer= corrected R; Re⇒Fractional Remainder = % of 50 D.P.'s of full scale.

Table 5: Radiosonde Temperature Profile Listing for Great Salt Lake, UT., 13 September 1973.

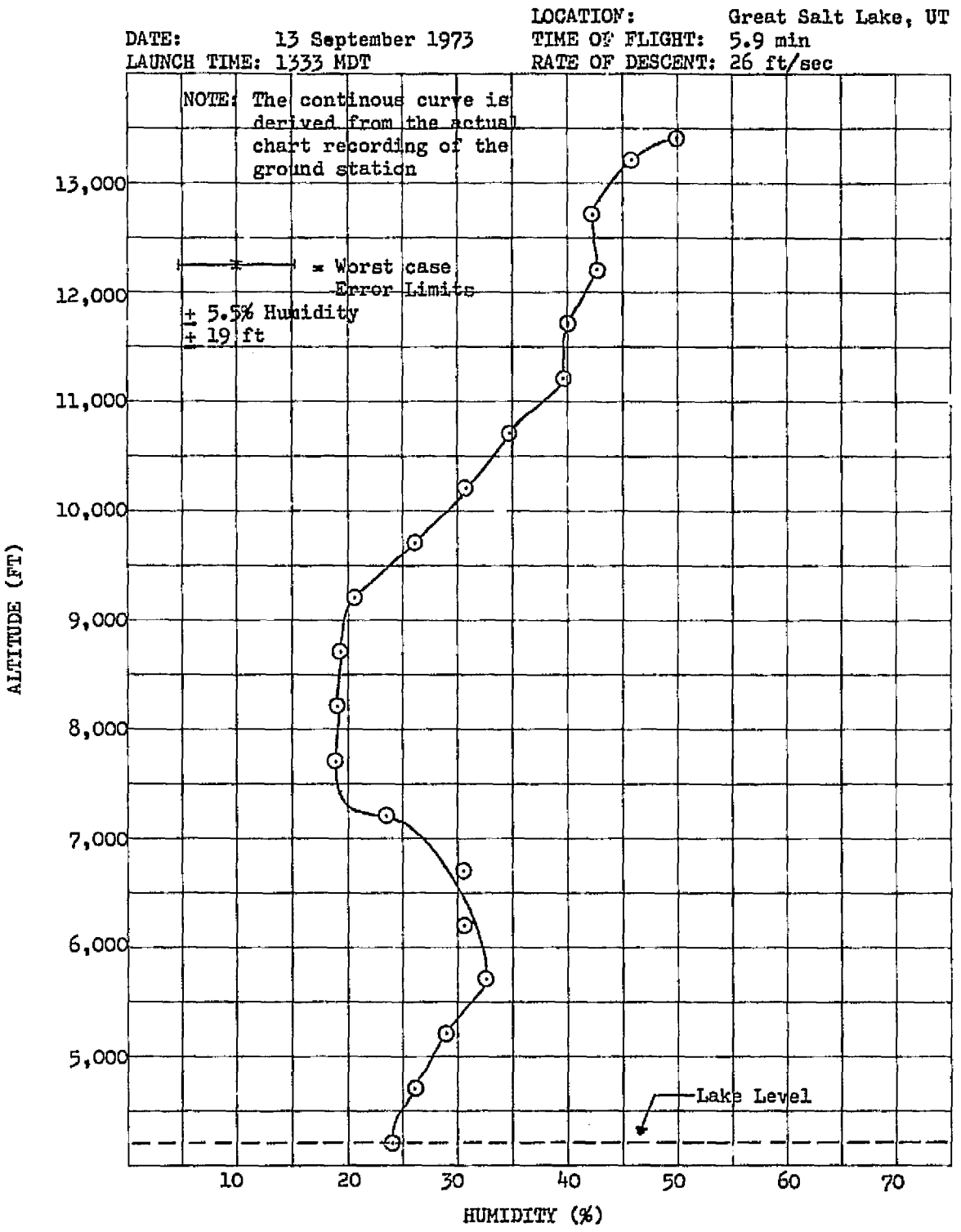

Fig. 10: Radiosonde Humidity Profile Plot for Great Salt Lake, UT., 13 September 1973.

RADIOSONDE EVALUATION DATA

NUMBER OF ¼" FROM LANDING	RAW DATA FROM ST.CH.	TIME FROM LANDING	ALTITUDE REF: 0'	ALTITUDE (A.S.L.)	TEMP OR HUM FROM TABLE	COMMENTS
0	1- 16.0	0 sec	000 ft	4200 ft	24.0 %	
7.70	1- 17.0	19.29	500	4700	26.0	
15.38	1- 18.5	38.46	1000	5200	28.7	
23.08	1- 21.5	57.69	1500	5700	32.5	
30.77	1- 19.5	76.92	2000	6200	30.3	
38.46	1- 19.5	96.15	2500	6700	30.3	
46.15	1- 15.5	115.38	3000	7200	23.3	
53.85	1- 12.0	134.62	3500	7700	18.7	
61.54	1- 12.0	153.62	4000	8200	18.7	
69.23	1- 12.5	173.08	4500	8700	19.2	
76.92	1- 13.5	192.31	5000	9200	20.3	
84.62	1- 17.0	211.54	5500	9700	26	
92.30	1- 20.0	230.77	6000	10200	30.7	
100.00	1- 23.5	250.00	6500	10700	34.7	
107.69	1- 28.0	269.23	7000	11200	39.5	
115.38	1- 28.5	288.46	7500	11700	40	
123.08	1- 31.0	307.69	8000	12200	42.3	
130.77	1- 31.0	326.92	8500	12700	42.3	
138.46	1- 35.0	346.15	9000	13200	45.7	
141.54	1- 42.5	353.85	9200	13400	50	

TEMPERATURE ___ HUMIDITY X LOCATION Great Salt Lake, UT

DATE 09-13-73

NOTES: 1) Recorder travels at 2.5 sec / ¼" Div
2) Descent rate: 26 ft/sec

Table 6: Radiosonde Humidity Profile Listing for Great Salt Lake, UT., 13 September 1973.

WATER TEMPERATURE AND BRIGHTNESS TEMPERATURE

A.S.L. ELEVATION	TIME (MDT)	SURFACE TEMP (°C)	BRIGHTNESS TEMP (°C)	LAKE POSITION	COMMENTS
4200 ft	1250		32.5	Sand	Near lake shore
00			19.5	Next to Shore	PRT-5
4. .0		25.0			YSI Probe
4400	1250		18.0	North side	(of causeway)
4400	1250		17.5	South side	
4700			17.8	North side	
4800			18.2	North side	
5200			17.5	South side	
5300			18.5	North side	
5700			17.5	South side	
6200			18.5	North side	
6500			18.5	North side	
6800			18.5	South side	
7000			18.0	South side	
7500			18.5	North side	
8000			17.5	South side	
8500			17.0	South side	
9000			17.0	South side	
9000			17.5	South side	
9200			18.5	North side	
9200			17.5	South side	
9200			19.0	Center	
9200			17.0	Center	
9300			17.0	South side	
9300			19.0	North side	
9600			17.0	South side	
9700			18.5	North side	
10000			18.0	South side	
10000			19.0	North side	
10700			18.5	North side	
10900	1325		17.0	South side	
11200			17.0	South side	
12400			16.0	South side	
13200			15.5	South side	
13500	1332		17.0	North side	

SITE Great Salt Lake MISSION S.L. III DATE 09-13-73

INSTRUMENT PRT-5 (M.M.A.)

Y.S.I. THERMISTOR PROBE

Table 7: Great Salt Lake, UT., Water Brightness Temperature Measurements.

3. SOLAR RADIATION CALIBRATION MEASUREMENTS AND ANALYSES

3.1 Instrumentation and Techniques - Two types of instrumentation were used to measure direct, diffuse, total, and reflected solar radiation.

The first type of instruments used were two interference wedge, spectral scanning, spectroradiometers, manufactured by I.S.C.O. (Instrumentation Specialties Company, Lincoln, Nebr.). The wavelength range covered was 400 to 1300 nanometer (nm), with halfband widths of 15 nm, from 400 to 750 nm, and 30 nm from 750 to 1300 nm. The sensing element is a planar diode and the light gathering element consists of fiber optics probes with a teflon diffuser at the acceptance end of the probe. One I.S.C.O. was used to periodically ($\tilde{\sim}$ 1/2 hour increments) measure the direct solar beam, using a 6° collimator placed over the above mentioned diffuser. As discussed later, these measurements allowed the atmospheric optical depth to be derived. The other I.S.C.O. was used to measure total, diffuse, and reflected solar radiation. The total incident solar radiation was measured by simply allowing the diffuser light collector to view (180° F.O.V.) the sky hemisphere, making certain that the diffuser was horizontal. The diffuse solar was measured by shading the diffuser from the direct solar beam. The reflected solar radiation was measured by rotating the diffuser 180°, so that it viewed the target. The detailed calibration of the I.S.C.O's is presented in the Appendix.

The second type of instrument used was a Bendix Model 100 Radiant Power Measuring Instrument (R.P.M.I); basically, it is a bandpass filter radiometer. The bandpasses normally used are those of the ERTS Multispectral Scanner (MSS), referred to as B1-.500 to .600 micrometers (μm), B2-.600 to .700 μm, B3-.700 to 800 μm, and B4-.800 to 1.100 μm. The real halfbands, as a result of the sensor/filter combination, are referred to as B1R-.505 to .590 μm,

B2R-.600 to .720 μm B3R-.680 to .815 μm, and B4R-.810 to 1.02 μm. Both the ERTS and real R.P.M.I. bands are reported. The R.P.M.I. was chiefly used to measure directional (normal to target, 7° F.O.V.) reflected solar radiation, and atmospheric optical depth. The detailed calibration of the R.P.M.I. is presented in the Appendix. The R.P.M.I. was kindly supplied by the Bendix Aerospace Corporation (Dr. R. Rogers).

3.2 Measurements and Analyses

3.2.1 *GREAT SALT LAKE DESERT, UTAH, 03 AUGUST 1973*

3.2.1.1 General Conditions - Overcast (80 - 90%).

3.2.1.2 Near Surface Meteorology -

3.2.1.3 Total and Diffuse Solar Radiation -

3.2.1.4 Atmospheric Optical Depth -

3.2.1.5 Target Reflectivity and Radiance At Ground Level -

} No Measurements

3.2.1.6 Target Radiance at EREP -

3.2.2 *GREAT SALT LAKE DESERT, UTAH, 08 AUGUST 1973*

Site Coordinates:	40° 45" N. Latitude 113° 24" W. Longitude (See Figure 11)
EREP Pass:	Track 34, Pass No. 16, Rev. 1241/1242
Time of Overpass:	220:16:01:12 GMT 10:01 Local Time (M.D.T.)

3.2.2.1 General Conditions - Clear

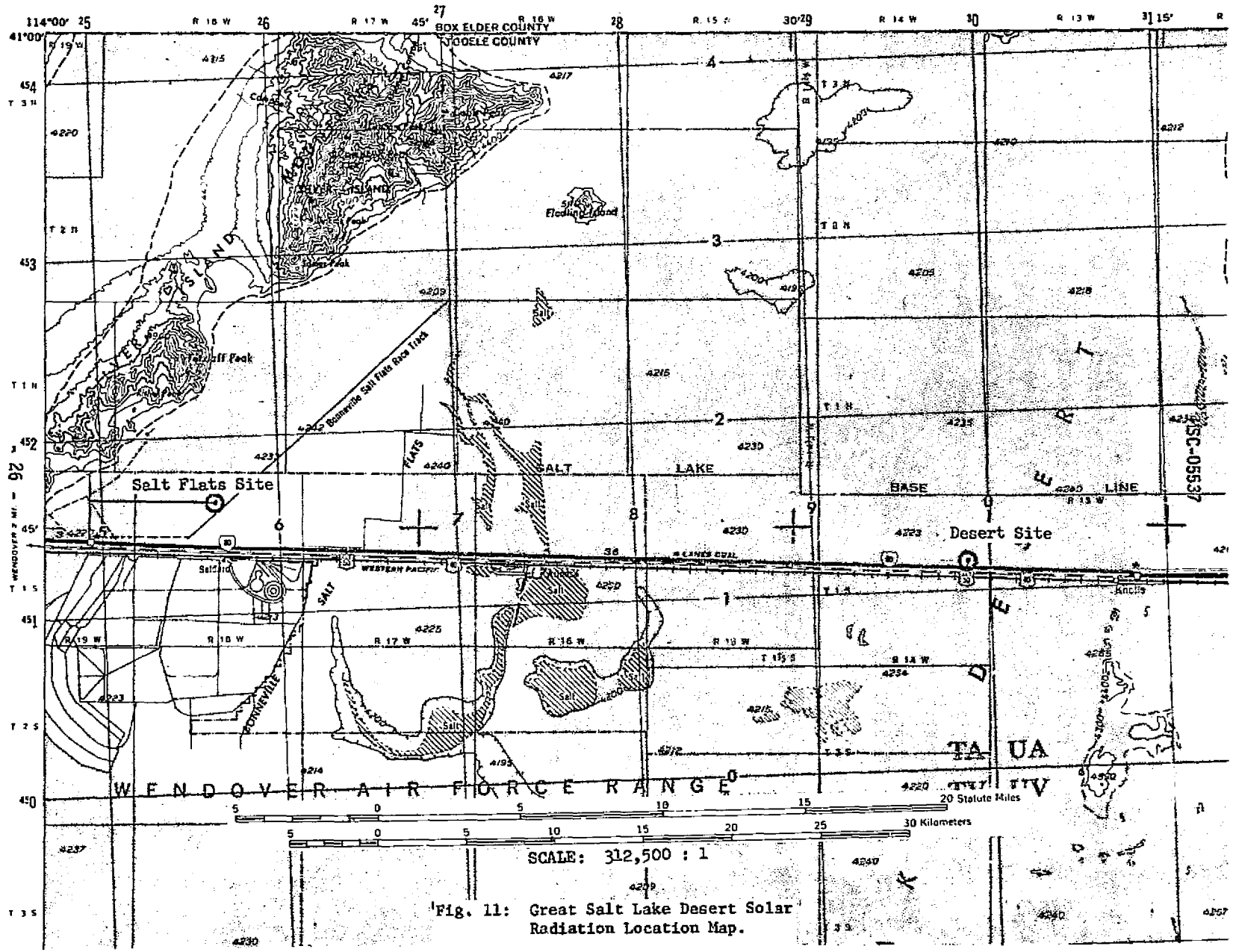

Fig. 11: Great Salt Lake Desert Solar Radiation Location Map.

3.2.2.2 Near Surface Meteorology - Field data was taken but subsequently lost.

3.2.2.3 Total and Diffuse Solar Radiation - Total and diffuse solar radiation were obtained with the Bendix R.P.M.I. unit only,because of an electronic malfunction in the I.S.C.O. spectroradiometer. The absolute amounts of total and diffuse solar radiation are shown in Figures 12 and 13, respectively. The quantitites are given in the normally used (with respect to the R.P.M.I.) units of watts per square meter per wavelength increment - $W\ m^{-2}\ \Delta\lambda^{-1}$. The $\Delta\lambda$'s shown are for the ERTS and actual R.P.M.I. bands, as defined in Section 3.1. The quantities of direct (I_h) diffuse (D) and total (H) solar radiation are also listed in Table 8. These three quantities are related by

$$H = I_h + D \qquad (1)$$

where I_h is the quantity of direct solar radiation on a horizontal surface. The field measurements consisted of diffuse and the normal incident solar beam (I). The horizontal direct solar radiation was subsequently derived by

$$I_h = I \cos \Theta_o \qquad (2)$$

where Θ_o is the solar zenith angle. The diffuse was obtained by simply shading the sensor from the direct solar beam. All measurements were taken sufficiently close to overpass so that no temporal influences existed.

The ratio of diffuse to total solar radiation is shown in Figure 14 and listed in Table 8. This ratio is simply D/H, and is sensitive to atmospheric aerosol content, i.e., the higher the atmospheric aerosol concentration, the greater D/H. For a detailed presentation of D/H, consult "Studies of Spectral Discrimination", W.A. Malila, et.al.,

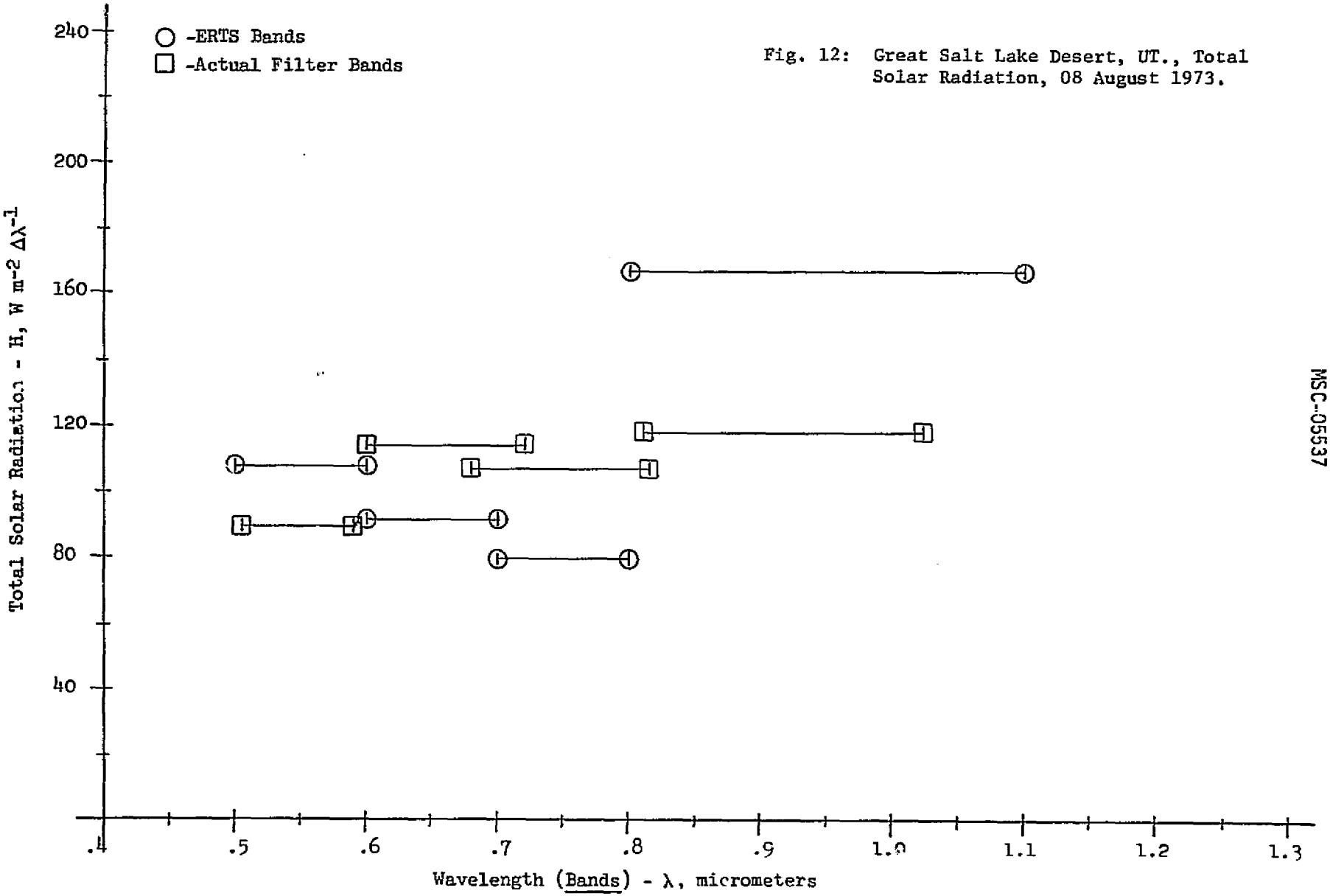

Fig. 12: Great Salt Lake Desert, UT., Total Solar Radiation, 08 August 1973.

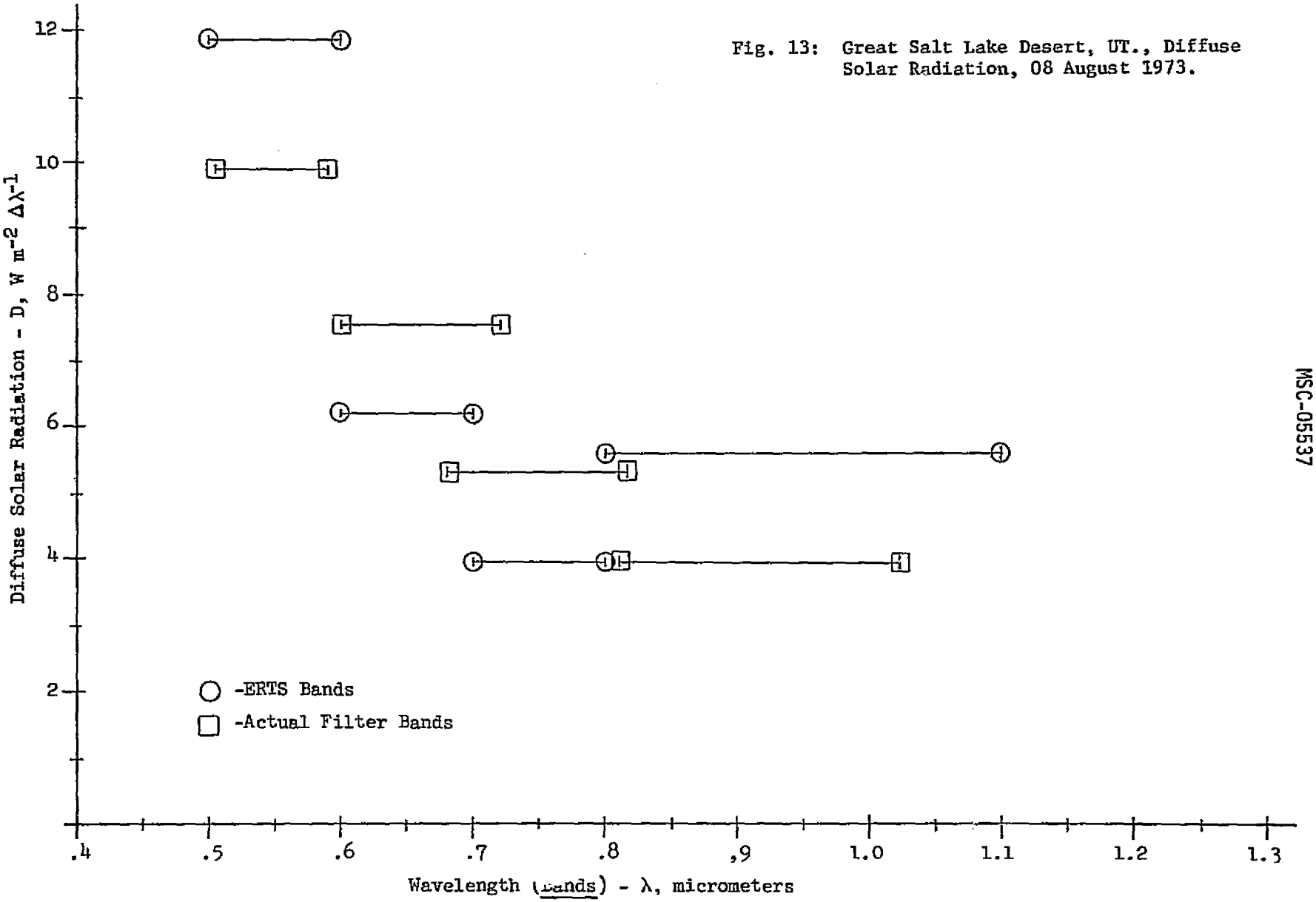

Fig. 13: Great Salt Lake Desert, UT., Diffuse Solar Radiation, 08 August 1973.

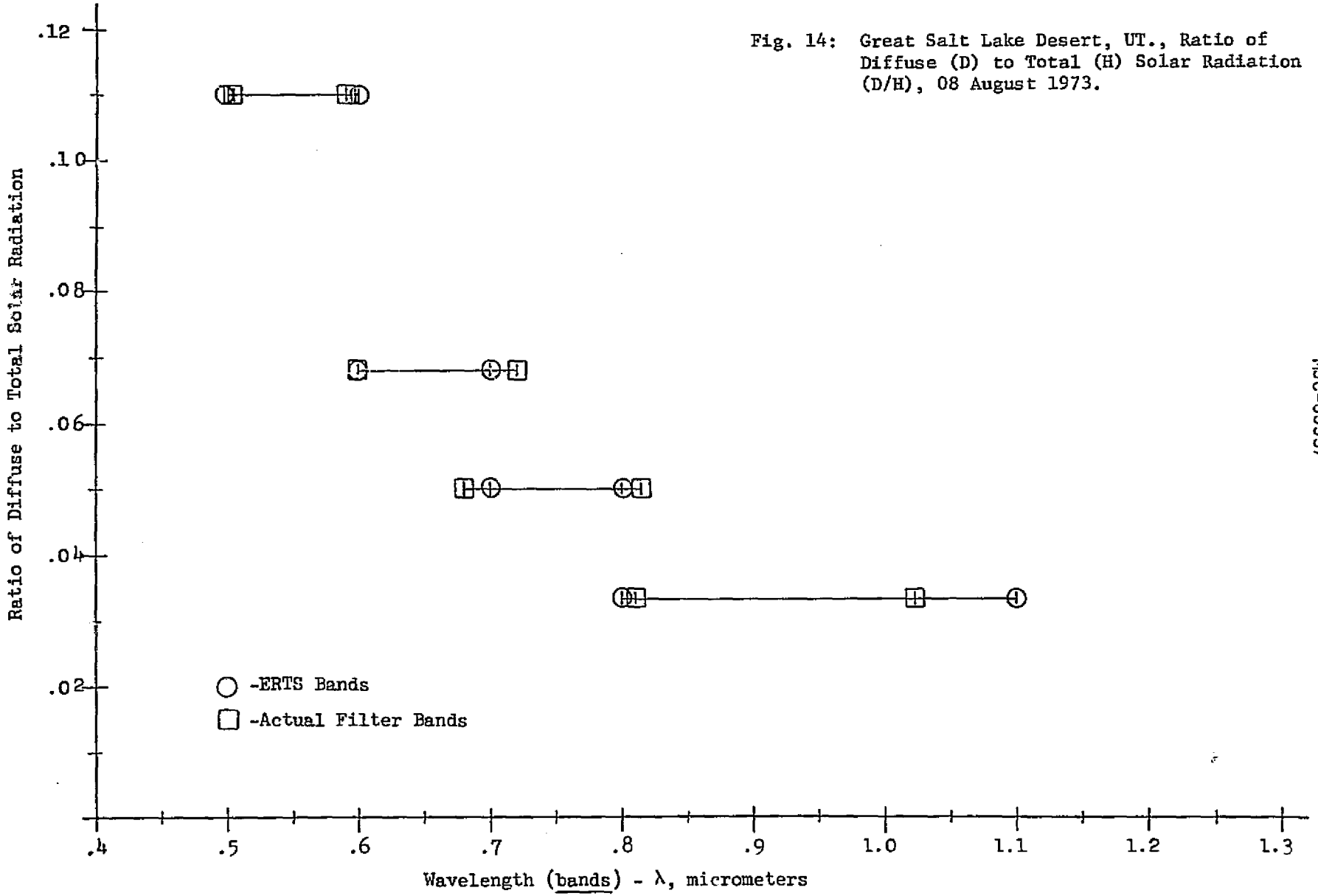

Fig. 14: Great Salt Lake Desert, UT., Ratio of Diffuse (D) to Total (H) Solar Radiation (D/H), 08 August 1973.

MSC-05537

Great Salt Lake Desert (08/08/73) Solar Radiation and Reflectance Measurements

Band	Direct (I_h)	Diffuse (D)*	Total (H)*	D/H	Dry Area (ρ)	Wet Area (ρ)
B1	95.51	11.86	107.4	.110	.356	.228
B1R	79.49	9.88	89.37	.110		
B2	85.26	6.22	91.48	.0680	.376	.262
B2R	106.5	7.77	114.3	.0680		
B3	75.59	3.96	79.55	.0498	.387	.285
B3R	101.73	5.32	107.0	.0497		
B4	161.43	5.59	167.0	.0335	.388	.293
B4R	114.17	3.95	118.1	.0334		

$H = I_h + D$

* Watts $(meter)^{-2}$ $\Delta\lambda^{-1}$

$\Delta\lambda$(micrometers) ⇒ B1 = .500-.600 B1R = .505-.590
B2 = .600-.700 B2R = .600-.720
B3 = .700-.800 B3R = .680-.815
B4 = .800-1.10 B4R = .810-1.02

Table 8: Great Salt Lake Desert, UT., Direct, Total and Diffuse Solar Radiation, and Target Reflectivities, 08 August 1973.

NASA CR-WRL 31650-22-T, NASA Manned Spacecraft Center, NAS9-9784, May 1971.

The relative temporal nature of the total solar radiation in a broadband from .400 to 1.1 μm, is shown in Figure 15. This was measured with a Y.S.I. (Yellow Springs Instruments) pyranometer. The pyranometer meter readings can roughly be taken as the total solar radiation from .3 to 3.0 μm, in units of cal cm^{-2} min^{-1}. However, this assumes that the relationship between total solar radiation from .4 to 1.1 μm (the region of actual sensing) is in a constant proportion to the radiation to the radiation from .3 to 3.0 μm; but, because of variable atmospheric water vapor content and absorption between .750 to 3.0 μm, this is not always the case. The chief use of the Y.S.I. in the field was to provide monitoring and assurance of steady solar radiation conditions, during the other solar measurements.

3.2.2.4 Atmospheric Optical Depth/Transmittance - Measurements of the direct solar beam were made, over a period of time, in order to subsequently derive the optical depth of the atmosphere (τ). These two parameters are related by Lambert's law, as follows

$$T = e^{-\tau m} \qquad (3)$$

where m is the relative air mass, defined as the ratio of the slant path length of the direct solar beam at some solar zenith angle (Θ_o), to the slant path at Zenith. For solar zenith angles of less than about 70°, the relative air mass can be givan as sec Θ_o; For greater angles atmospheric refraction has to be taken into account. This was performed using an equivalent solution of Bemporad's formula as follows

$$C.F. = 5.534 \times 10^{-4} \sec \Theta^{3.34}, \quad 2<\Theta<3 \qquad (4a)$$

$$\text{Air Mass} = \sec \Theta - [C.F.\ p/p_o] \qquad (4b)$$

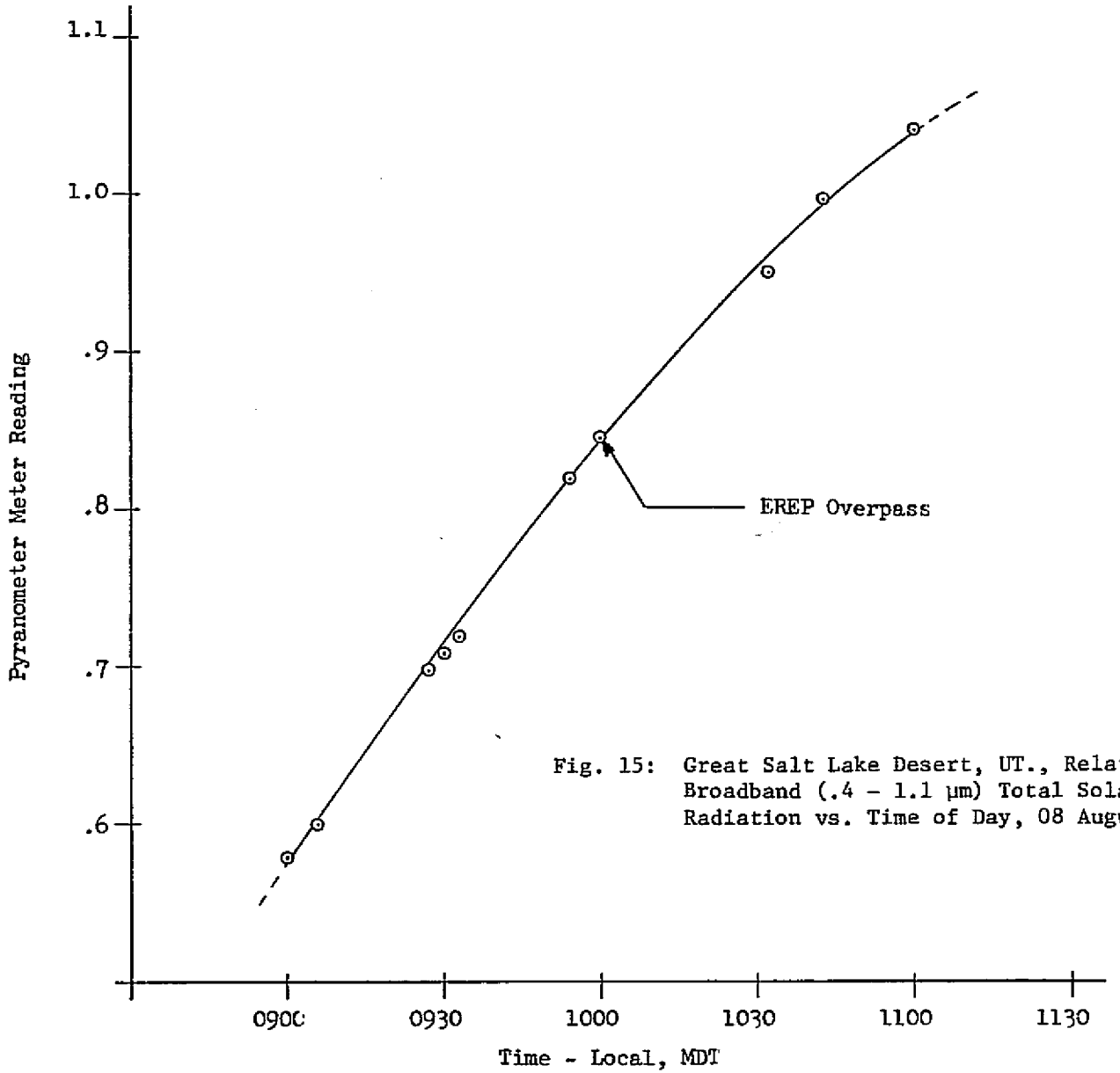

Fig. 15: Great Salt Lake Desert, UT., Relative Broadband (.4 – 1.1 μm) Total Solar Radiation vs. Time of Day, 08 August 1973.

where p_o is atmospheric pressure at sea level, and p is the pressure at the site in question. For more details concerning optical depth and transmittance consult "Spectral Distribution of Solar Radiation at the Earth's Surface", D. M. Gates, Science, Vol. 151, Number 3710, 4 February 1966.

The meter reading (M) of the instruments, when they viewed the direct solar beam (pyrheliometers), are related to atmospheric transmittance by

$$T = M/M_o \qquad (5)$$

where M_o is the meter reading of the pyrheliometer if it observed the sun outside of the atmosphere. Hence,

$$M = M_o e^{-\tau \sec \Theta_o} \qquad (6)$$

and

$$\ln M = -\tau \sec \Theta_o + \ln M_o \qquad (7)$$

In order to derive optical depth from the field measurements (M's and sec Θ_o's) , the pyrheliometer meter readings were plotted vs. air mass (m), as shown in Figures 16 through 17e. The slope of the lines drawn is (from Eq. 7) atmospheric optical depth and an extrapolation of the line yields M_o at m = o. The I.S.C.O. spectradiometer measurements are given in 25 nm and 50 nm increments, and the Bendix broadband measurements are shown for the four bands (B1, B2, B3, and B4). The resultant optical depths are shown in Figure 18. As can be seen, excellent agreement exists between the two instruments. The actual Bendix filter bands are the appropriate ones to compare to the I.S.C.O. determinations. Also shown in Figure 18 is the optical depth of a model, Visual Range = 40 km, derived from models given by Elterman "Vertical-Attenuation Model with Eight Surface Meteorological

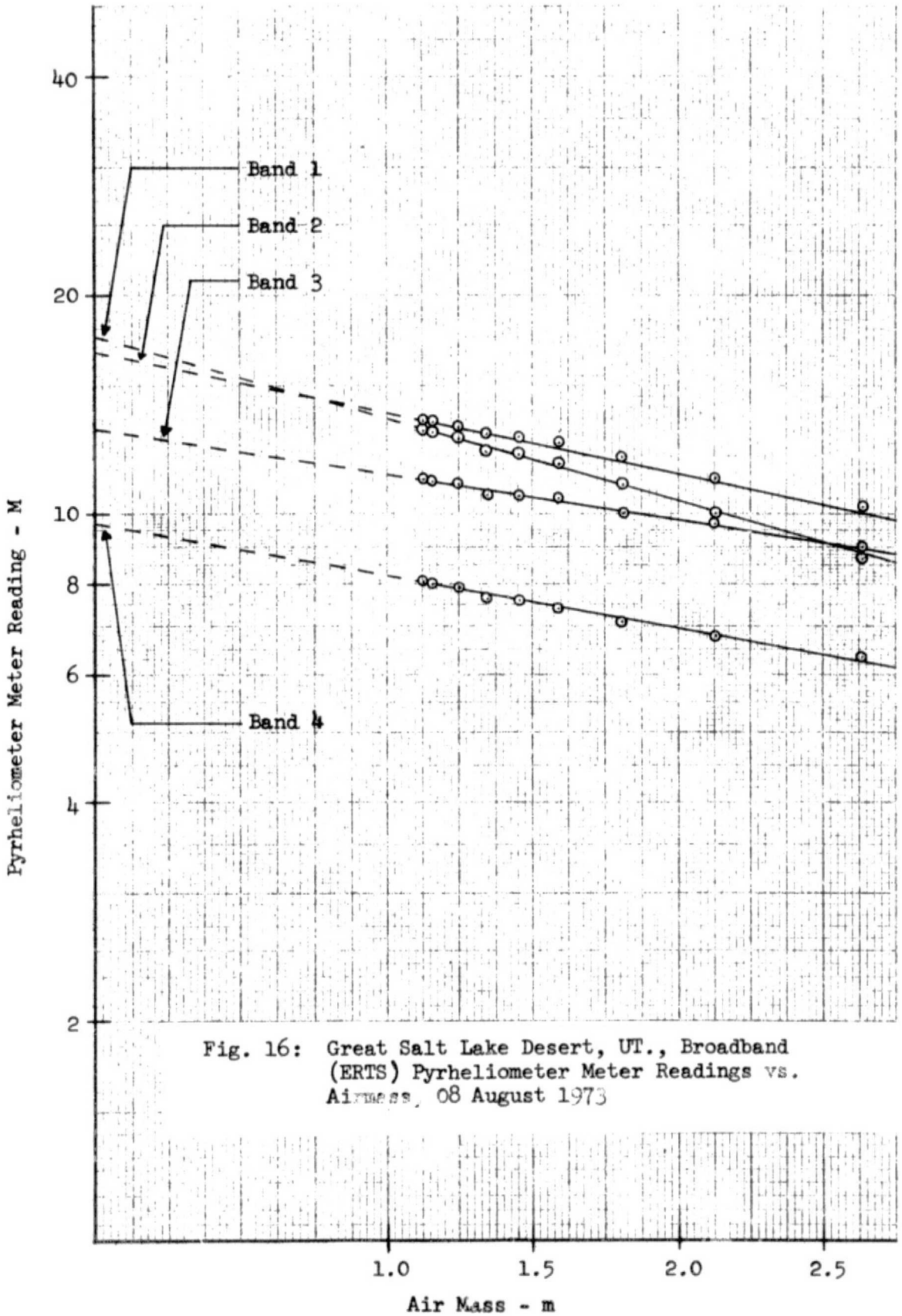

Fig. 16: Great Salt Lake Desert, UT., Broadband (ERTS) Pyrheliometer Meter Readings vs. Airmass, 08 August 1973

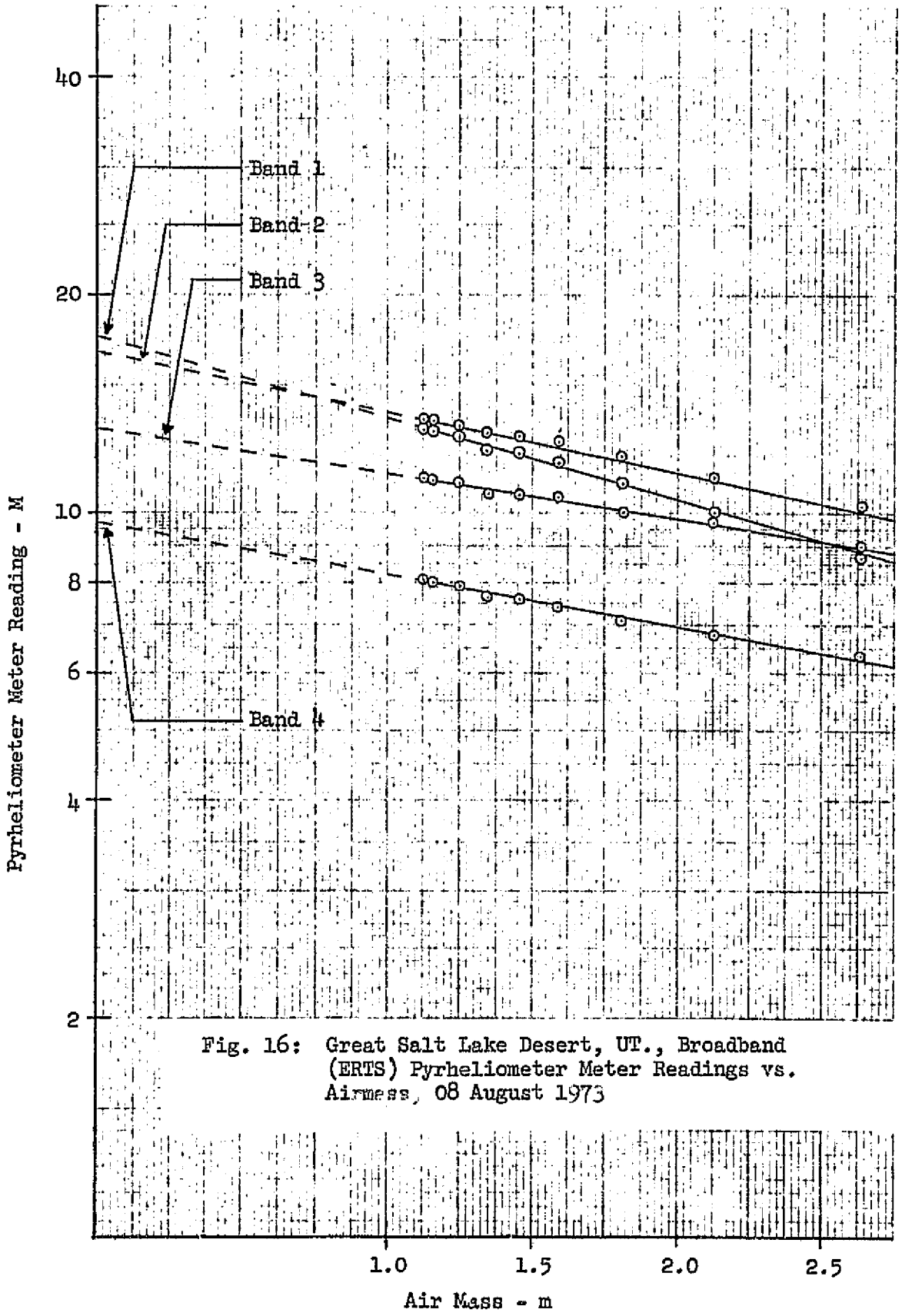

Fig. 16: Great Salt Lake Desert, UT., Broadband (ERTS) Pyrheliometer Meter Readings vs. Airmass, 08 August 1973

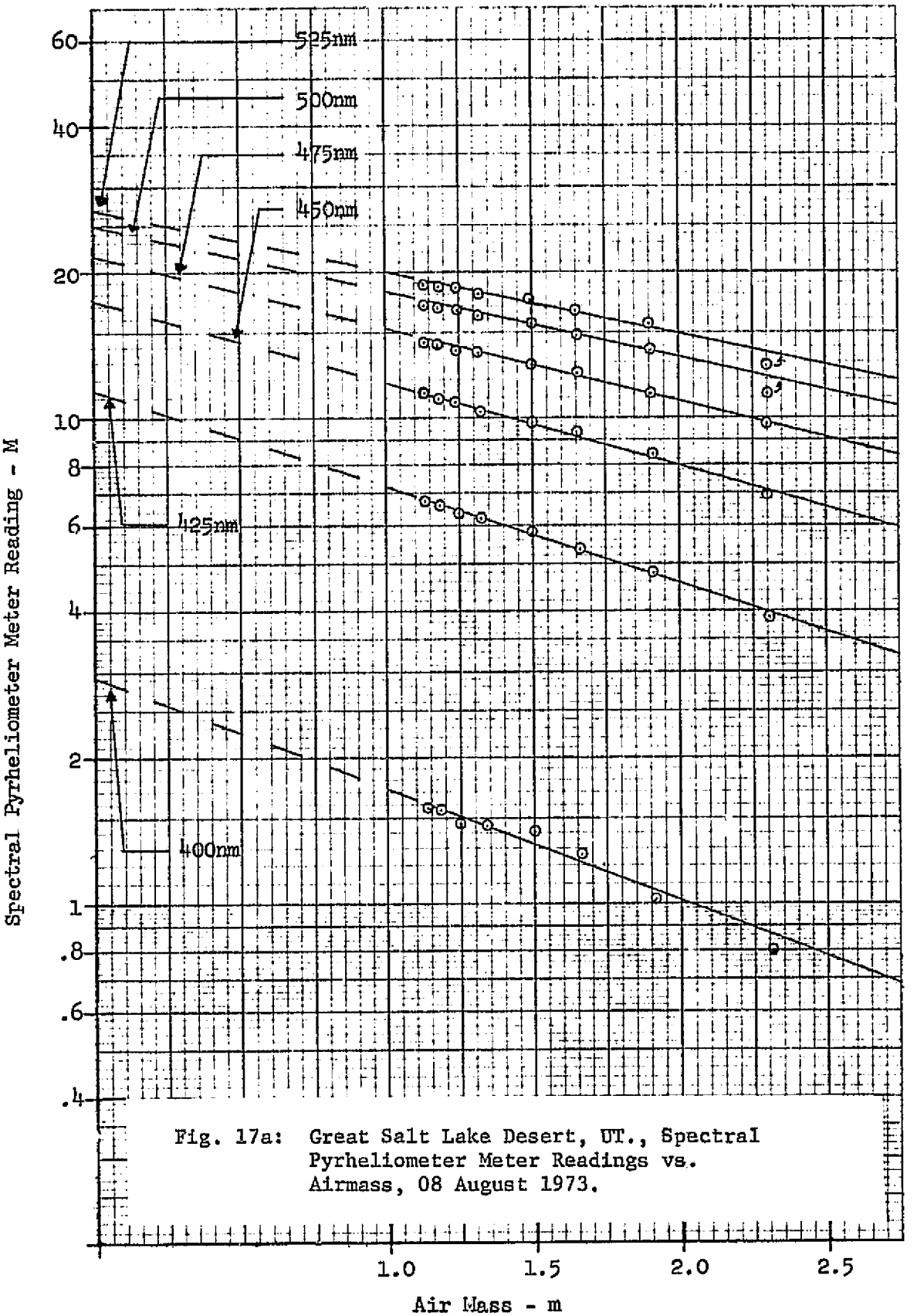

Fig. 17a: Great Salt Lake Desert, UT., Spectral Pyrheliometer Meter Readings vs. Airmass, 08 August 1973.

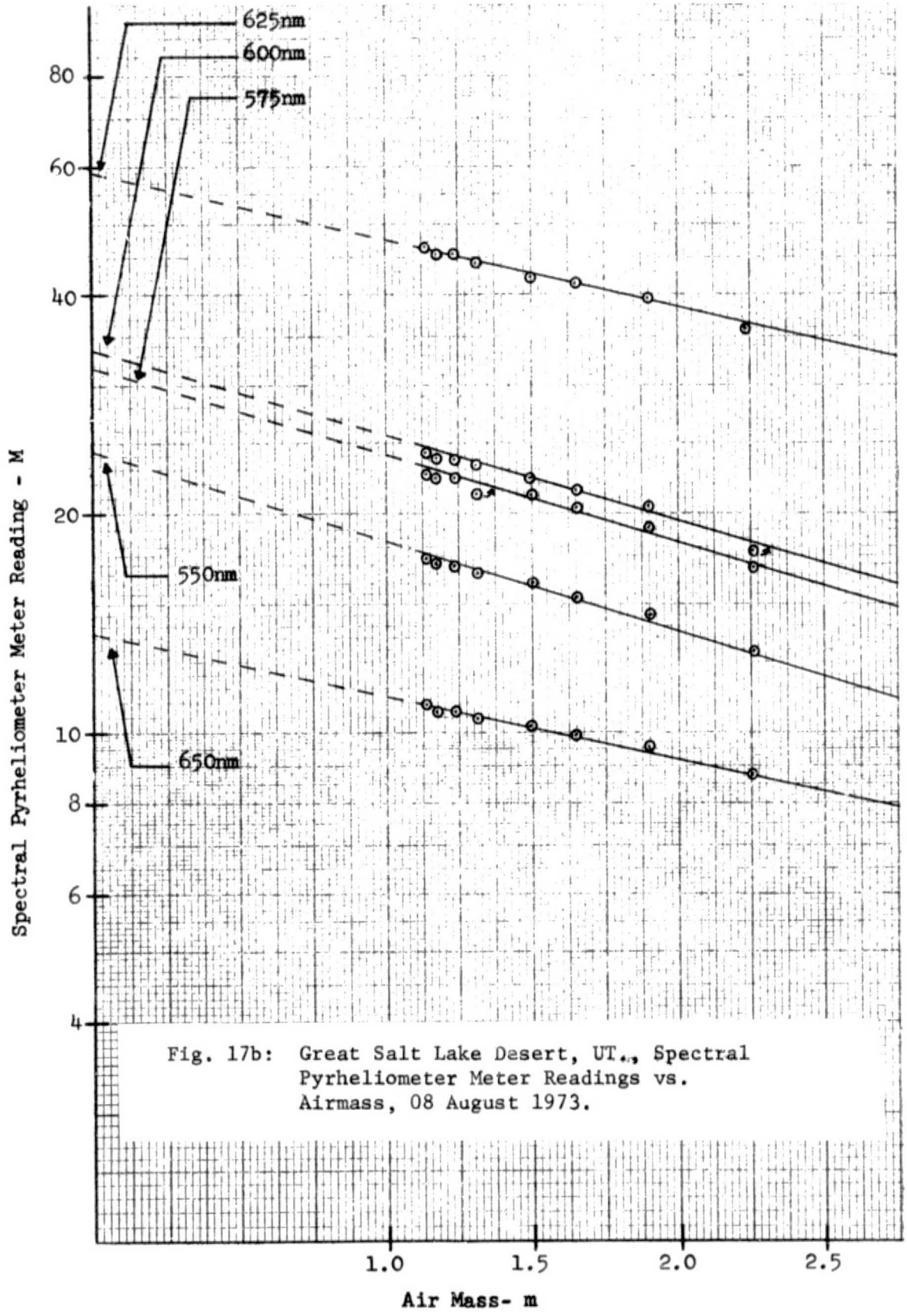

Fig. 17b: Great Salt Lake Desert, UT., Spectral Pyrheliometer Meter Readings vs. Airmass, 08 August 1973.

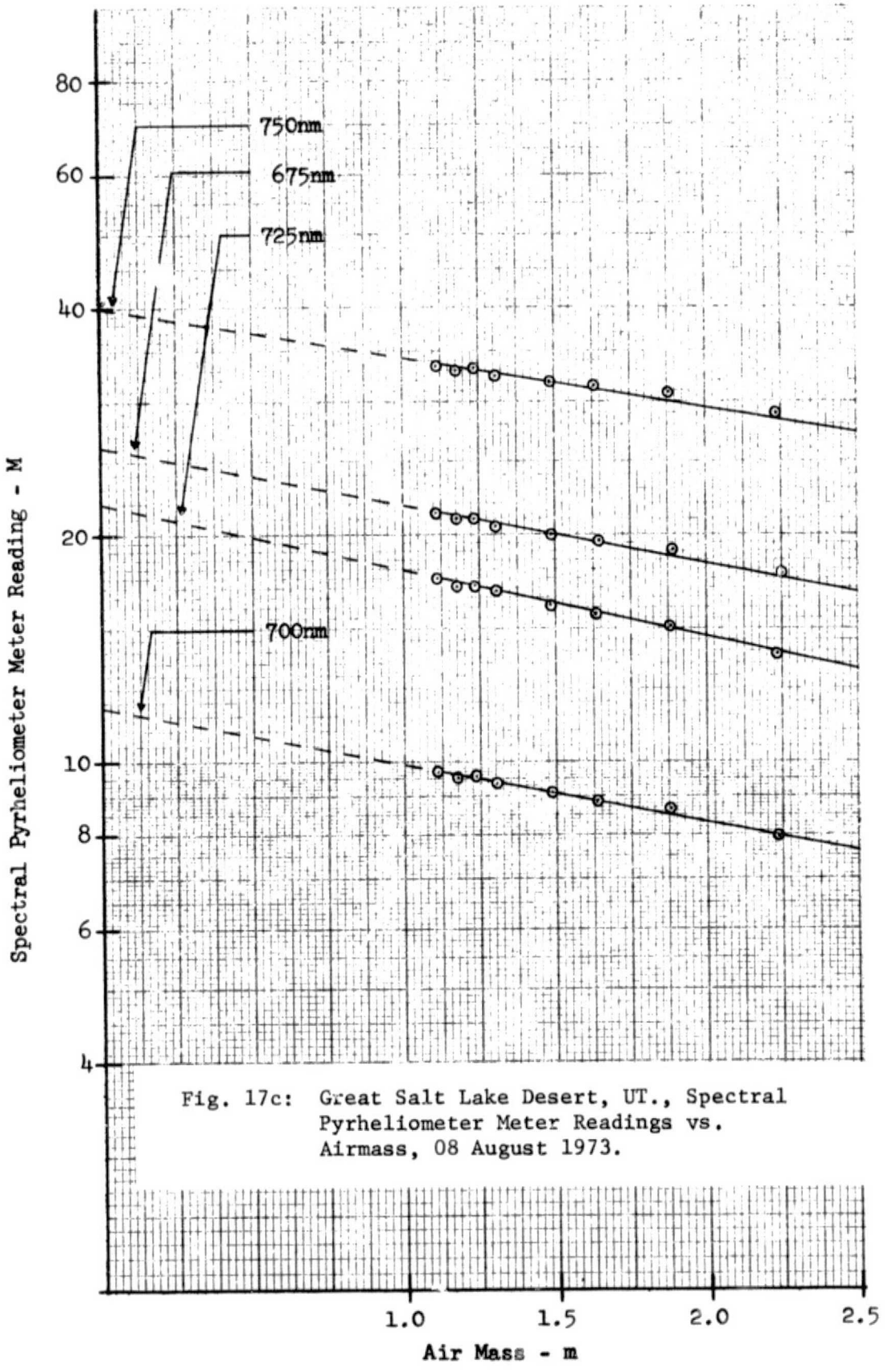

Fig. 17c: Great Salt Lake Desert, UT., Spectral Pyrheliometer Meter Readings vs. Airmass, 08 August 1973.

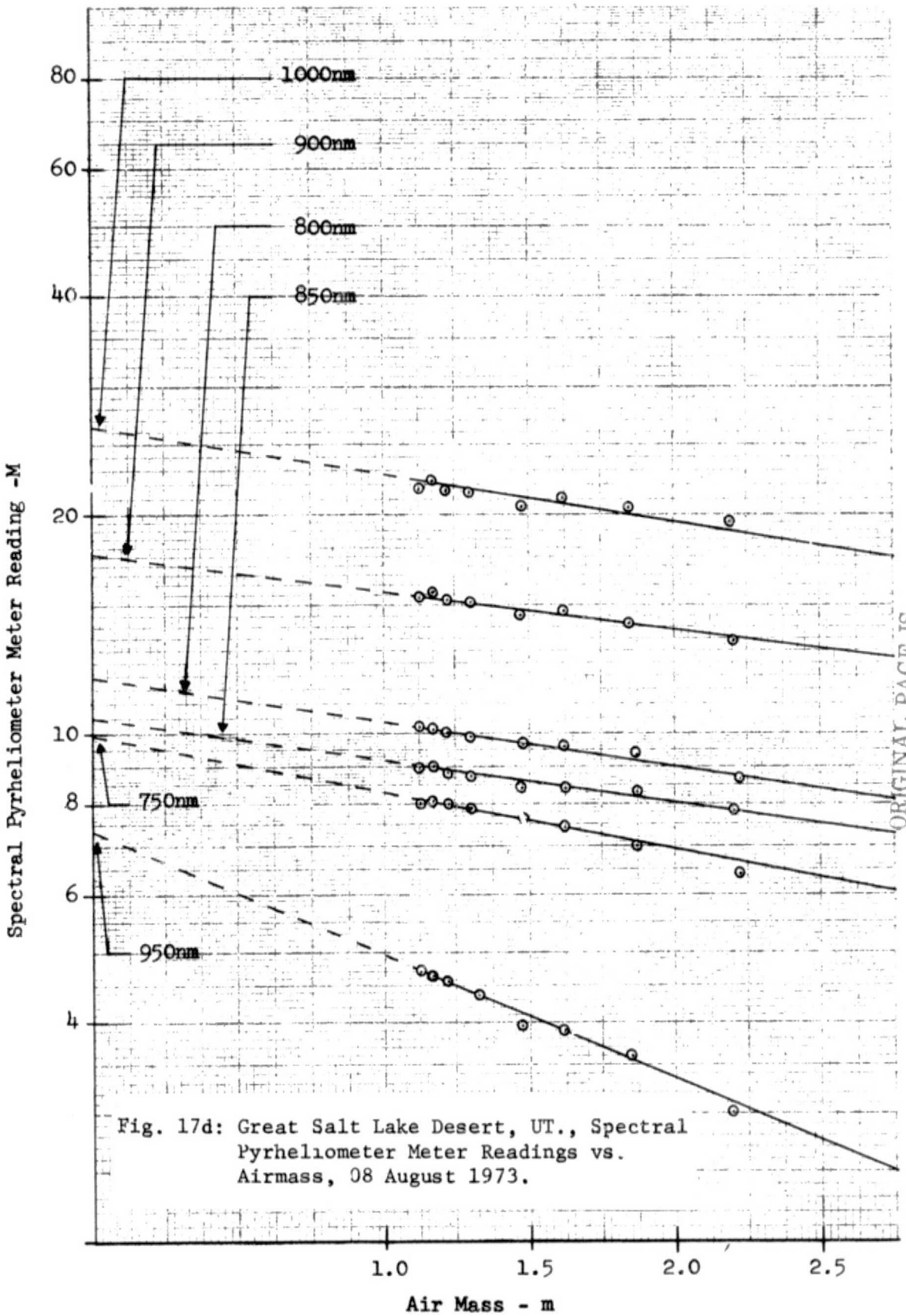

Fig. 17d: Great Salt Lake Desert, UT., Spectral Pyrheliometer Meter Readings vs. Airmass, 08 August 1973.

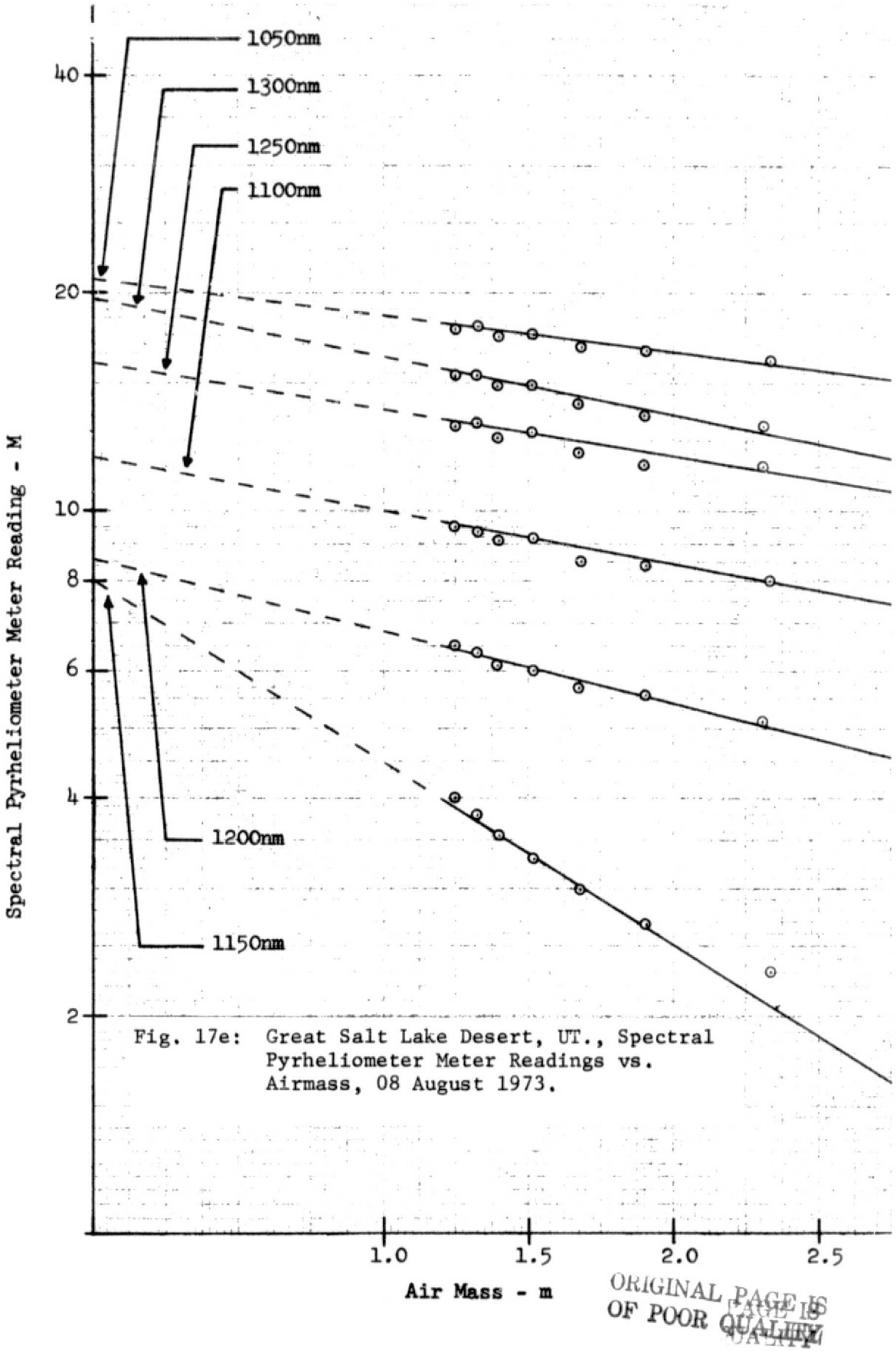

Fig. 17e: Great Salt Lake Desert, UT., Spectral Pyrheliometer Meter Readings vs. Airmass, 08 August 1973.

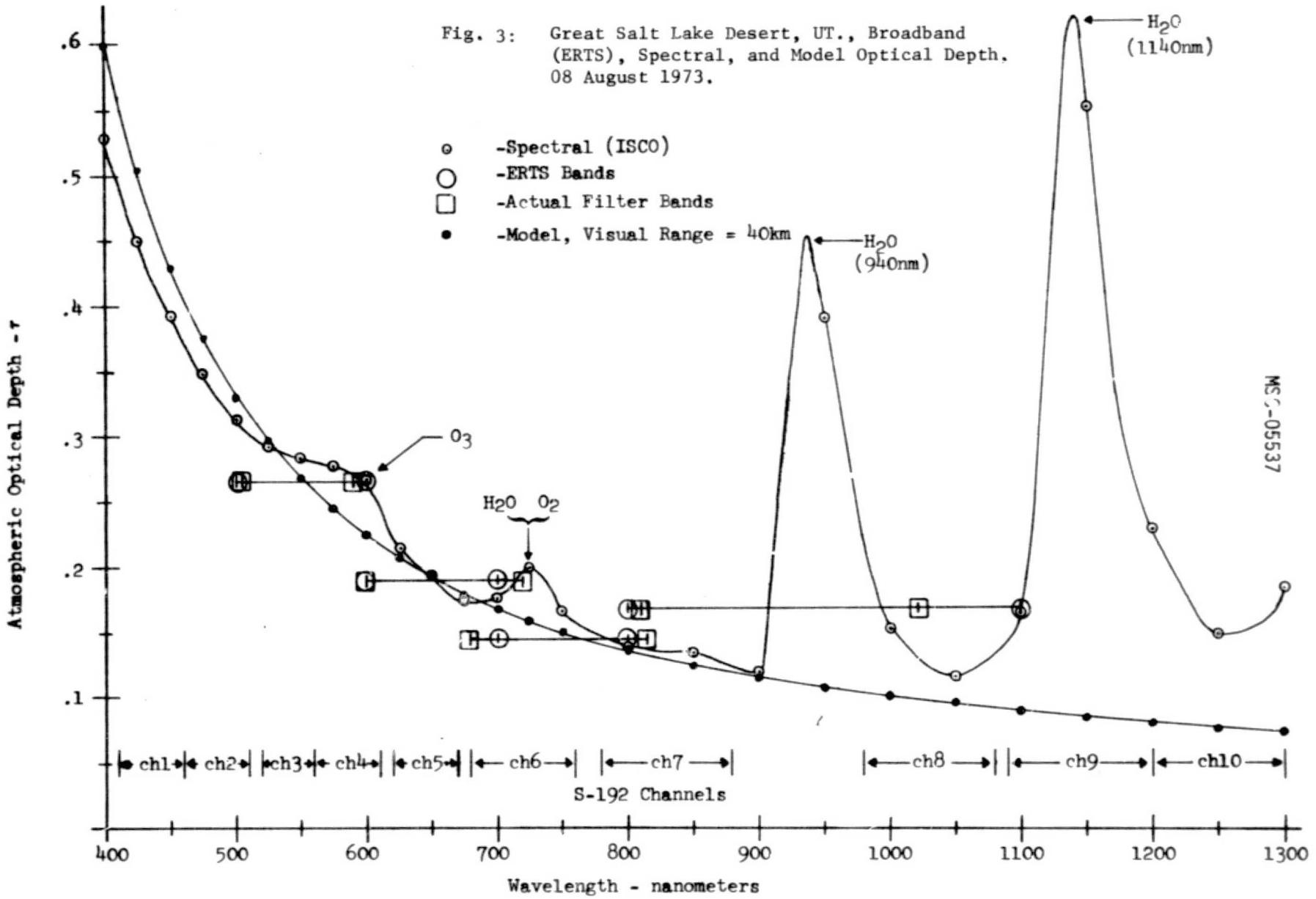
Fig. 3: Great Salt Lake Desert, UT., Broadband (ERTS), Spectral, and Model Optical Depth. 08 August 1973.
-Spectral (ISCO)
-ERTS Bands
-Actual Filter Bands
-Model, Visual Range = 40km
H2O (1140nm)
H2O (940nm)
O3
H2O O2
Atmospheric Optical Depth - τ
.6
.5
.4
.3
.2
.1
ch1
ch2
ch3
ch4
ch5
ch6
ch7
ch8
ch9
ch10
S-192 Channels
400
500
600
700
800
900
1000
1100
1200
1300
Wavelength - nanometers
MSC-05537

Ranges 2 to 13 Km", AFCRL-70-0200. The methods of applying these optical depths will be discussed in a following section, 3.2.2.6. Shown in Figure 18, are some of the related atmospheric relationships to optical depth, i.e., water vapor, ozone, and oxygen absorptions. The model does not take such absorptions into account. It applies only to molecular scattering and aerosol scattering components of the optical depth. Molecular scattering (Rayleigh) accounts for the rapid decrease in optical depth as wavelength increases (a $1/\lambda^4$ relationship), while aerosol scattering dominates the longer wavelengths (about 750 to 1300 nm).

3.2.2.5 Target Reflectivity and Radiance at Ground Level - Two types of targets existed in the general area shown in Figure 11. One type was a wet mud, low albedo area, while the other was a dry, high albedo area. All other areas appeared to be combinations of these two types. The dry area had very fine, precipitated, salt dust overlaying a dry, hard, mud flat surface.

Two methods of determining the target radiance were used. The first method involved simply pointing at the vertical (normal to the surface), the Bendix R.P.M.I. (equipped with the 7° F.O.V. collimator tube) and measuring the radiance directly; this target radiance will be referred to as N_g (meas.). These measurements were made in a two hour period immediately following EREP overpass, which was at 1001 local time - MDT. In order to normalize measurements made of target radiance, made at times other than overpass, the following equations were used:

$$N_g = \frac{H\rho}{\pi} \qquad (7)$$

where N_t is the targer radiance, H is the total amount of solar radiation and ρ is the target reflectivity. From Equation 7 it can be seen that,

$$\frac{N_g\ (1)}{N_g\ (2)} = \frac{H\ (1)}{H\ (2)} \qquad (8)$$

where N_g (1) and H (1) are target radiance and total solar radiation at a given time (1); N_g (2) and H (2) are the corresponding parameters at some other time (2). Hence, letting N_g (1) and H (1) be the desired parameters at overpass time,

$$N_g (1) = N_g (2) * \left(H (1)/_{H (2)}\right) \qquad (9)$$

the normalizing factor is then $H (1)/_{H (2)}$. Due to the fact that the total solar radiation measurements were not always made, due to a higher priority task of measuring the direct solar beam, the $H (1)/_{H (2)}$ normalization factor could not always be used. Instead, because the direct horizontal solar radiation makes up about 90 to 97% of the total solar radiation (shown in Table 8), the following normalization factor was used

$$\frac{H (1)}{H (2)} \approx \frac{I_1 \text{ Cos } \Theta_o (1)}{I_2 \text{ Cos } \Theta_o (2)} \qquad (10)$$

where I_1 and I_2 are the direct solar beam measurements and Cos Θ_o (1) and Cos Θ_o (2) are the respective cosines of the solar zenigh angle. The data for deriving the normalization factors for the 08 August mission are shown in Figure 19. Also shown are the corresponding total solar radiation measurements. As can be seen, the slopes of the I Cos Θ_o curves are in good agreement with the total solar measurements; hence, for the times near overpass, the I Cos Θ_o factors should be accurate for deriving target radiance at overpass.

The second method of determining target radiance was by measuring the total amount of solar radiation, H, and the target reflectivity (discussed later), and using Equation 7 to calculate the target radiance. The results obtained with this method will be referred to as N_t (calc.).

The results of both methods of determining target

radiance, at ground level, are shown in Table 9. A comparison of N(g) meas./N(g) calc. reveals that the directly measured radiances are consistently and significantly higher than the calculated values. In addition, this variance seems to depend strongly upon target reflectivity. A candidate explanation is the possibility that the collimator tube, having no baffles, collects stray radiance from areas other than the field of view for which it is calibrated (see Appendix). This was checked out in the laboratory and similar results were obtained (see Appendix). However, the nature and magnitude of this collimator radiance depends specifically upon the nature of the target's reflectivity, specifically bi-directional reflectance properties, and viewing conditions. The targets and conditions for the other sites measured in this report (Katherine Playa, NM, and a repeat of Great Salt Lake Desert), were similar to the dry target case (see Table 9). Therefore, the measured target radiances were adjusted for collimator radiance, using the factors shown for N_{meas}/N_{calc} - dry target in Table 9. Shown in Figure 20 is the derived target radiance (average of $N_{meas.}$ and $N_{calc.}$), with the appropriate correction factors for collimator radiance. Shown in Figure 21 and listed in Table 9, are the ratios of wet to dry target radiances. These give an indication of contrast between the two types of targets. As can be seen, the highest contrast exists .n the visible wavelengths, and diminishes somewhat in the near infrared.

Target reflectivities, both dry and wet areas were measured with the Bendix R.P.M.I. by viewing standard reflectance cards along with the target. The reflectivity of the target is determined by comparing the meter readings of the R.P.M.I. when viewing the target, "gray", and "white" cards as shown in Figures 22 and 23. The resultant target reflectivities

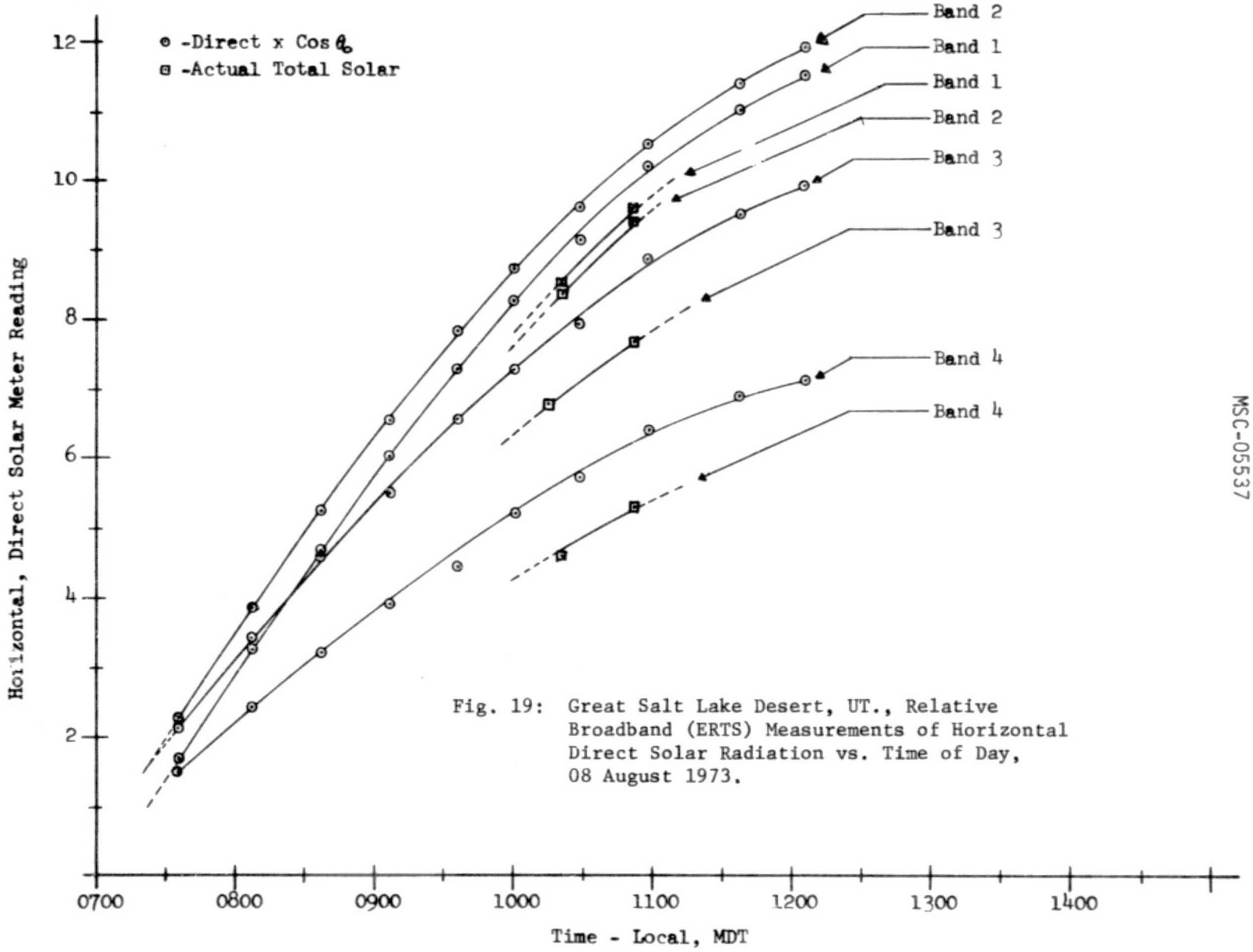

Fig. 19: Great Salt Lake Desert, UT., Relative Broadband (ERTS) Measurements of Horizontal Direct Solar Radiation vs. Time of Day, 08 August 1973.

MSC-05537

Great Salt Lake Desert (08/08/73) Target Radiance - Ground Level

Band	Nt(g) calc.		Nt(g) meas.		Avg.		N_{meas}/N_{calc}		Ratio-Wet/Dry
	Wet	Dry	Wet	Dry	Wet	Dry	Wet	Dry	
B1	7.79	12.17	8.27	13.68	8.03	12.92	1.06	1.12	.622
B1R	6.48	10.12	6.86	11.36	6.67	10.74	1.06	1.12	.621
B2	7.63	10.95	8.14	12.18	7.88	11.56	1.07	1.11	.682
B2R	9.53	13.68	10.12	15.15	9.82	14.41	1.06	1.11	.681
B3	7.22	9.80	7.32	10.75	7.27	10.28	1.01	1.10	.707
B3R	9.71	13.18	10.16	14.92	9.94	14.05	1.05	1.13	.707
B4	15.58	20.62	15.80	22.00	15.69	21.31	1.01	1.07	.736
B4R	11.02	14.59	11.72	16.32	11.37	15.46	1.06	1.12	.735

Table 9: Great Salt Lake Desert, UT., Target Radiance at Ground Level, 08 August 1973.

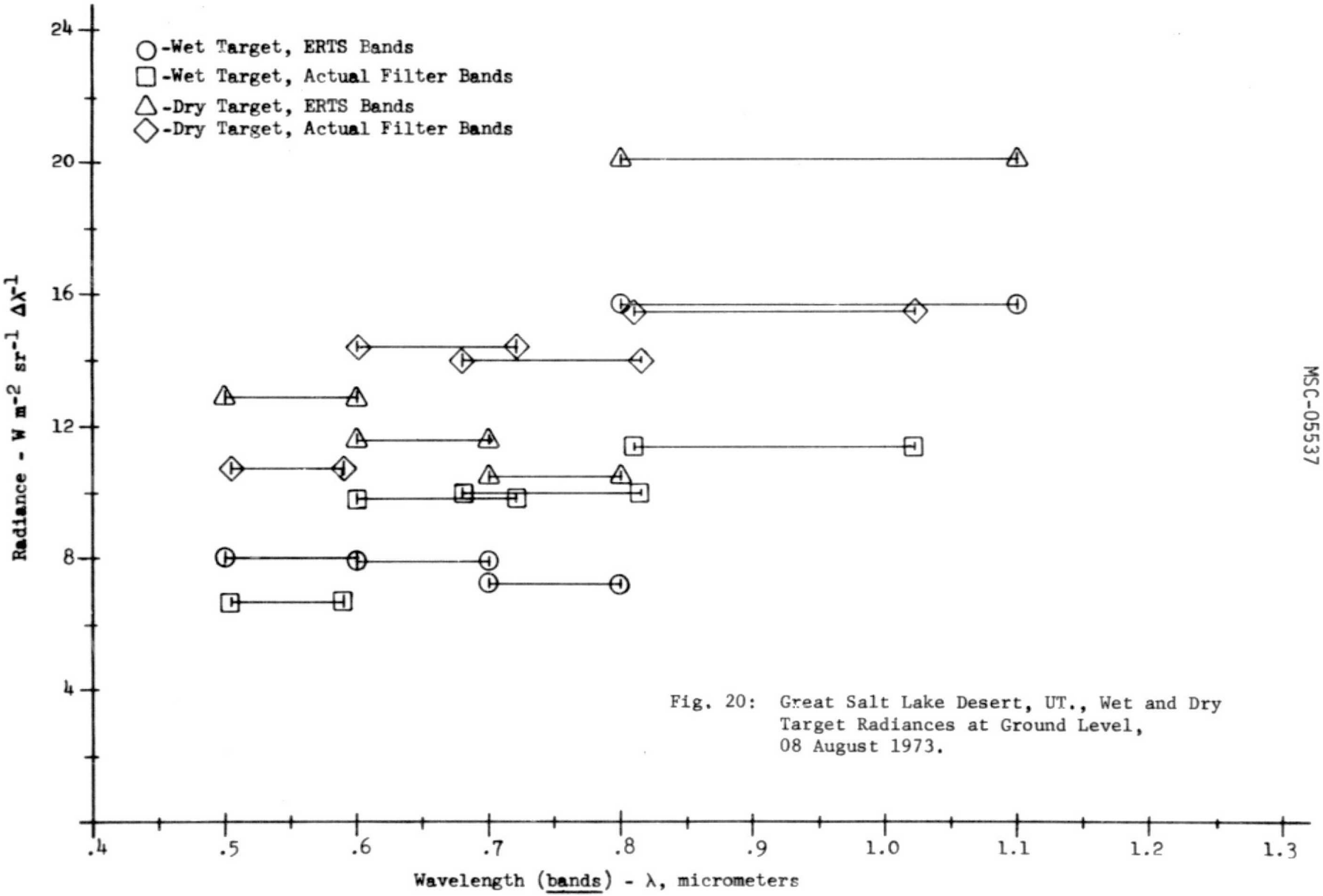

Fig. 20: Great Salt Lake Desert, UT., Wet and Dry Target Radiances at Ground Level, 08 August 1973.

MSC-05537

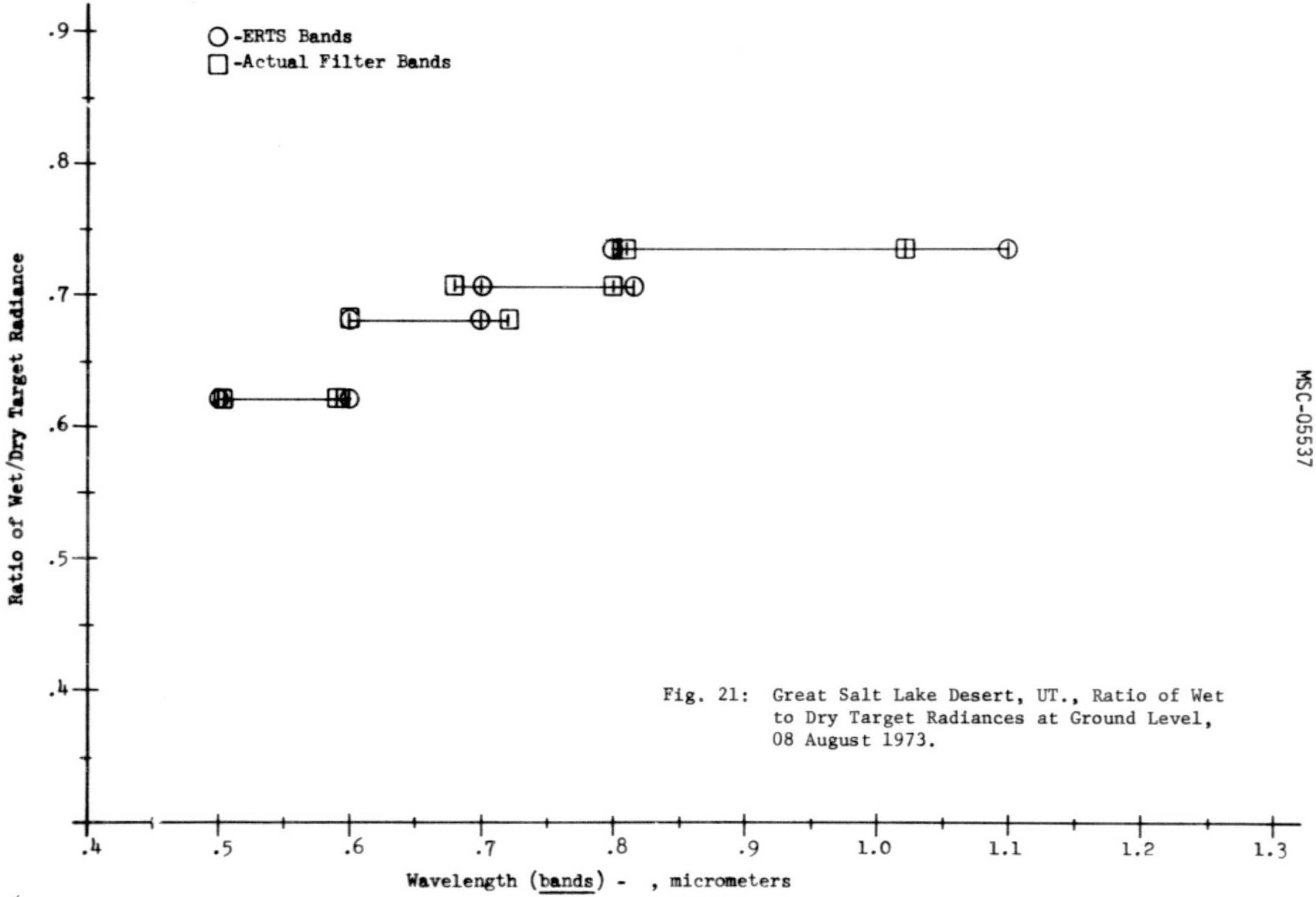

Fig. 21: Great Salt Lake Desert, UT., Ratio of Wet to Dry Target Radiances at Ground Level, 08 August 1973.

MSC-05537

Fig. 22: Great Salt Lake Desert, UT, Determination of Dry Target Reflectivity Using Cards, 08 August 1973.

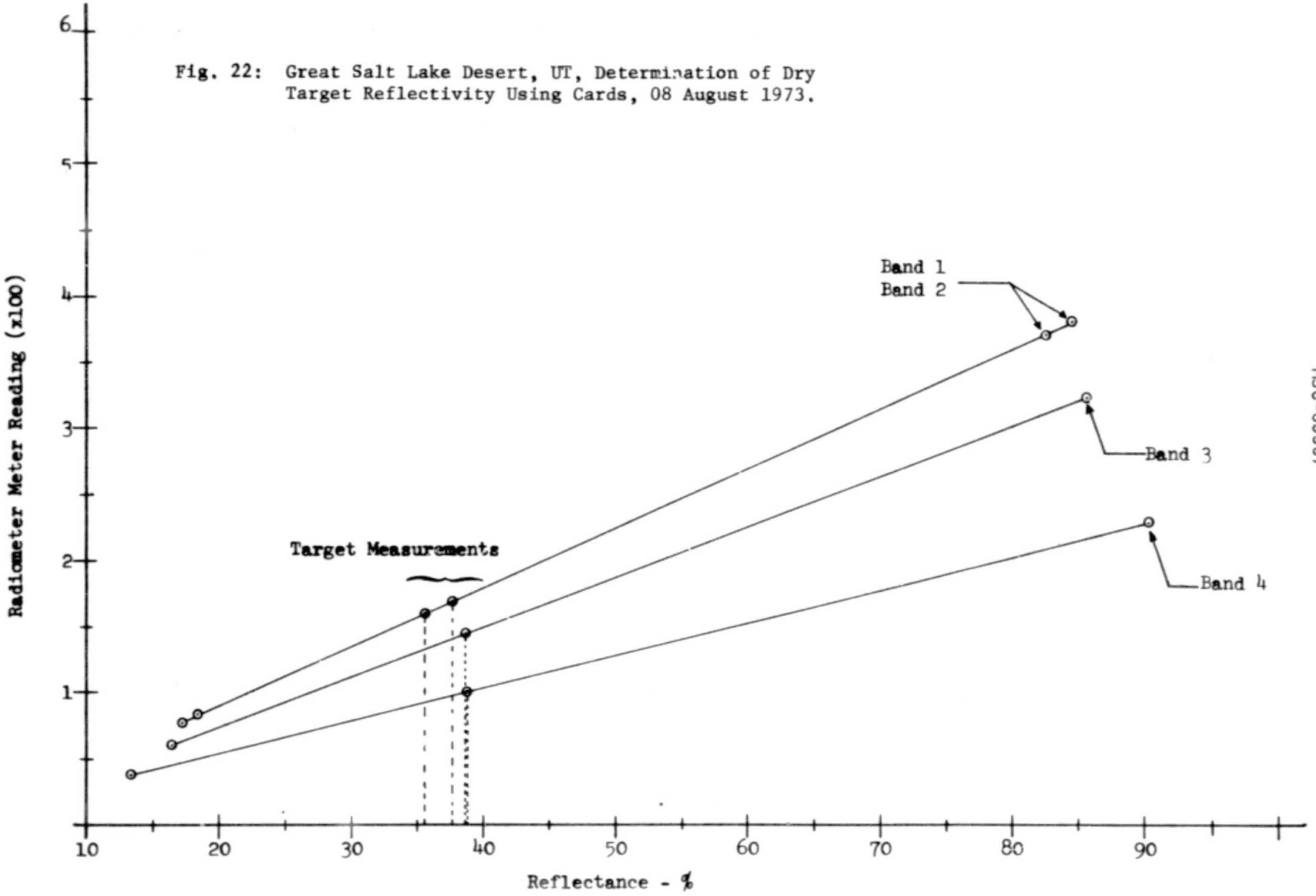

MSC-05537

Fig. 23: Great Salt Lake Desert, UT, Determination of Wet Target Reflectivity Using Cards, 08 August 1973.

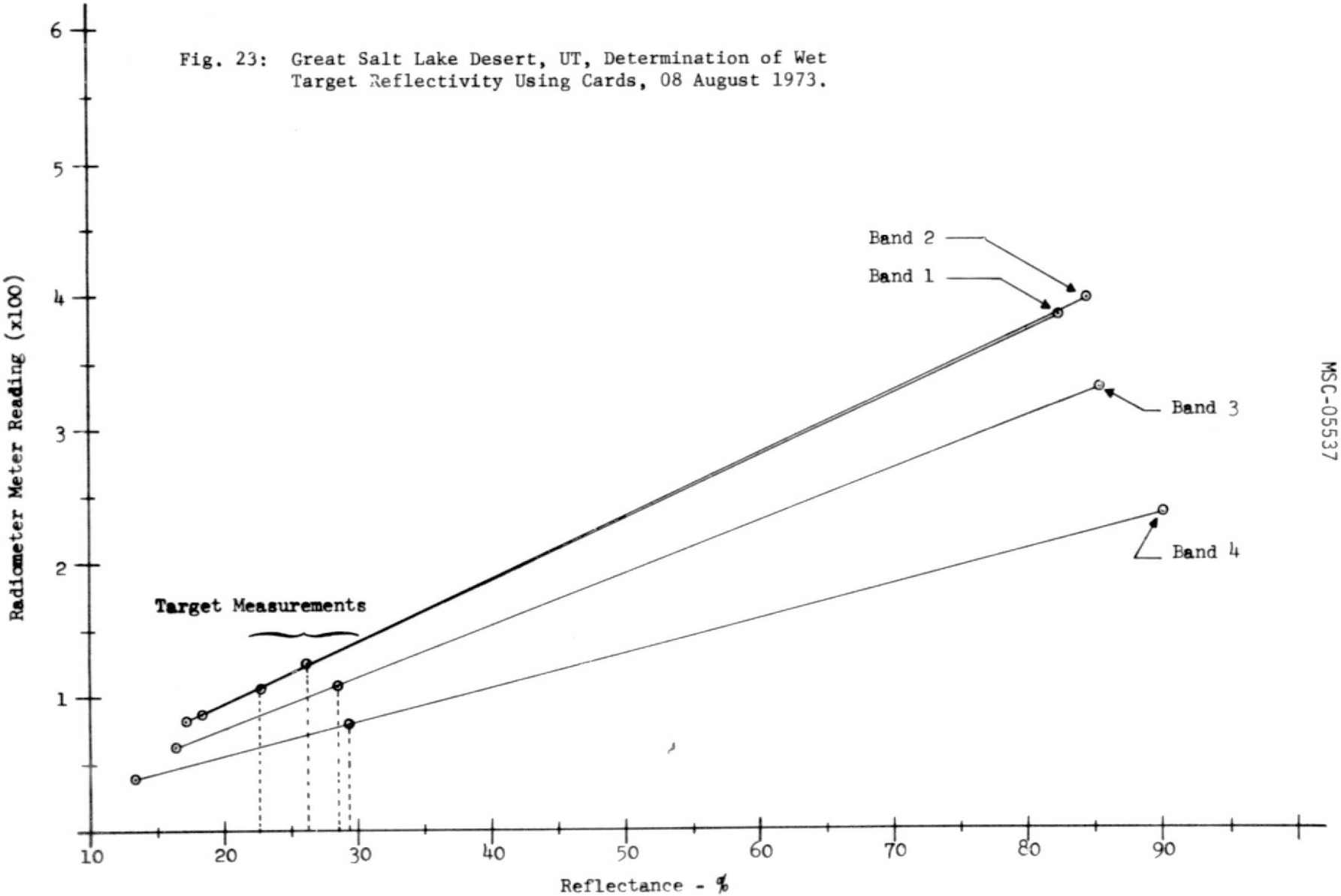

MSC-05537

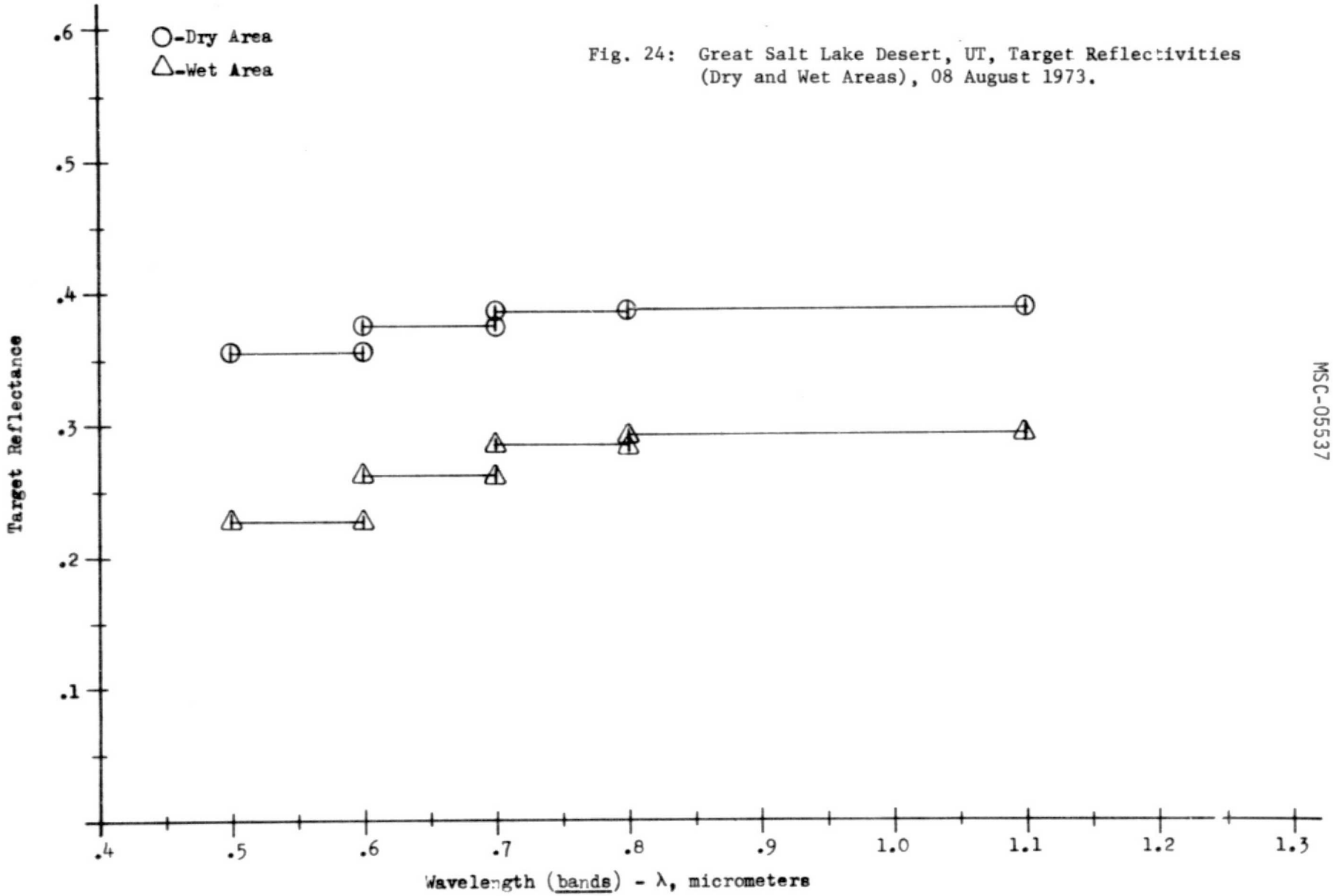

Fig. 24: Great Salt Lake Desert, UT, Target Reflectivities (Dry and Wet Areas), 08 August 1973.

MSC-05537

are shown in Figure 24 and listed in Table 8.

3.2.2.6 Target Radiance at EREP - The apparent radiance of the ground target at the satellite sensor (N_s), Skylab-EREP, is made up of the directional target radiance - $N_t(d)$, and the atmospheric path radiance - N_a (often called "airlight", "haze-light", etc.). The directional target radiance can be given as

$$N_t(d) = N_t(g)\ T \qquad (11)$$

where $N_t(g)$ and T are the previously discussed (and measured) target radiance at ground level and atmospheric fractional transmittance. Hence $N_t(d)$ is calculated from actual ground-based measurements. The radiance at EREP is then

$$N_s = N_t(g)\ T + N_a \qquad (12)$$

No direct measurement of the atmospheric path radiance, N_a, can be made from ground-based instrumentation. The method used to obtain N_a, in this report, consists of combining the field measurements of optical depth and target reflectivity, with a radiative transfer computer program which calculates N_a. The computer program was originally developed by the Environmental Research Institute of Michigan and is reported in detail in "Studies of Spectral Discrimination", W. A. Malila, et. al., Report No. NASA CR-WRL 31650-22-T, Contract No. NAS9-9784, NASA Manned Spacecraft Center, Houston, Texas, May 1971. The required inputs to the program are (1) altitude of the sensor, (2) target reflectivity as a function of wavelength, (3) target background albedo as a function of wavelength, (4) solar zenith angle, (5) solar-sensor azimuth angle, (6) sensor scan angle (viewing angle), and (7) atmospheric visual range. The altitude of the sensor was input as 50 Km, which is equivalent to the outer extremity of the atmosphere. The target reflectivity was a measured input parameter, target background albedo was reasonably assumed to be

similar to an average of the measured target reflectivities (wet and dry areas), solar zenith and solar-sensor azimuth angles were available from EREP SKYBET data, sensor scan angle (viewing angle) was taken to be a nadir view. It was determined that for the EREP sensors scan angles of 0 to 5°, varying the sensor scan angle (from 0 to 5°) had little effect on the resultant radiance at EREP. The atmospheric visual range (visibility) is that distance at which the contrast between a dark object and the surrounding sky is about 2%, which allows it to be discernible. In practice, it is nearly impossible to make such a measurement with any degree of confidence or accuracy. Instead, the measured atmospheric optical depth was used to quantitatively select a visual range model that agreed with the field measurements of same. As can be seen in Figure 18, 35, and 54, this technique was successful and provided an accurate input of the derived visual range to the computer program. Having all the above inputs directly determined from or based on actual field measurements, the computer program then calculated the corresponding atmospheric path radiance. The resultant path radiances, integrated for the Bendix R.P.M.I. bands are shown in Figure 25. The resultant target radiances at EREP ($N_t(g) + N_a$) are shown in Figures 26 and 27, and all parameters are listed in Table 10. Near the bottom of Table 10 are the collimator radiance factors to be multiplied by the values listed under N_s in order to correct the readings for the influence of collimator radiance.

A discussion of the possible errors associated with the above methods of determining $N_t(g)$, $N_t(d)$, N_a, and N_s is given in the Appendix.

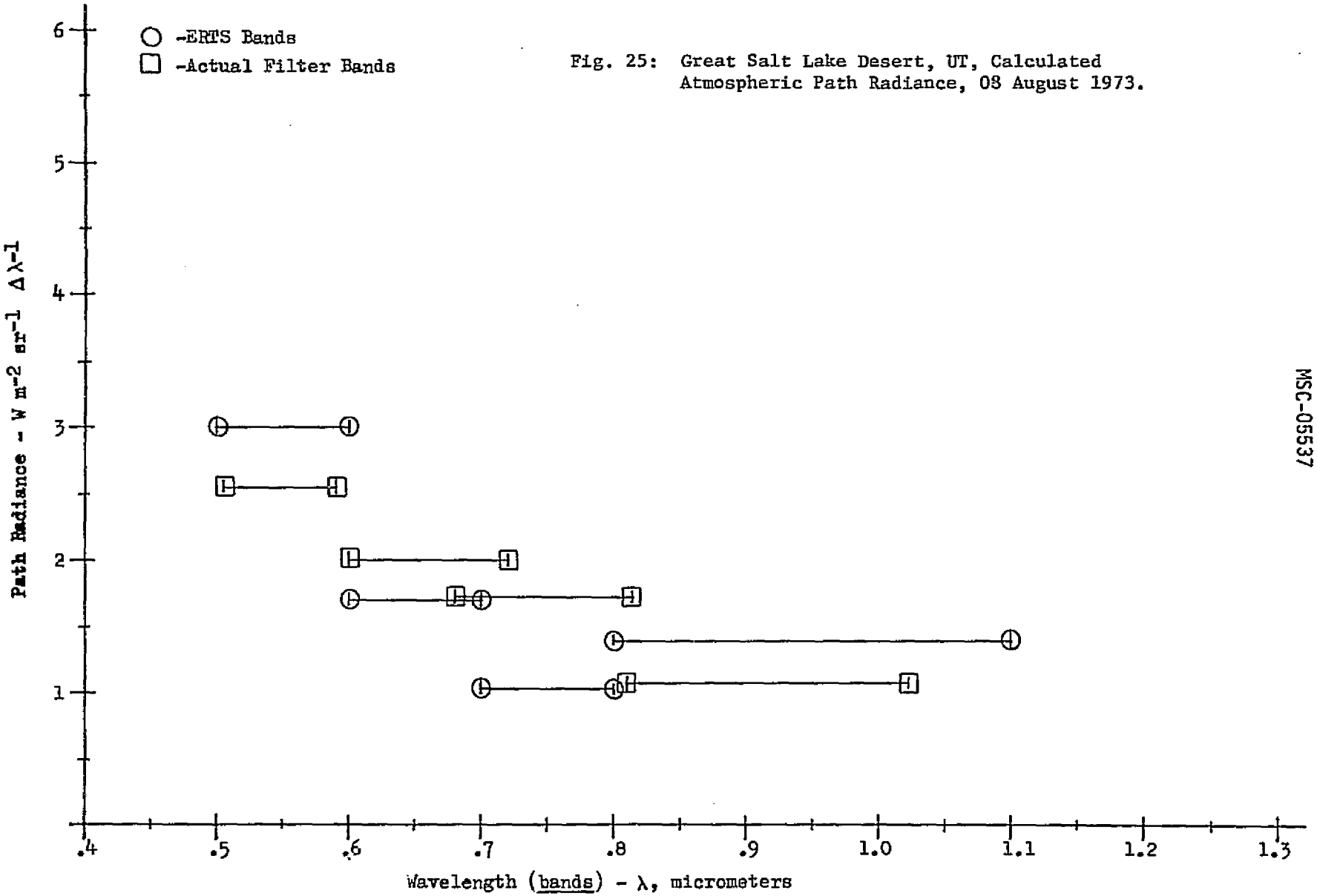

Fig. 25: Great Salt Lake Desert, UT, Calculated Atmospheric Path Radiance, 08 August 1973.

MSC-05537

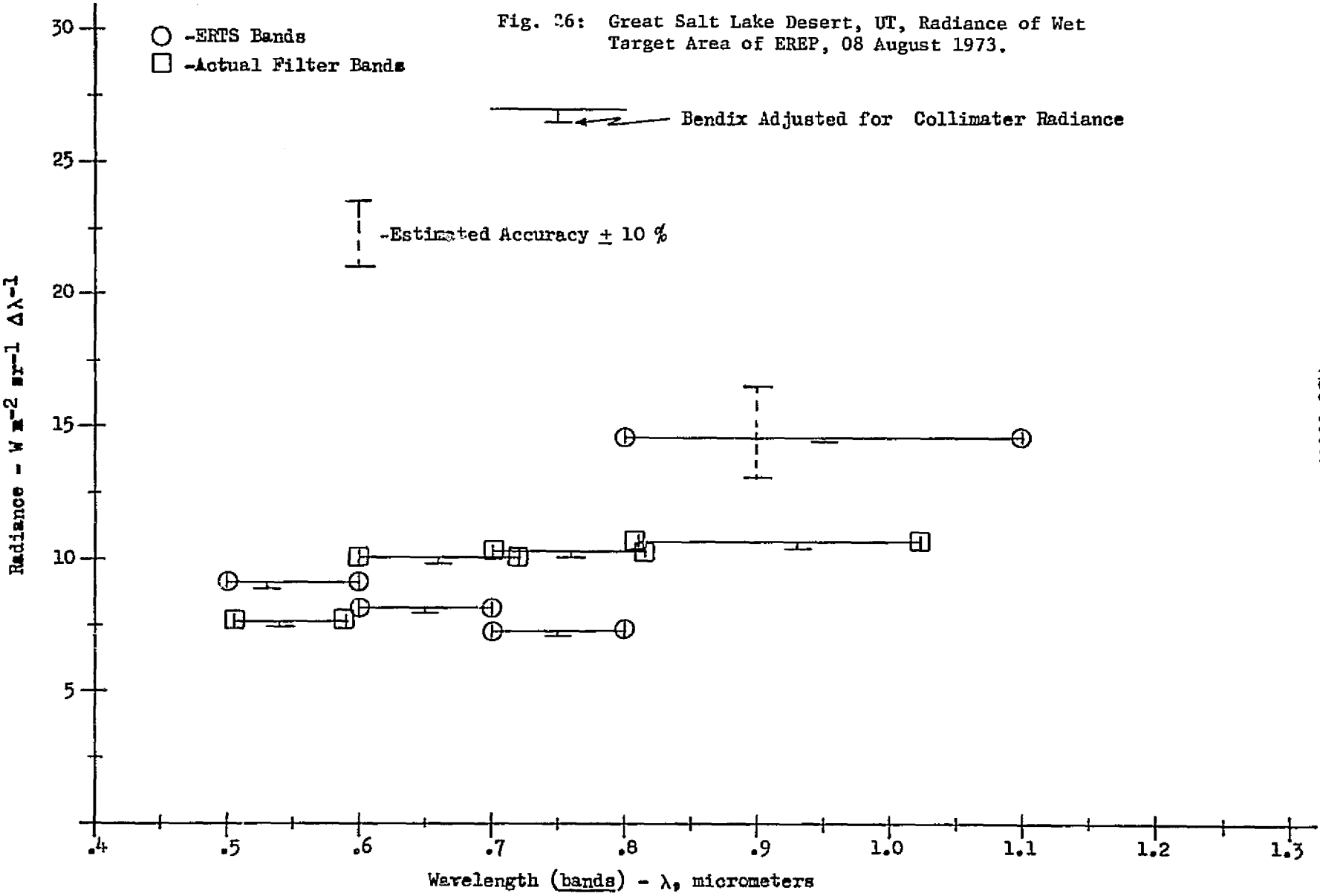

Fig. 36: Great Salt Lake Desert, UT, Radiance of Wet Target Area of EREP, 08 August 1973.

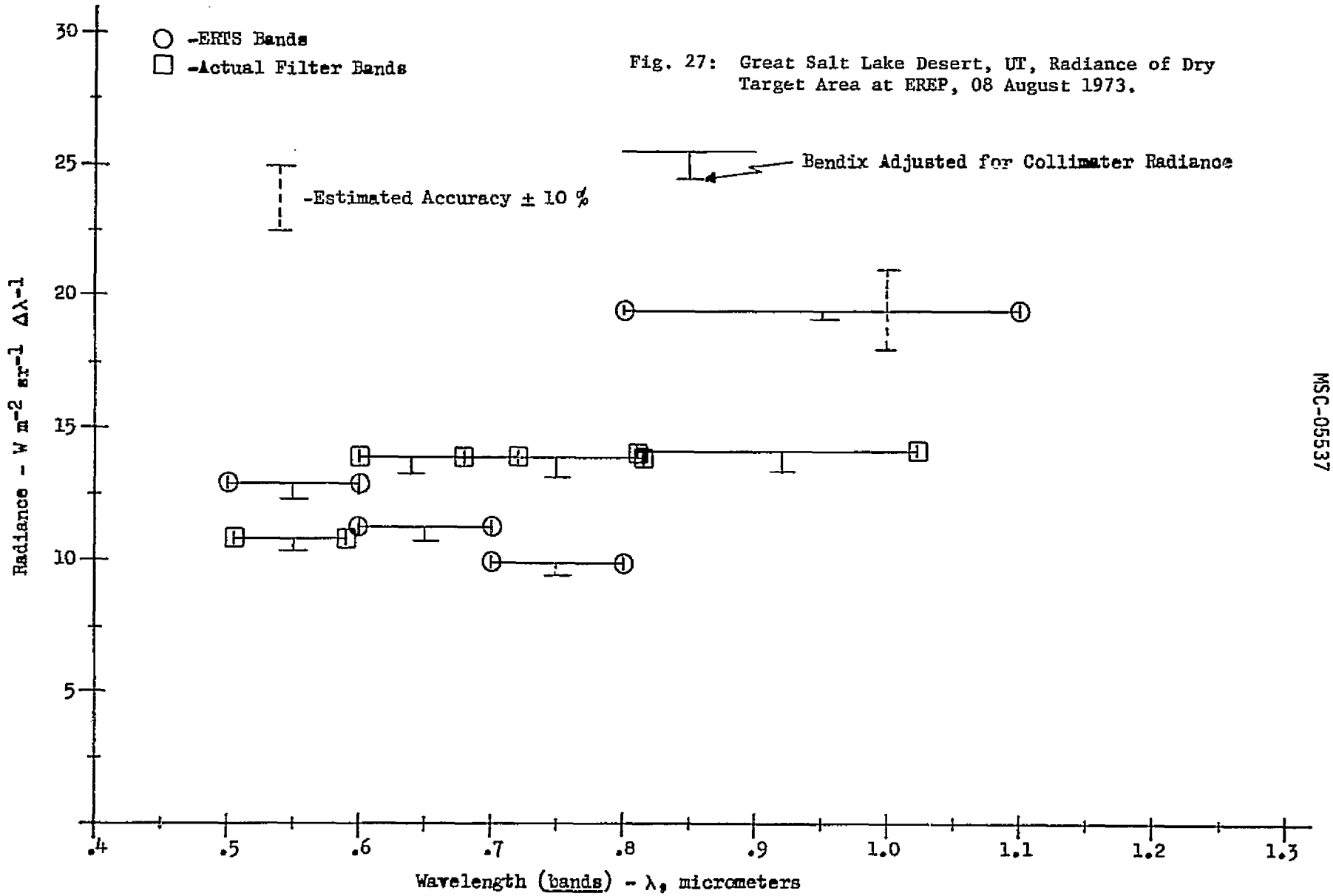

Fig. 27: Great Salt Lake Desert, UT, Radiance of Dry Target Area at EREP, 08 August 1973.

MSC-05537

Great Salt Lake Desert (08/08/73) Atmospheric and Target Radiance

BAND	Optical depth (τ)	Transmittance (T)	$N_t(g)$		$N_t(d)$		N_a	N_s	
			Wet	Dry	Wet	Dry		Wet	Dry
B1	.266	.766	8.03	12.92	6.15	9.90	3.01	9.16	12.91
B1R	.266	.766	6.67	10.74	5.11	8.23	2.56	7.67	10.79
B2	.191	.826	7.88	11.56	6.51	9.55	1.70	8.21	11.25
B2R	.191	.826	9.82	14.41	8.11	11.90	2.00	10.11	13.90
B3	.145	.865	7.27	10.28	6.29	8.89	1.02	7.31	9.91
B3R	.145	.865	9.94	14.05	8.60	12.15	1.72	10.32	13.87
B4	.167	.846	15.69	21.31	13.27	18.03	1.40	14.67	19.43
B4R	.167	.846	11.37	15.46	9.62	13.08	1.08	10.70	14.16

$N_t(g)$ = Target Radiance at Ground Level
$N_t(d)$ = Target Directional Radiance at EREP
N_a = Atmospheric Path Radiance
N_s = Radiance at EREP
$= \frac{\rho HT}{\pi} + N_a$

Bendix Adjusted for Collimater Radiance

Wet Target:	B1(.98)	B1R(.98)	Dry Target:	B1(.96)	B1R(.96)
	B2(.97)	B2R(.98)		B2(.95)	B2R(.96)
	B3(.99)	B3R(.98)		B3(.96)	B3R(.94)
	B4(.99)	B4R(.97)		B4(.99)	B4R(.95)

Table 10: Great Salt Lake Desert, UT, Atmospheric and Target Radiances at EREP, 08 August 1973.

3.2.3 *KATHERINE PLAYA, NEW MEXICO, 11 AUGUST 1973*

Site Coordinates:	32° 18" N. Latitude 108° 53" W. Longitude (See Figure 28)
EREP Pass:	Track 06, Pass No. 18, Rev. 1284/1285
Time of Overpass:	223:15:30:05 GMT 0930 Local Time (MDT)

3.2.3.1 General Conditions - Clear

3.2.3.2 Near Surface Meteorology - Dry bulb temperature = 25.7°, wet bulb temperature = 13.3°C, surface pressure (measured) = 657.4 mm of Hg, wind - none.

3.2.3.3 Total and Diffuse Solar Radiation - Total and diffuse solar radiation were measured with the previously mentioned, section 3.1,I.S.C.O. spectroradiometer. The spectral total solar radiation is shown in Figure 29 and listed in Table 11. The spectral diffuse solar radiation is shown in Figure 30 and is listed in Table 11. The ratio of diffuse to total solar radiation is shown in Figure 31 and is also listed in Table 11. Shown in Figure 32 is the nature of the broadband (.4 to 1.1 μm - 400 to 1100 nm) total solar radiation, discussed in detail in section 3.2.2.3.

3.2.3.4 Atmospheric Optical Depth/Transmittance - The field data, pyrheliometer meter readings vs. air mass, used for deriving atmospheric optical depth (described in detail in section 3.2.2.4) are shown in Figures 34 and 34a, 35b, 34c, 34d, and 34e. The resultant optical depths, broadband and spectral, are shown in Figure 35, along with the derived visual range model (27.1 Km). As can be seen, excellent agreement is obtained between the measured spectral (I.S.C.O.) and broadband (Bendix) and the model.

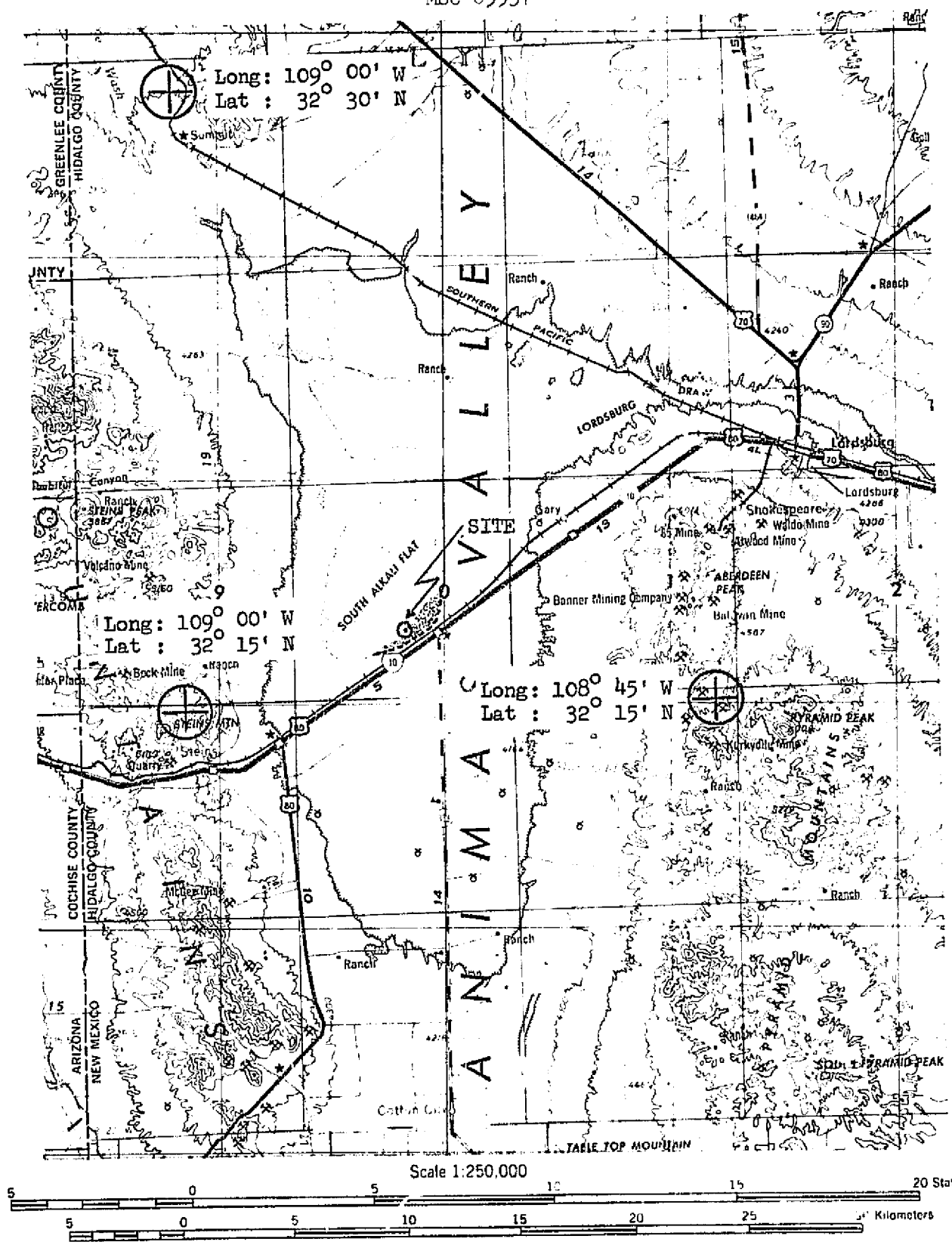

Fig. 28 Katherine Playa, NM, Location Map

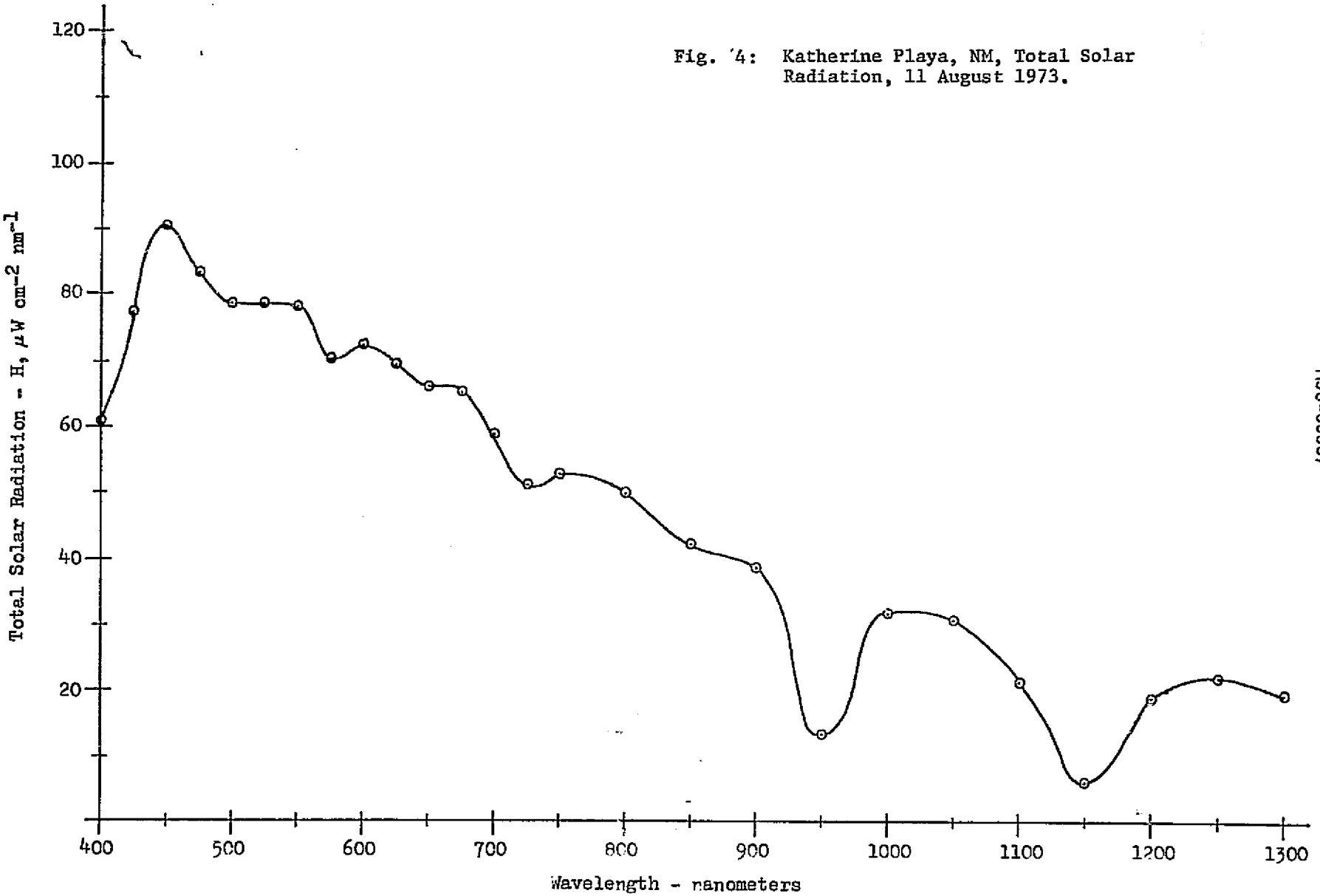

Fig. 4: Katherine Playa, NM, Total Solar Radiation, 11 August 1973.

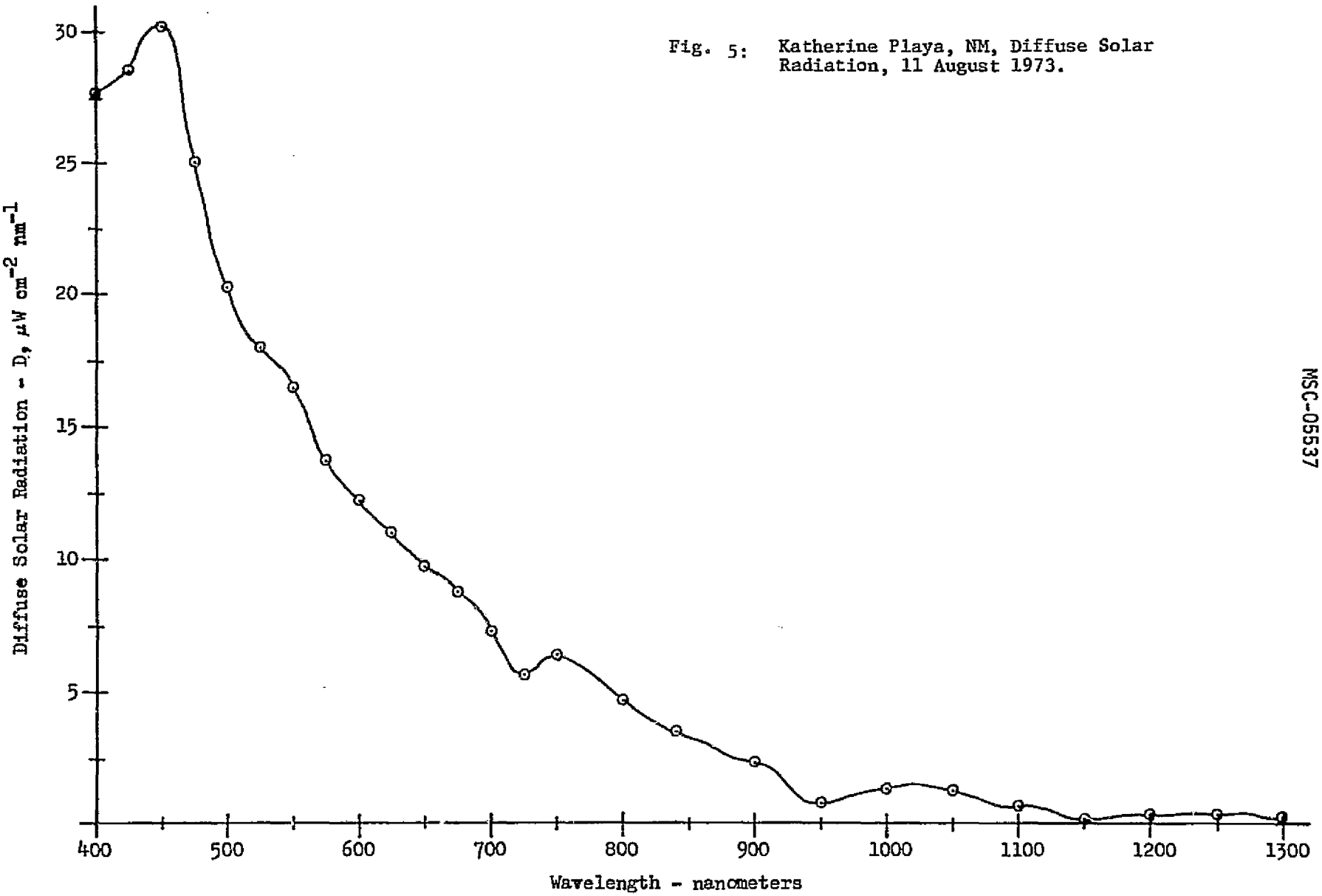

Fig. 5: Katherine Playa, NM, Diffuse Solar Radiation, 11 August 1973.

Fig. 6: Katherine Playa, NM, Ratio of Diffuse (D) to Total (H) Solar Radiation (D/H), 11 August 1973.

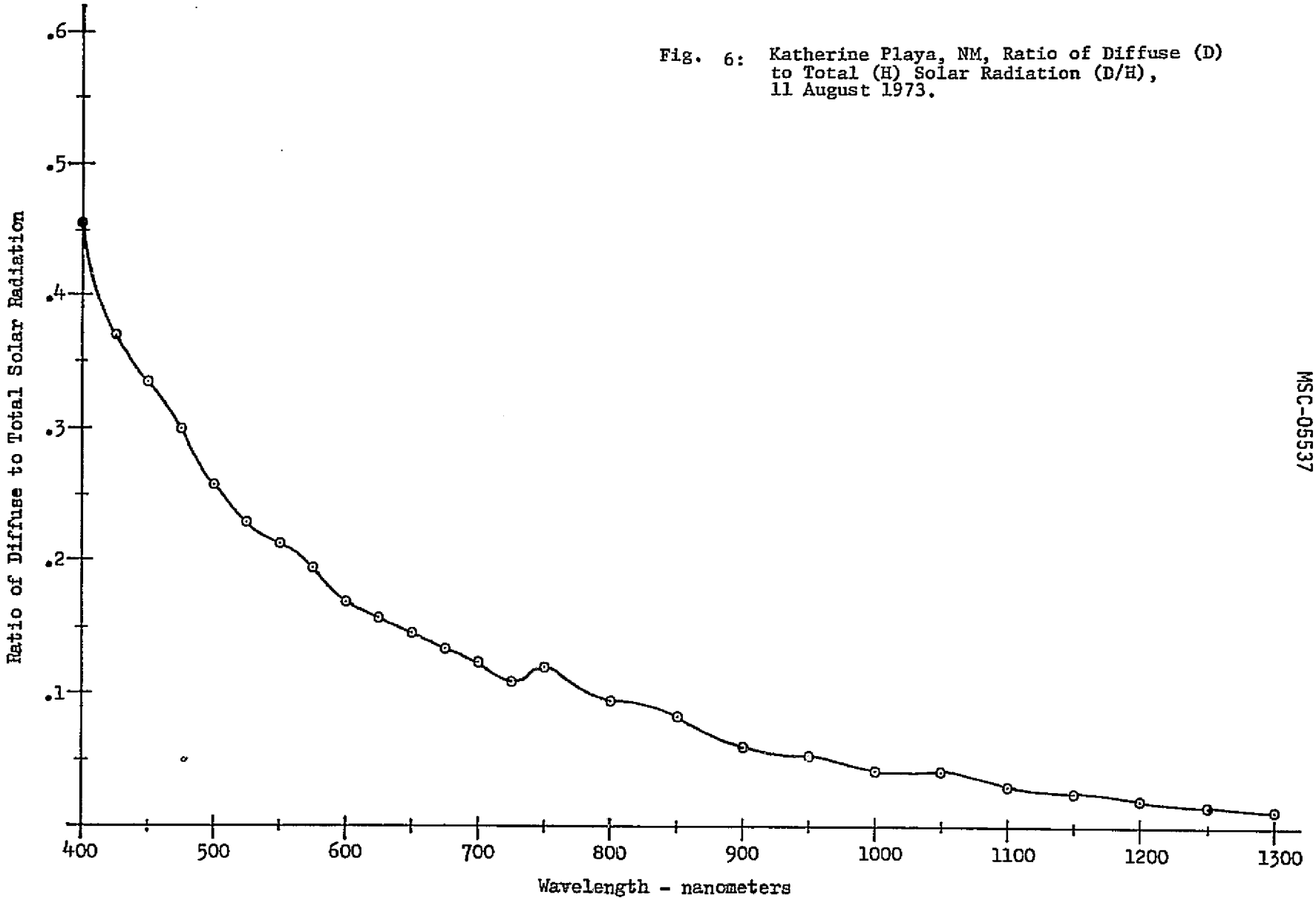

Katherine Playa (08/11/73) Total and Diffuse Solar Radiation

Wavelength (nm)	H *	D *	D/H
400	60.86	27.73	.456
425	77.35	28.54	.369
450	90.42	30.26	.335
475	83.39	24.98	.300
500	78.57	20.25	.258
525	78.57	17.96	.228
550	77.94	16.49	.212
575	70.32	13.73	.195
600	72.30	12.23	.169
625	69.95	11.04	.158
650	66.39	9.77	.147
675	65.52	8.80	.134
700	59.13	7.35	.124
725	51.29	5.67	.110
750	52.76	6.39	.121
800	49.78	4.71	.0950
850	42.30	3.52	.0832
900	39.09	2.35	.0601
950	13.78	.74	.0537
1000	32.00	1.36	.0425
1050	31.23	1.30	.0416
1100	21.56	.654	.0303
1150	6.19	.162	.0262
1200	19.35	.386	.0199
1250	21.99	.333	.0151
1300	19.65	.263	.0134

* microWatts (centimeter)$^{-2}$ (nanometer)$^{-1}$

Table 11: Katherine Playa, NM, Total and Diffuse Solar Radiation, 11 August 1973.

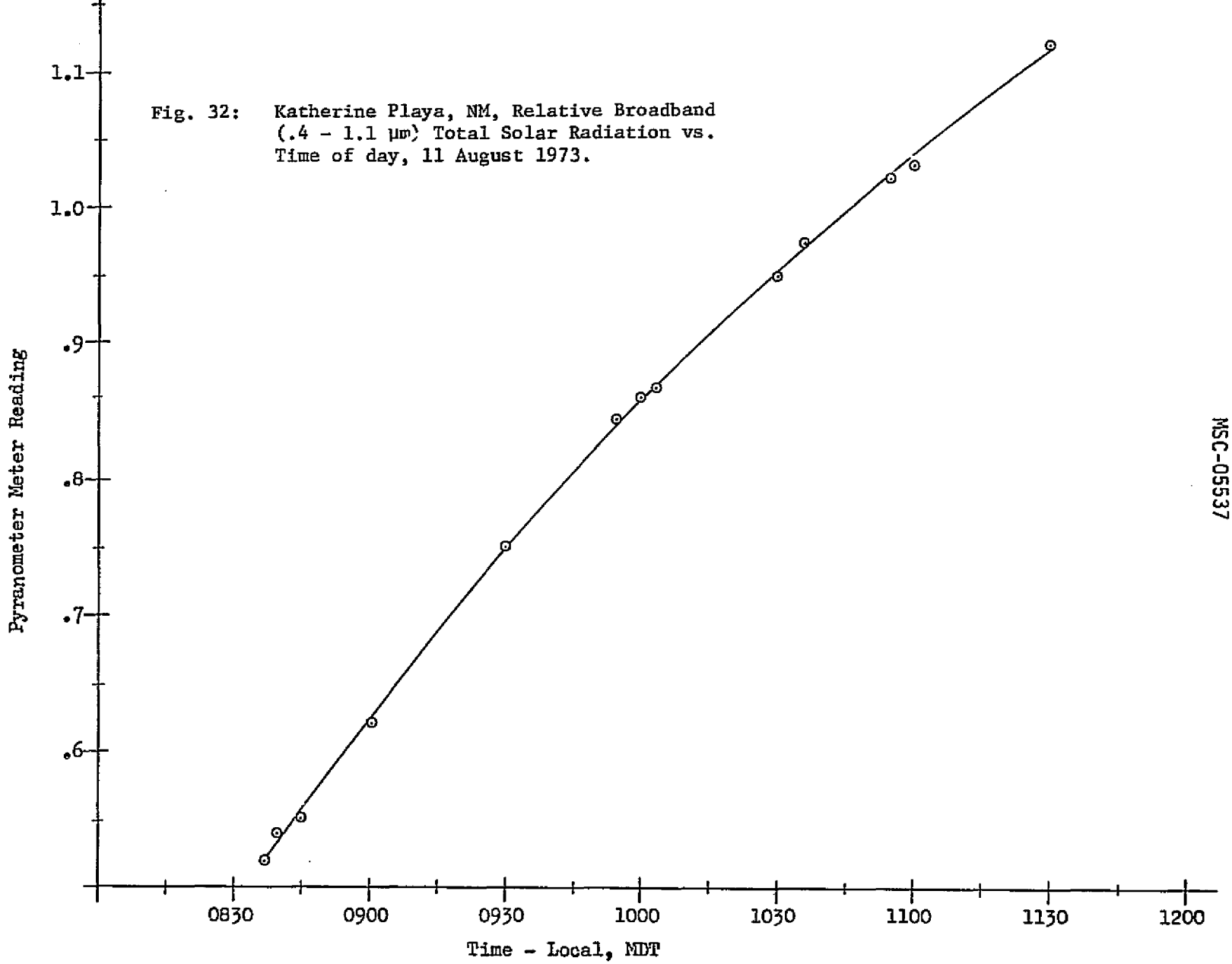

Fig. 32: Katherine Playa, NM, Relative Broadband (.4 - 1.1 μm) Total Solar Radiation vs. Time of day, 11 August 1973.

MSC-05537

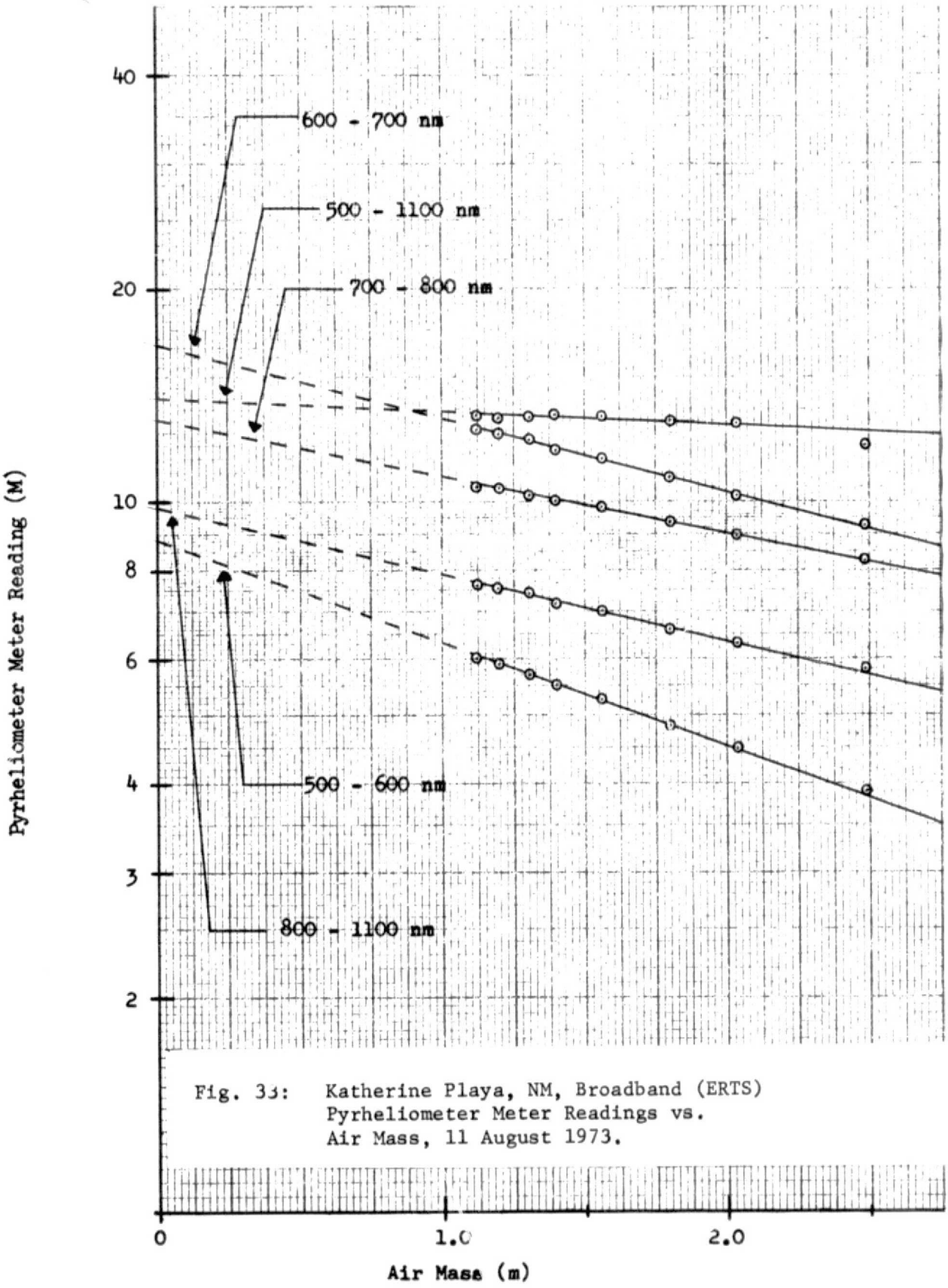

Fig. 33: Katherine Playa, NM, Broadband (ERTS) Pyrheliometer Meter Readings vs. Air Mass, 11 August 1973.

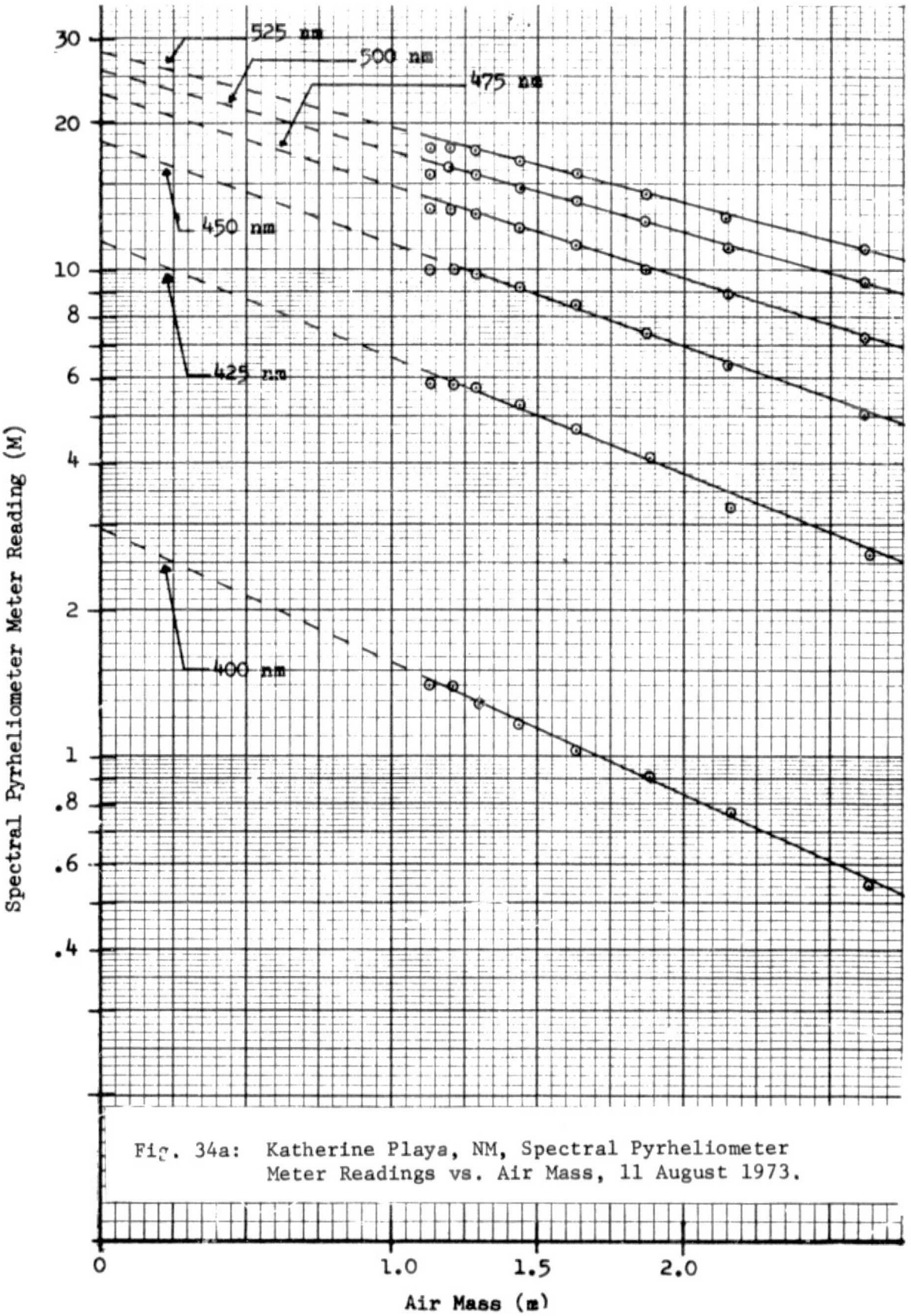

Fig. 34a: Katherine Playa, NM, Spectral Pyrheliometer Meter Readings vs. Air Mass, 11 August 1973.

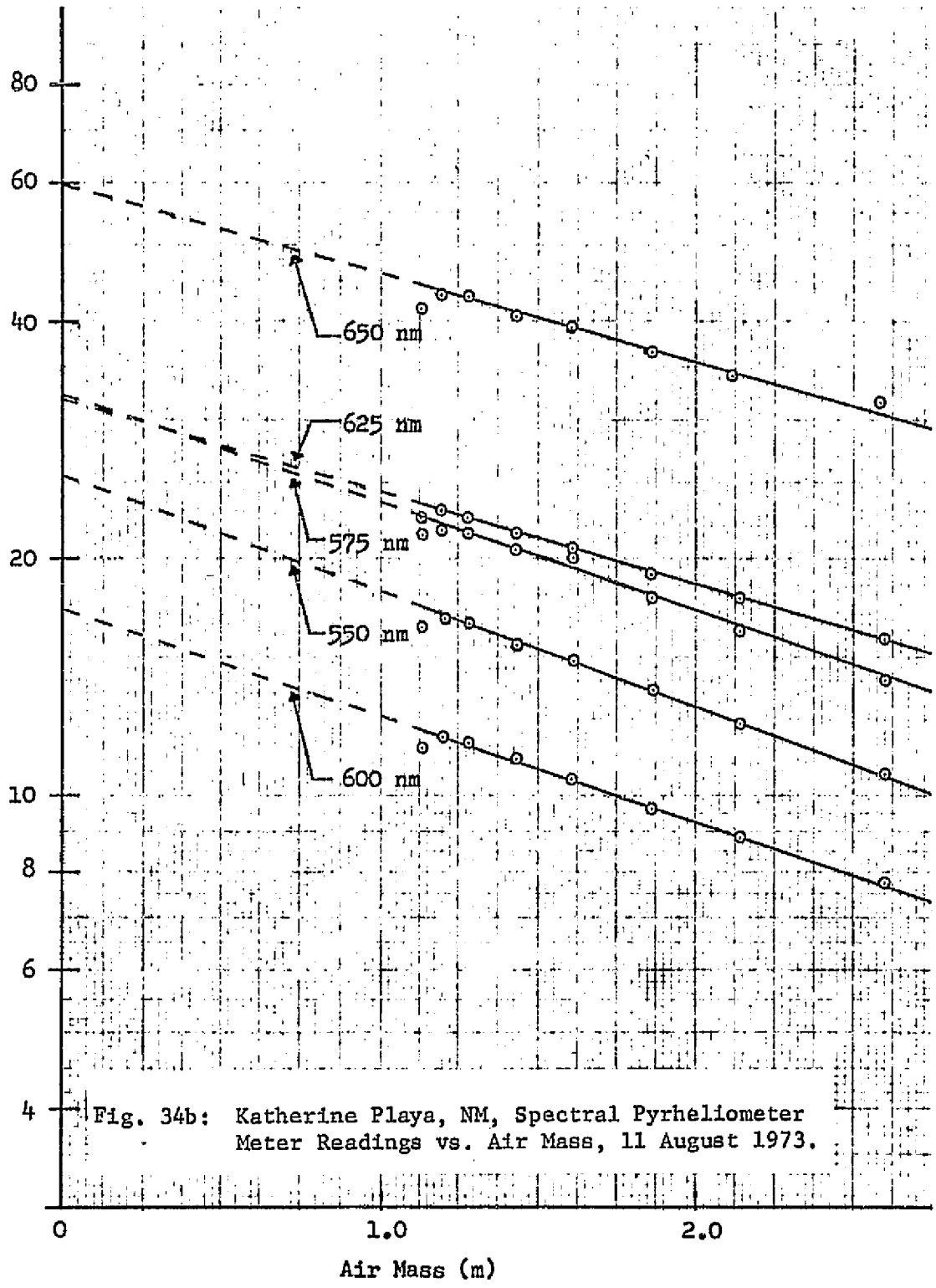

Fig. 34b: Katherine Playa, NM, Spectral Pyrheliometer Meter Readings vs. Air Mass, 11 August 1973.

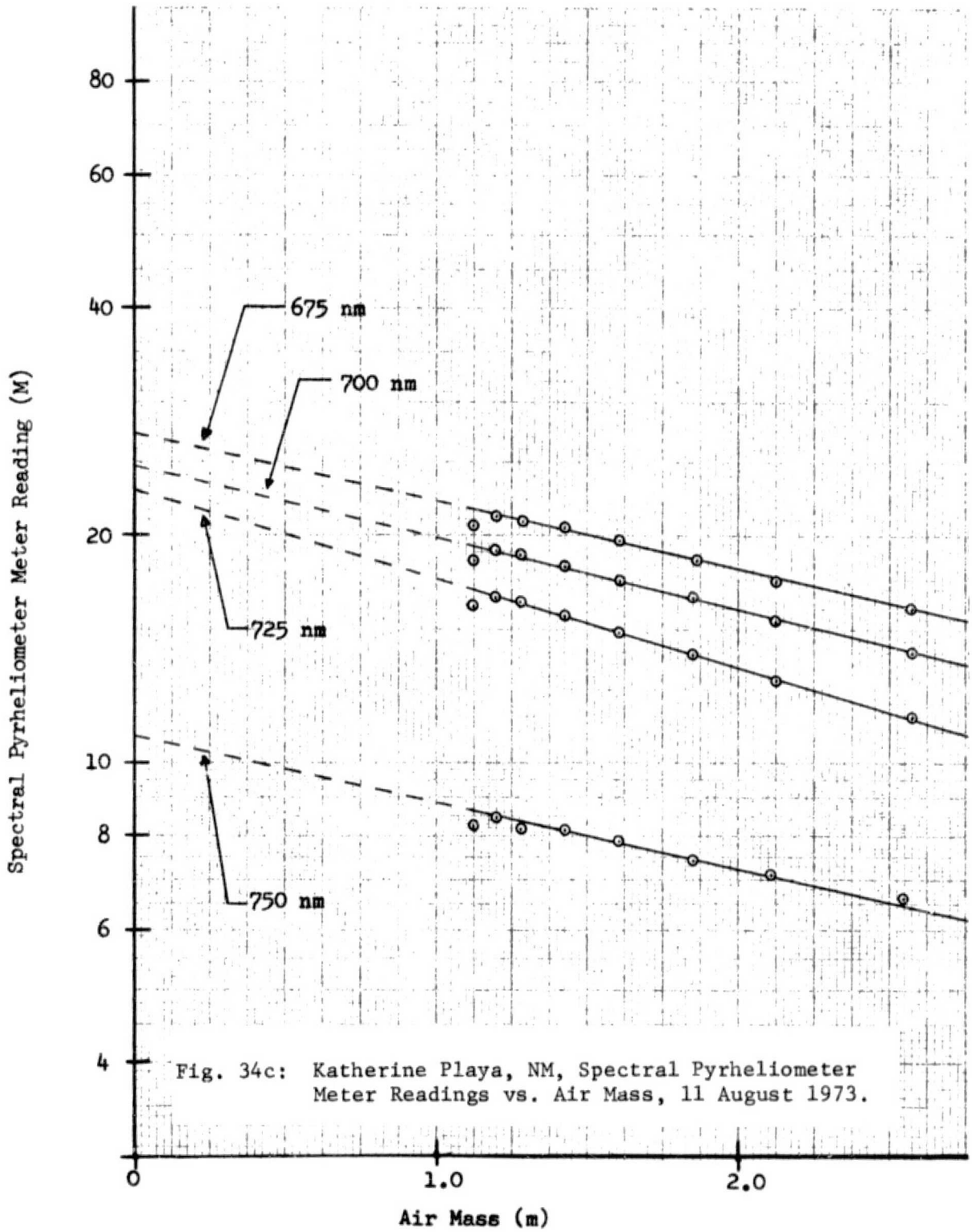

Fig. 34c: Katherine Playa, NM, Spectral Pyrheliometer Meter Readings vs. Air Mass, 11 August 1973.

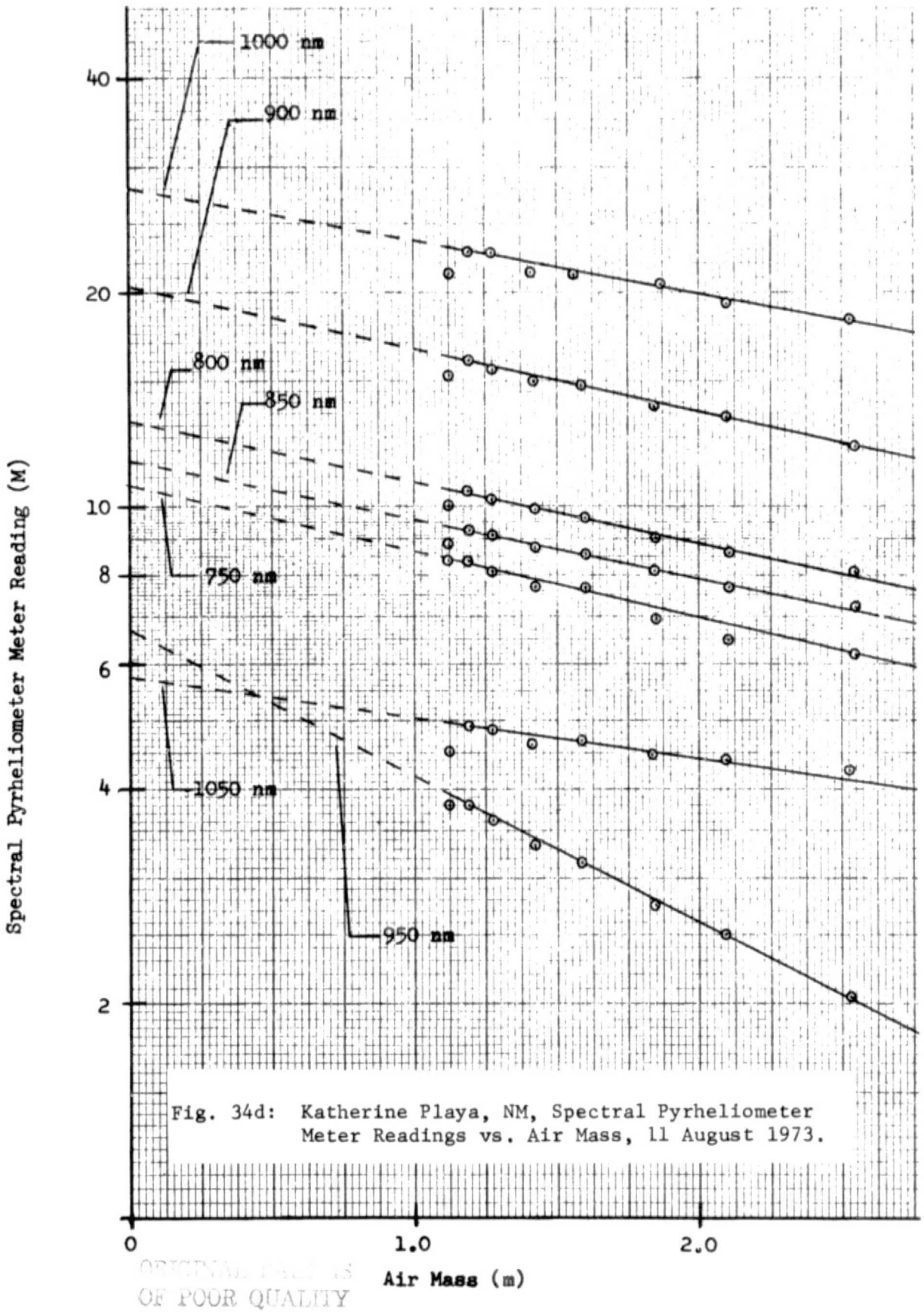

Fig. 34d: Katherine Playa, NM, Spectral Pyrheliometer Meter Readings vs. Air Mass, 11 August 1973.

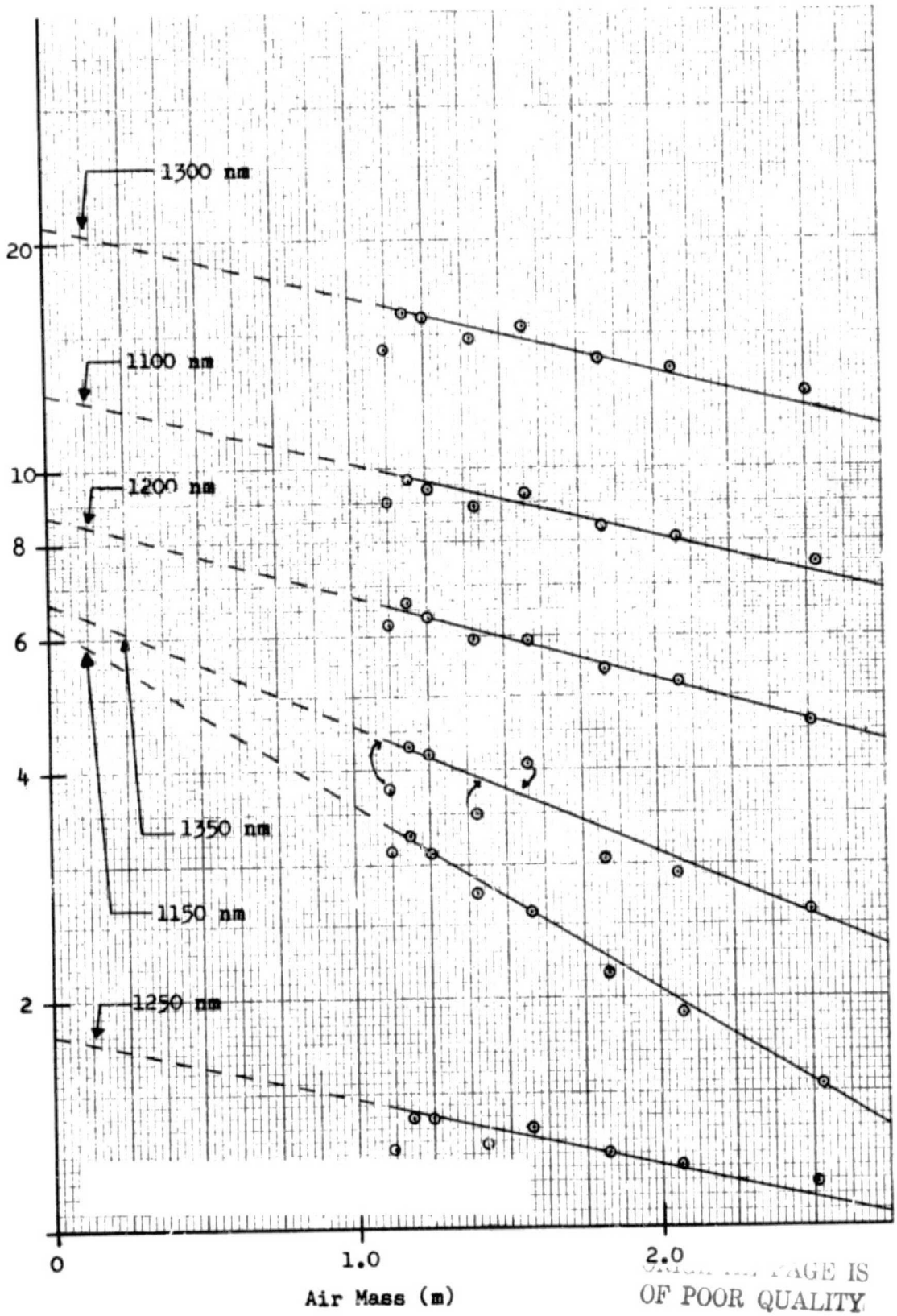

Fig. 34e: Katherine Playa, NM, Spectral Pyrheliometer Meter Readings vs. Air Mass, 11 August 1973.

Fig. 35: Katherine Playa, NM, Broadband (ERTS), Spectral, and Model Optical Depth, 11 August 1973.

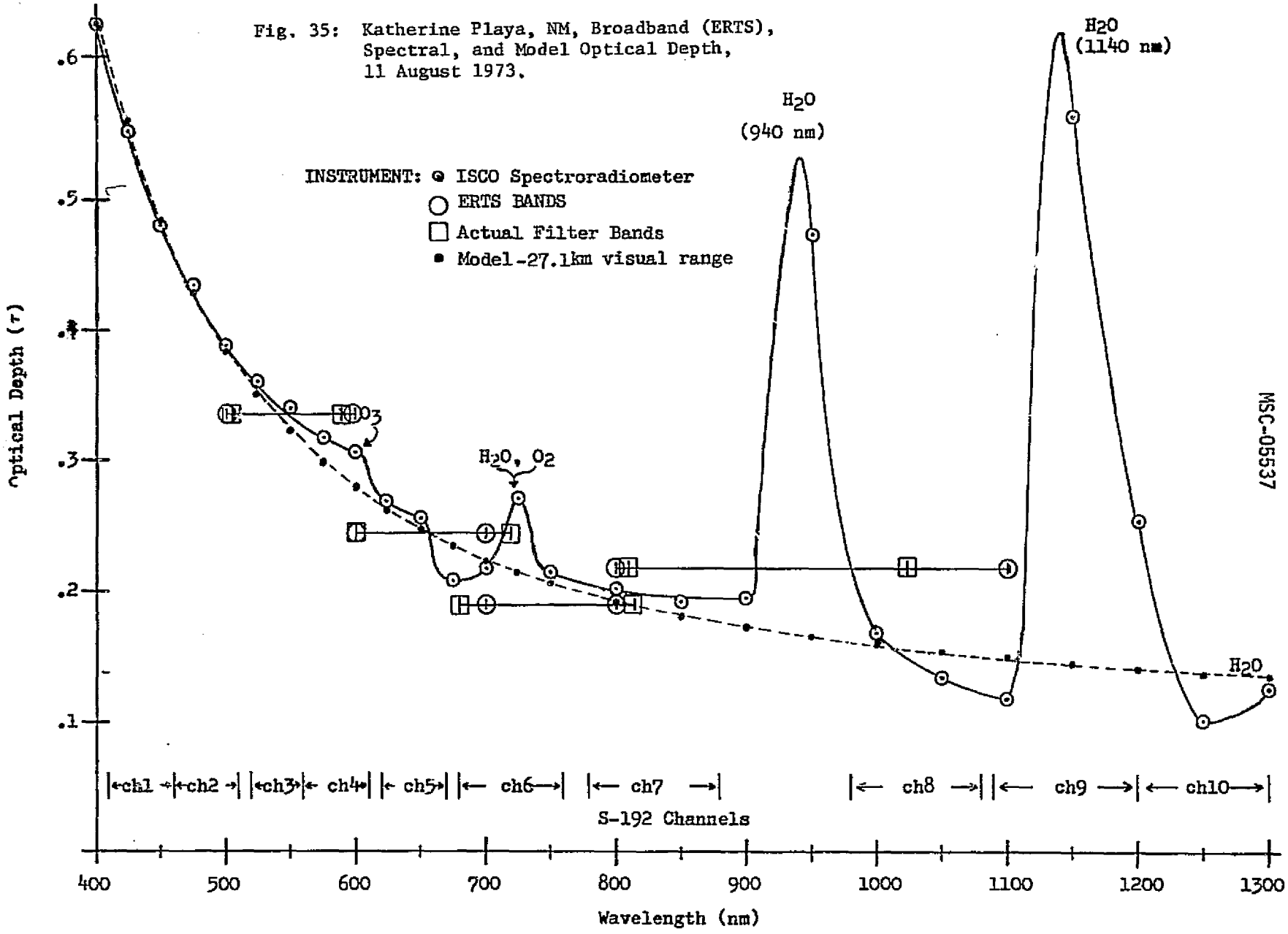

3.2.3.5 Target Reflectivity and Radiance at Ground Level - The appropriate normalization data for normalizing target radiances taken at other times than EREP overpass are shown in Figure 36. The technique of normalization is discussed in section 3.2.2.5.

The Bendix R.P.M.I. was used to measure target radiance normal to the target surface - $N_t(g)$. In order to assess target uniformity, two different sites on Katherine Playa were measured, see Figure 28. One site corresponded to the site where the I.S.C.O. spectradiometer was used (to measure spectral target radiance/reflectivity. The other site was randomly selected at a significant distance (approximately 600 ft.) from the I.S.C.O. site. The Playa target consisted of dry mud in polygon shapes, with small depressions bordering each dry mud polygon feature. In the bottom of such depressions there was a much lighter colored, smaller grain dust/crust. The polygons varied from about 2 to 6 in. across, while the lighter depressions were about 1 inch across. At both sites, the Bendix was positioned at different heights above the target, such that circular spot sizes of 3, 5, and 6 in. diameter were viewed. Shown in Figures 37 and 38 are the resultant average of the six measurements (3 spot sizes at two targets), and their range. The range probably results from varying mixtures of the darker mud polygons with the lighter depressions. These measurements are also lsited in Table 12. Shown in Figure 39 is the spectral target radiance determined by

$$N_t(g) = H\rho/\pi \qquad \text{(Eq. 7)}$$

where the spectral total solar radiation (H) and the spectral target reflectivity (ρ) were measured with the I.S.C.O.
Also shown in Figure 39 is a direct comparison of absolute units and spectral distribution of the two independent derivations -

I.S.C.O (Eq. 7) vs. Bendix direct radiance measurement. As can be seen, when the collimator radiance adjustment is made, excellent agreement is obtained. Since the I.S.C.O. and Bendix were both rigorously calibrated, see Appendix, with the same set of N.B.S. standard lamps; the collimator radiance adjustment appears to be accurate. The spectral shape of each curve is also in close agreement.

The field data and derivations, as explained in section 3.2.2.5, for the broadband (Bendix R.P.M.I.) target reflectivities are shown in Figures 40, 41, and 42. Shown in Figure 43 is the spectral target reflectivity determined by the I.S.C.O. spectroradiometer (explained in section 3.1). A comparison of the Bendix determined target reflectivity (at the same site) with that of the I.S.C.O. is also shown in Figure 43 and excellent agreement is obtained. The average broadband target reflectivity is listed in Table 12 and the spectral target reflectivity is listed in Table 13.

3.2.3.6 Target Radiance at EREP - The apparent target radiance at EREP, as discussed in detail in section 3.2.2.6, was derived by

$$N_s = N_t(g)\ T + N_a \qquad \text{(Eq. 14)}$$

where $N_t(g)$ is the target radiance at ground level, T is the atmospheric transmittance, and N_a is the calculated atmospheric path radiance. For the 11 August Katherine Playa mission, an atmospheric visual range of 27.1 Km was derived, see Figure 35, and used to determine atmospheric path radiance. The derived broadband atmospheric path radiance is shown in Figure 44, and the resultant target radiance (broadband) at EREP is shown in Figure 45. In addition, all parameters are listed in Table 12. The derived spectral atmospheric path radiance, directional radiance, and radiance at EREP, are shown in Figure 46 and listed in Table 13.

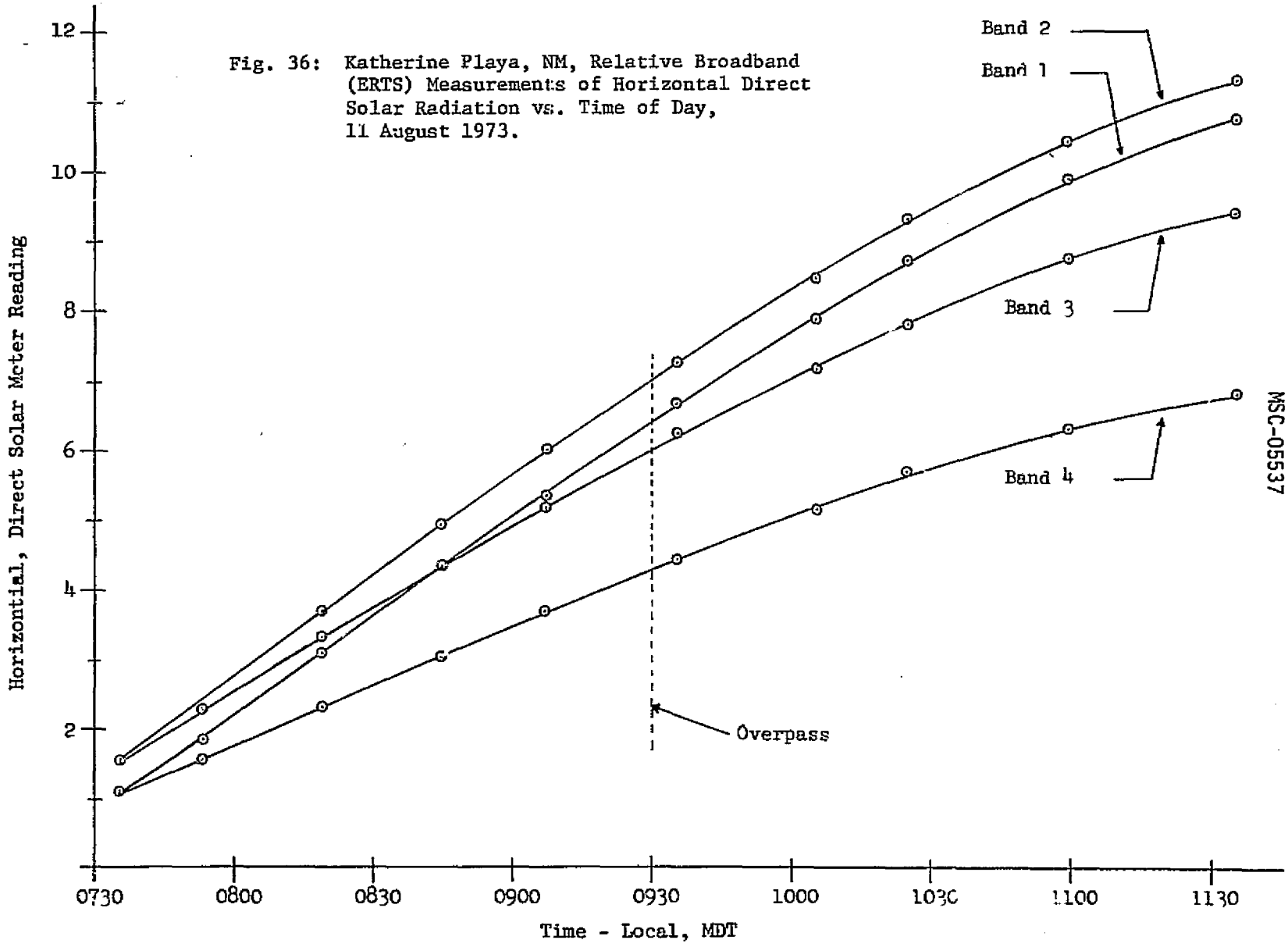

Fig. 36: Katherine Playa, NM, Relative Broadband (ERTS) Measurements of Horizontal Direct Solar Radiation vs. Time of Day, 11 August 1973.

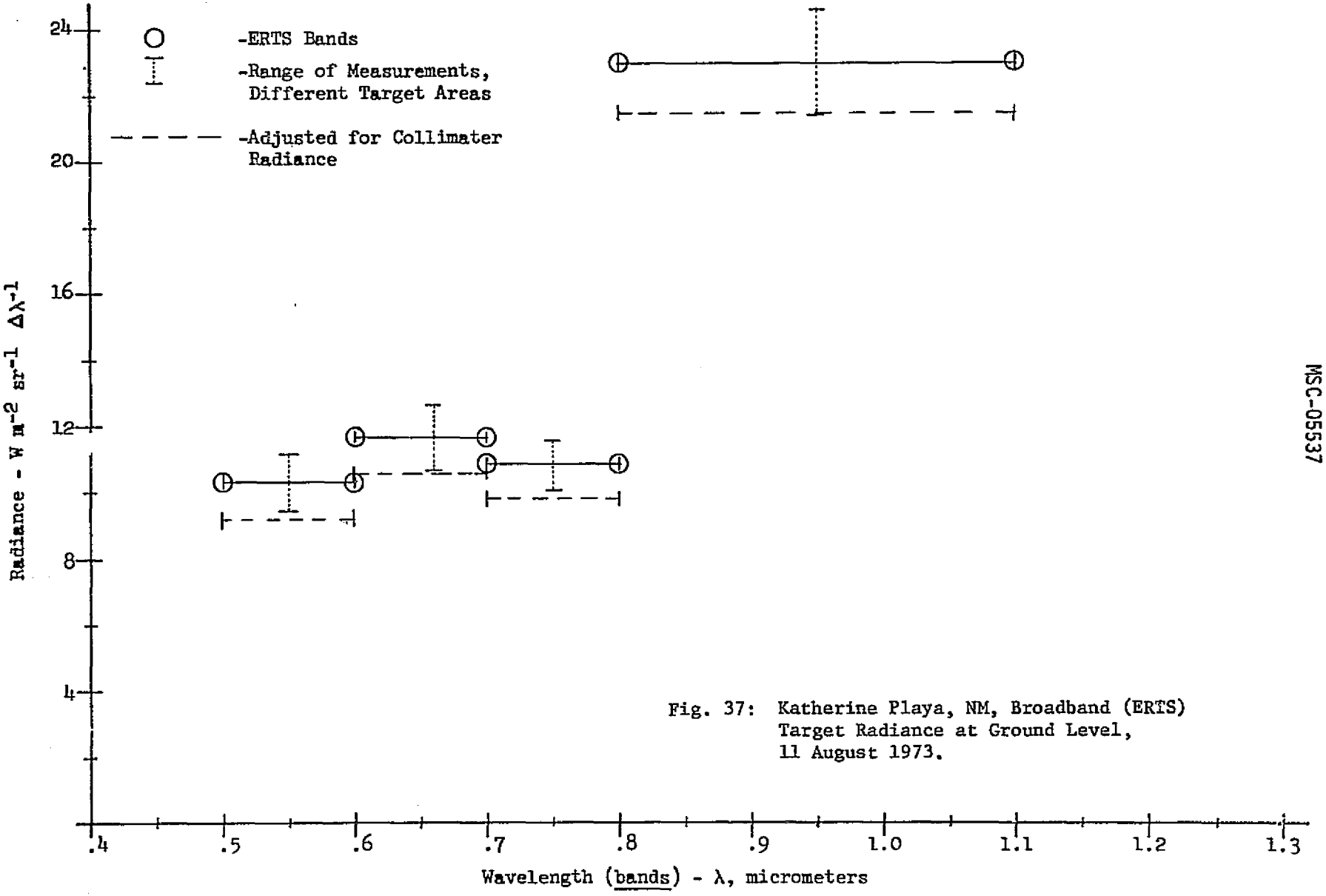

Fig. 37: Katherine Playa, NM, Broadband (ERTS) Target Radiance at Ground Level, 11 August 1973.

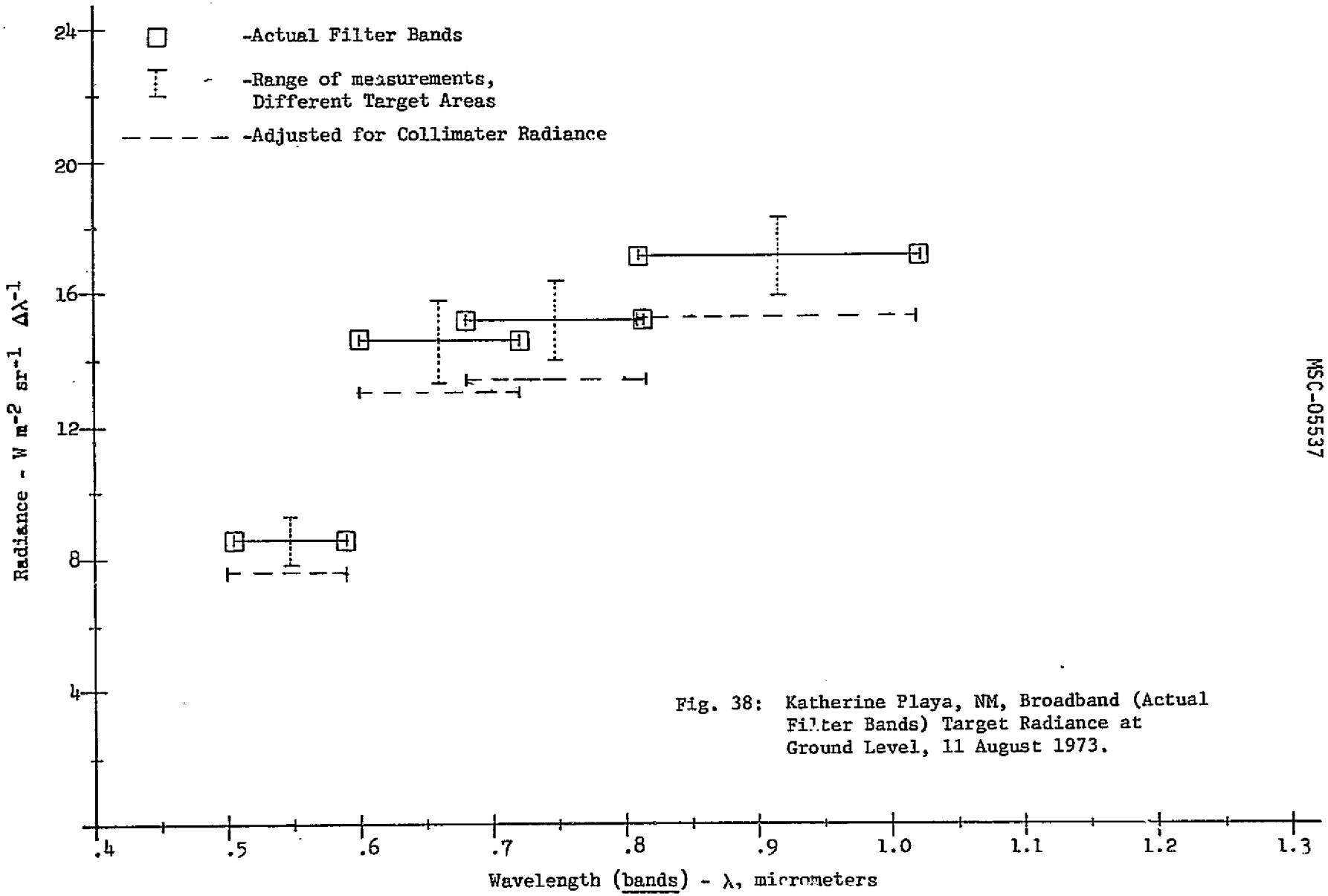

Fig. 38: Katherine Playa, NM, Broadband (Actual Filter Bands) Target Radiance at Ground Level, 11 August 1973.

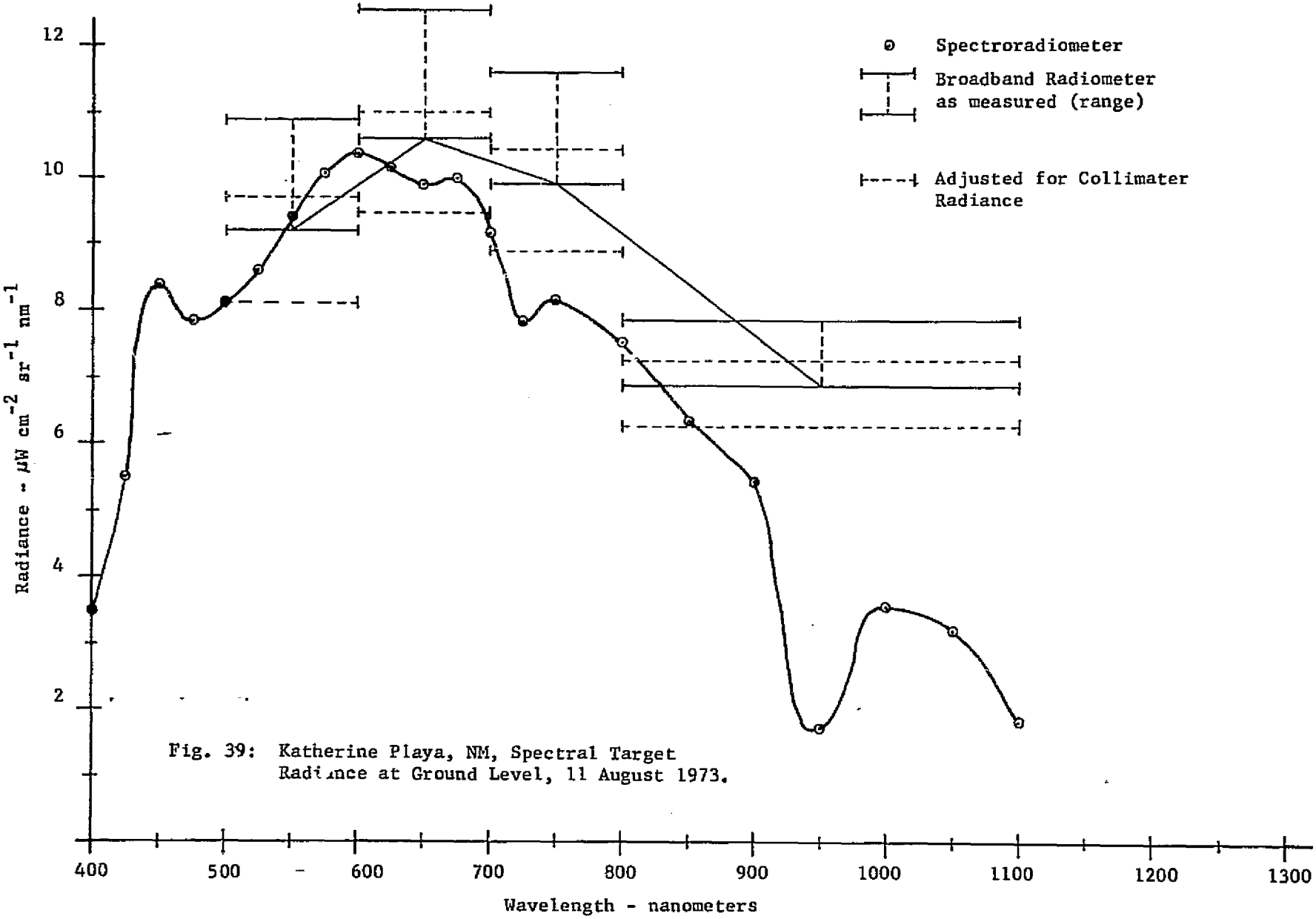

Fig. 39: Katherine Playa, NM, Spectral Target Radiance at Ground Level, 11 August 1973.

MSC-05537

Fig. 40: Katherine Playa, NM, Determination of Site #1 Reflectivity Using Cards, 11 August 1973.

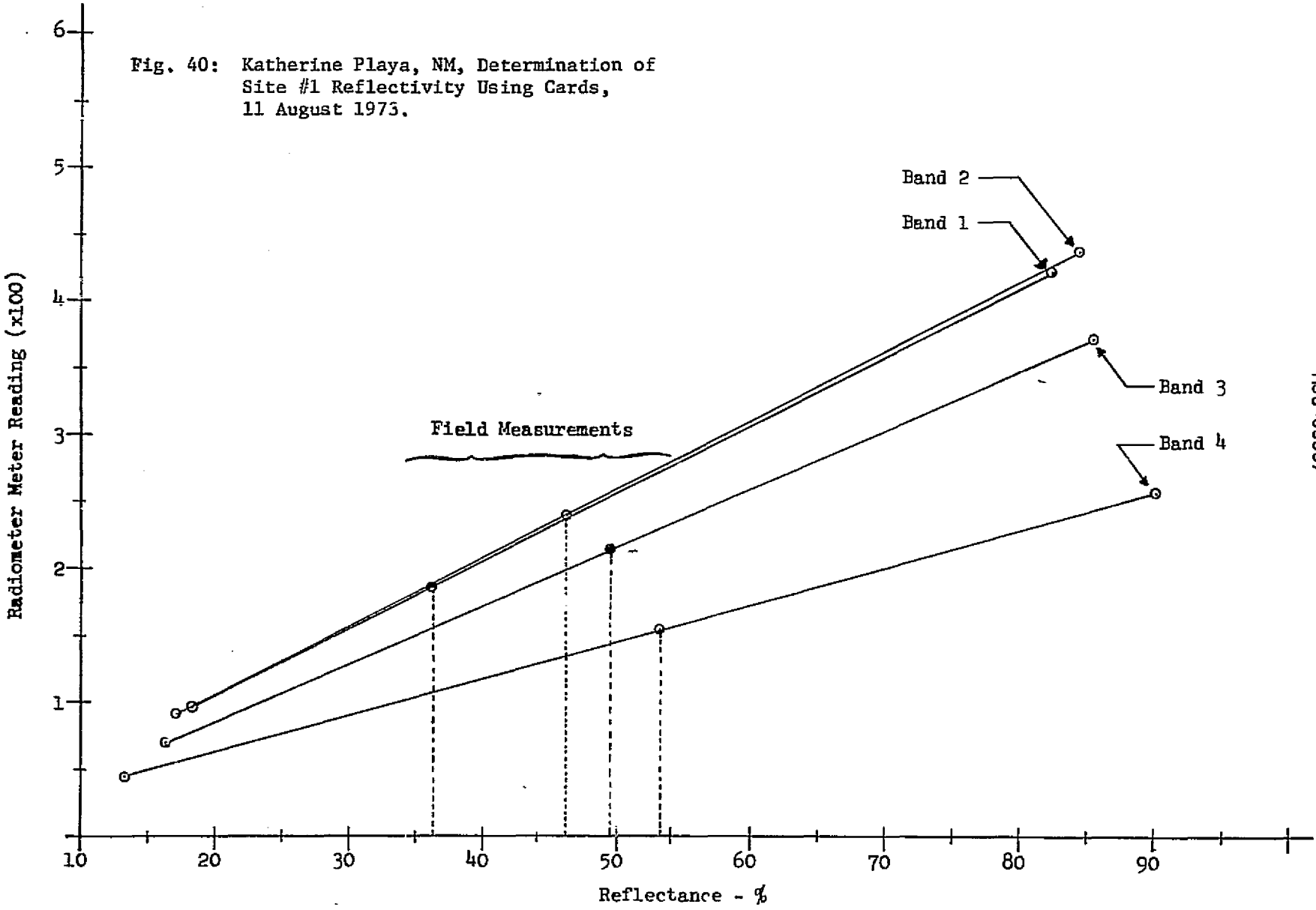

MSC-05537

Fig. 41: Katherine Playa, NM, Determination of Site #2 Reflectivity Using Cards, 11 August 1973.

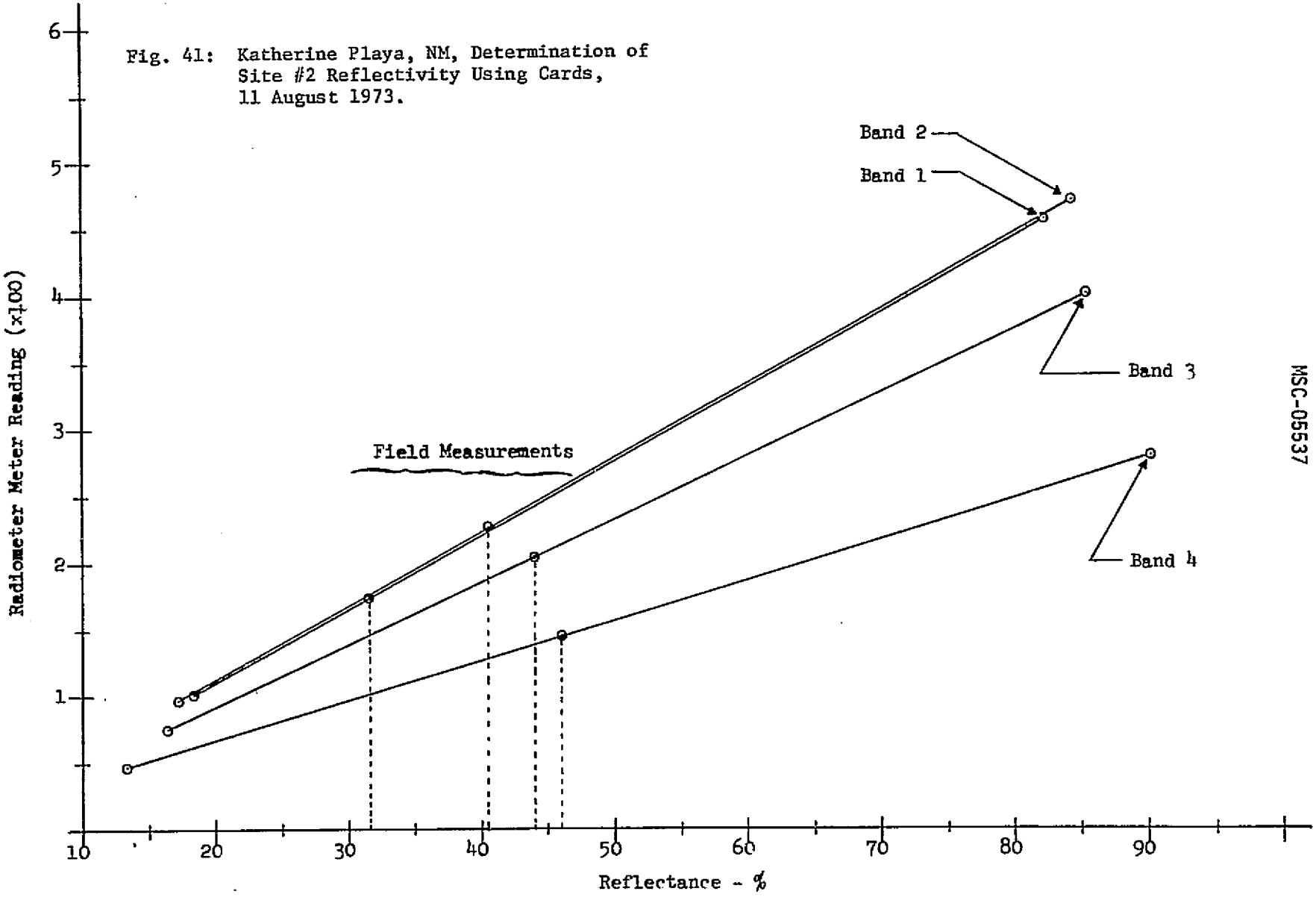

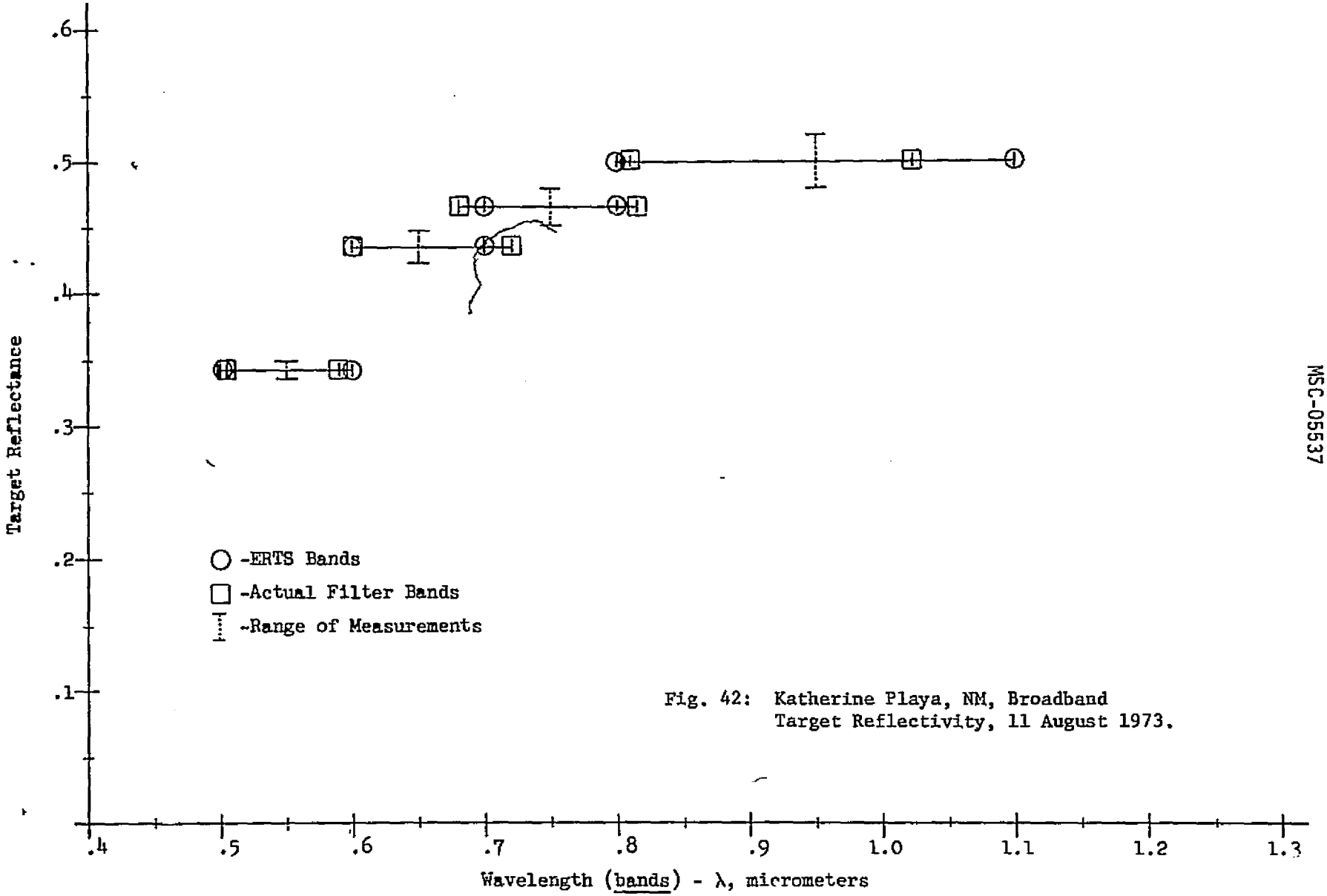

Fig. 42: Katherine Playa, NM, Broadband Target Reflectivity, 11 August 1973.

MSC-05537

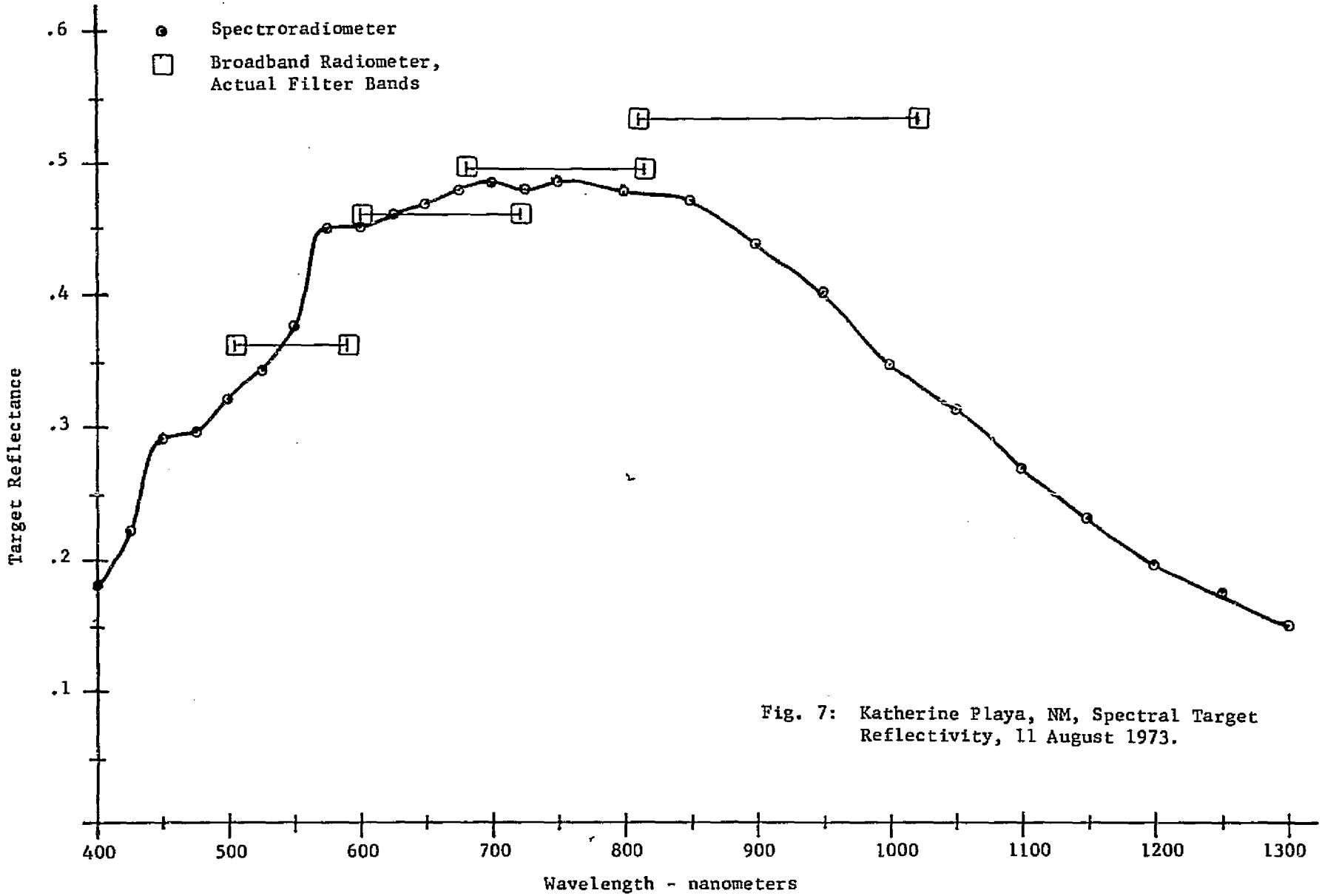

Fig. 7: Katherine Playa, NM, Spectral Target Reflectivity, 11 August 1973.

MSC-05537

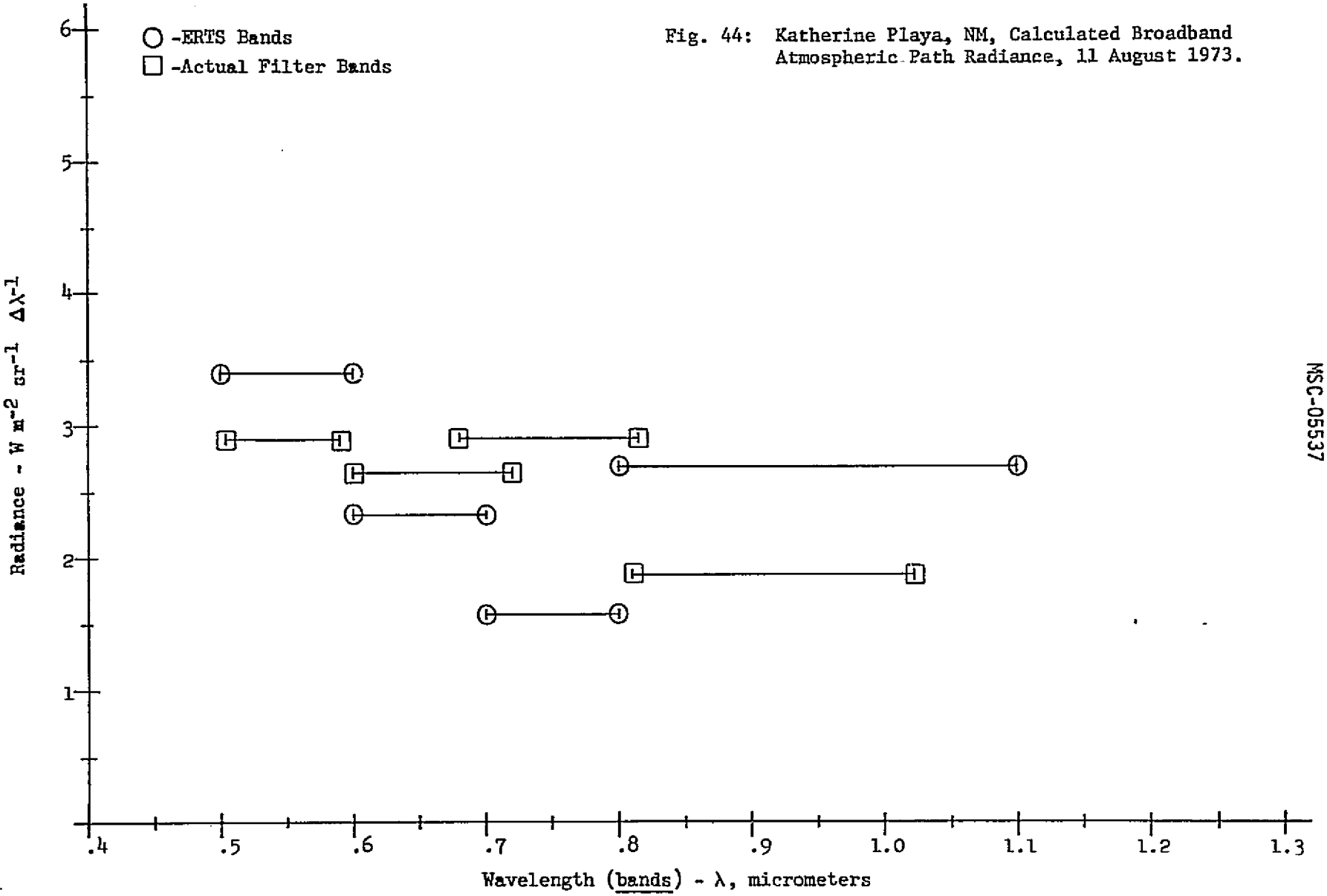

Fig. 44: Katherine Playa, NM, Calculated Broadband Atmospheric Path Radiance, 11 August 1973.

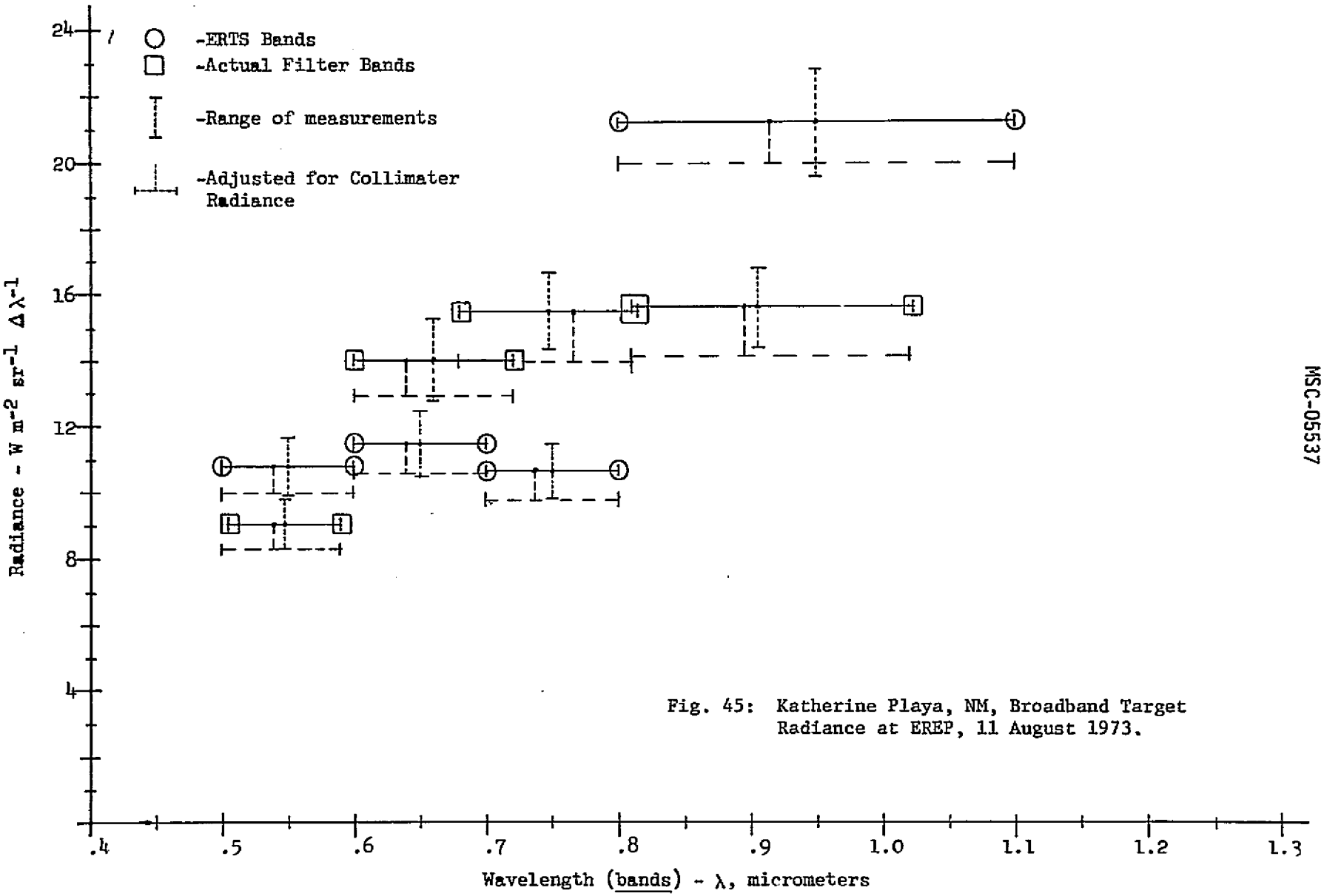

Fig. 45: Katherine Playa, NM, Broadband Target Radiance at EREP, 11 August 1973.

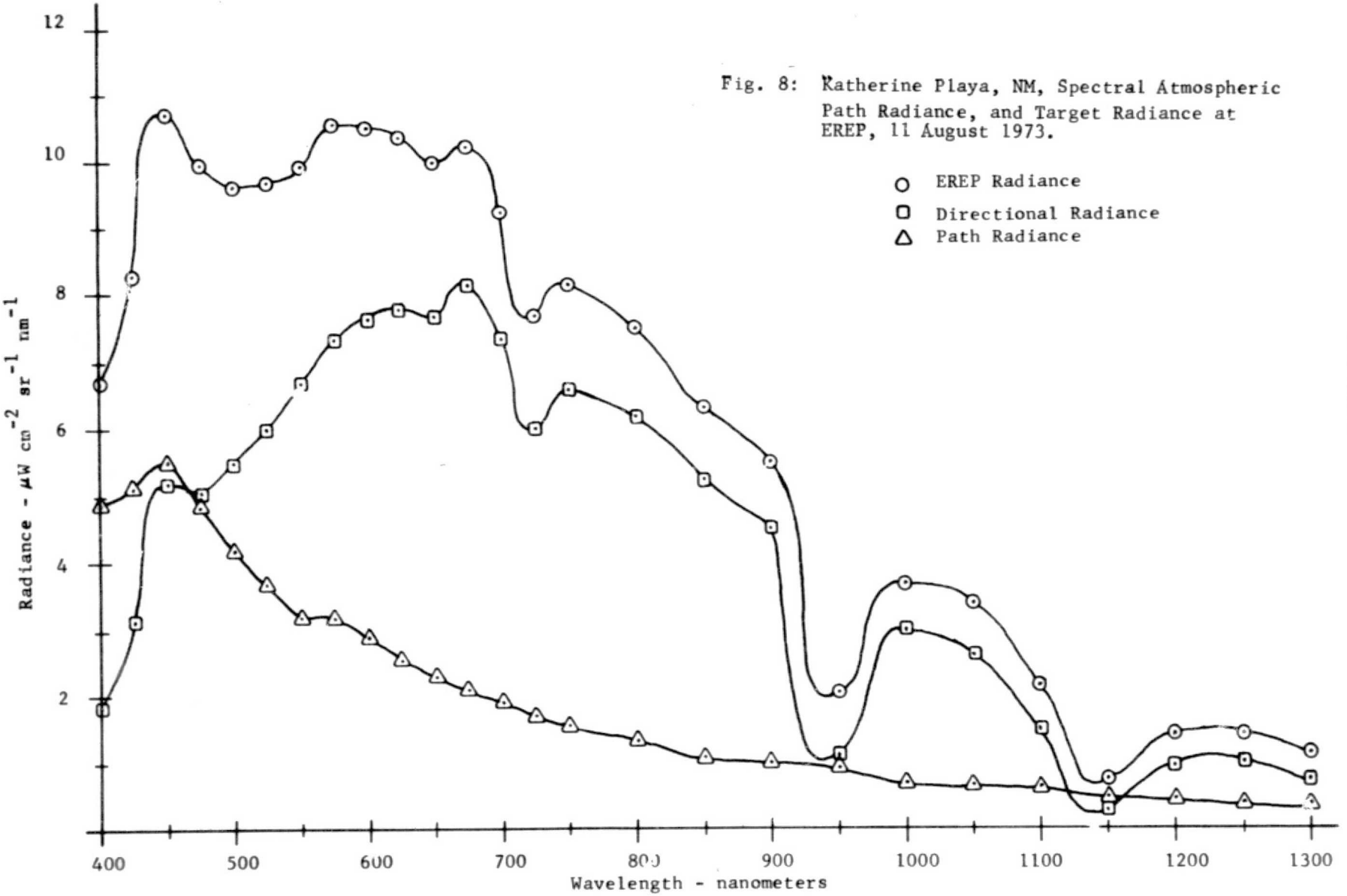

Fig. 8: Katherine Playa, NM, Spectral Atmospheric Path Radiance, and Target Radiance at EREP, 11 August 1973.

MSC-05537

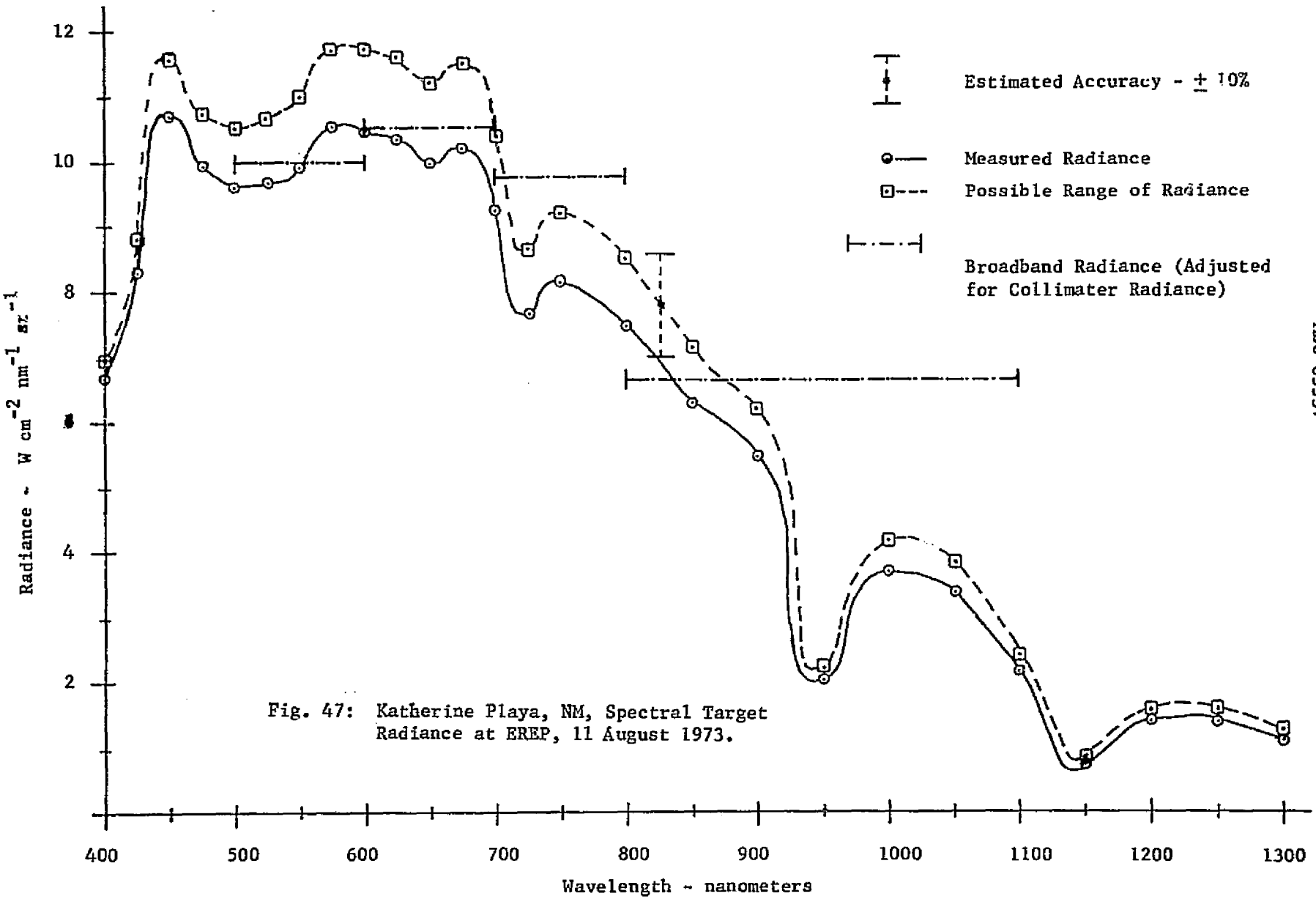

Fig. 47: Katherine Playa, NM, Spectral Target Radiance at EREP, 11 August 1973.

MSC-05537

Katherine Playa (08/11/73) Broadband Atmospheric and Target Radiance

Band	τ	T	Reflectance (ρ)	$N_t(g)$**		$N_t(d)$**		N_a **	N_s **	
				Meas.	Adj.*	Meas.	Adj.*		Meas.	Adj.*
B1	.335	.715	.343	10.34	9.23	7.39	6.60	3.41	10.80	10.01
L1R				8.58	7.66	6.13	5.48	2.90	9.03	8.38
B2	.244	.783	.435	11.72	10.56	9.18	8.27	2.33	11.51	10.60
B2R				14.58	13.13	11.42	10.28	2.65	14.07	12.93
B3	.188	.829	.466	10.94	9.94	9.07	8.24	1.58	10.65	9.82
B3R				15.17	13.42	12.58	11.13	2.91	15.49	14.04
B4	.217	.805	.500	23.03	21.52	18.54	17.33	2.69	21.23	20.02
B4R				17.08	15.25	13.75	12.28	1.88	15.63	14.16

** Watts $(meter)^{-2}$ $(steradian)^{-1}$ $\Delta\lambda^{-1}$

$\Delta\lambda$ (micrometers) = B1 = .500 - .600 B1R = .505 - .590
B2 = .600 - .700 B2R = .600 - .720
B3 = .700 - .800 B3R = .680 - .815
B4 = .800 - 1.100 B4R = .810 - 1.02

* Adjusted for Collimater Radiance. In addition, ground measurements indicated a $\pm$ 7.0% to $\pm$ 8.5% variation with respect to values reported.

τ = Atmospheric Depth

T = Transmittance = $e^{-\tau \sec\theta}$

$N_t(g)$ = Target Radiance at Ground Level

$N_t(d)$ = Target Directional Radiance at EREP = $\frac{\rho HT}{\pi}$

N_a = Atmospheric Path Radiance

N_s = Radiance at EREP = $N_t(d) + N_a$

Table 12: Katherine Playa, NM, Broadband Atmospheric and Target Radiance, 11 August 1973.

Katherine Playa (08/11/73) Spectral Atmospheric and Target Radiance

Wavelength (λ)	τ	T	H **	Reflectance (ρ)	$N_t(d)$ ***	N_a ***	N_s ***	
							Meas.	Adj.*
400	.638	.528	60.86	.181	1.85	4.84	6.69	6.99
425	.555	.574	77.35	.223	3.15	5.13	8.28	8.78
450	.481	.618	90.42	.292	5.20	5.51	10.71	11.54
475	.437	.646	83.39	.296	5.08	4.86	9.94	10.75
500	.389	.678	78.57	.323	5.48	4.17	9.65	10.53
525	.361	.697	78.57	.344	6.00	3.71	9.71	10.67
550	.340	.712	77.94	.379	6.70	3.22	9.92	11.00
575	.315	.730	70.32	.450	7.36	3.18	10.54	11.72
600	.305	.736	72.30	.451	7.64	2.87	10.51	11.73
625	.269	.764	69.65	.460	7.78	2.56	10.34	11.59
650	.256	.774	66.39	.470	7.68	2.30	9.98	11.21
675	.207	.813	65.52	.480	8.14	2.08	10.22	11.52
700	.218	.804	59.13	.485	7.35	1.88	9.23	10.40
725	.270	.763	51.29	.481	5.99	1.70	7.69	8.65
750	.214	.807	52.76	.487	6.60	1.56	8.16	9.22
800	.202	.817	49.78	.478	6.18	1.32	7.50	8.49
850	.191	.826	42.30	.472	5.25	1.08	6.32	7.16
900	.192	.825	39.09	.438	4.50	1.00	5.50	6.21
950	.472	.624	13.78	.401	1.10	0.93	2.03	2.20
1000	.169	.844	32.00	.348	3.00	0.70	3.70	4.17
1050	.133	.876	31.23	.313	2.72	0.67	3.39	3.83
1100	.218	.804	21.56	.268	1.48	0.67	2.15	2.39
1150	.516	.597	6.19	.232	0.27	0.49	0.76	0.81
1200	.251	.778	19.35	.196	0.94	0.46	1.40	1.55
1250	.202	.817	21.99	.174	1.00	0.40	1.40	1.56
1300	.224	.799	19.65	.149	0.75	0.38	1.13	1.25

* Adjusted for +16 % target radiance, as measured with Bendix R.P.M.I.

** microWatts $(\text{centimeter})^{-2}$ $(\text{nanometer})^{-1}$

*** microWatts $(\text{centimeter})^{-2}$ $(\text{nanometer})^{-1}$ $(\text{steradian})^{-1}$

τ = Atmospheric Depth

T = Transmittance = $e^{-\tau \sec\theta}$

H = Total Solar Radiation

$N_t(d)$ = Target Directional Radiance at EREP = $\frac{\rho H T}{\pi}$

N_a = Atmospheric Path Radiance

N_s = Radiance at EREP = $N_t(d) + N_a$

Table 13: Katherine Playa, NM, Spectral Atmospheric and Target Radiance Parameters, 11 August 1973.

The significance and relationships between these parameters can be seen in Figure 46. In the "blue" wavelengths from 400 to 500 nm, the atmospheric path radiance is greater than or equal to the target's directional radiance. Therefore, the radiance at EREP is dominated by atmospheric path radiance. However, as the wavelength increases, the path radiance quickly drops and becomes a much smaller influence. Shown in Figure 47 is a comparison of the Bendix derived radiances at EREP with those derived with the I.S.C.O.; as can be seen, good agreement exists. Also shown in Figure 47 is a spectral target radiance curve which represents the same range of target radiances measured by the Bendix. This upper curve is intended to represent possible target areas having a higher reflectivity (as determined with the Bendix) than the target site where the I.S.C.O. was used.

3.2.4 *GREAT SALT LAKE DESERT, UTAH, 13 SEPTEMBER 1973*

Site Coordinates:	40° 45" N. Latitude 113° 24" W. Longitude (see Figure 11)
EREP Pass:	Track 59A, Pass No. 39 Rev. 1763/1764
Time of Overpass:	256:19:34:18 GMT 1334 Local Time - MDT

3.2.4.1 General Conditions - Clear

3.2.4.2 Near Surface Meteorology - Dry bulb temperature = 29.4°C; wet bulb temperature = 17.22; surface pressure (measured) = 657.1 mm of Hg; wind = 5 m.p.h. WSW.

3.2.4.3 Total and Diffuse Solar Radiation - Total and diffuse solar radiation were measured with the previously mentioned section 3.1, I.S.C.O. spectroradiometer. The spectral total solar radiation is shown in Figure 48, and listed in Table 14. The spectral diffuse solar radiation

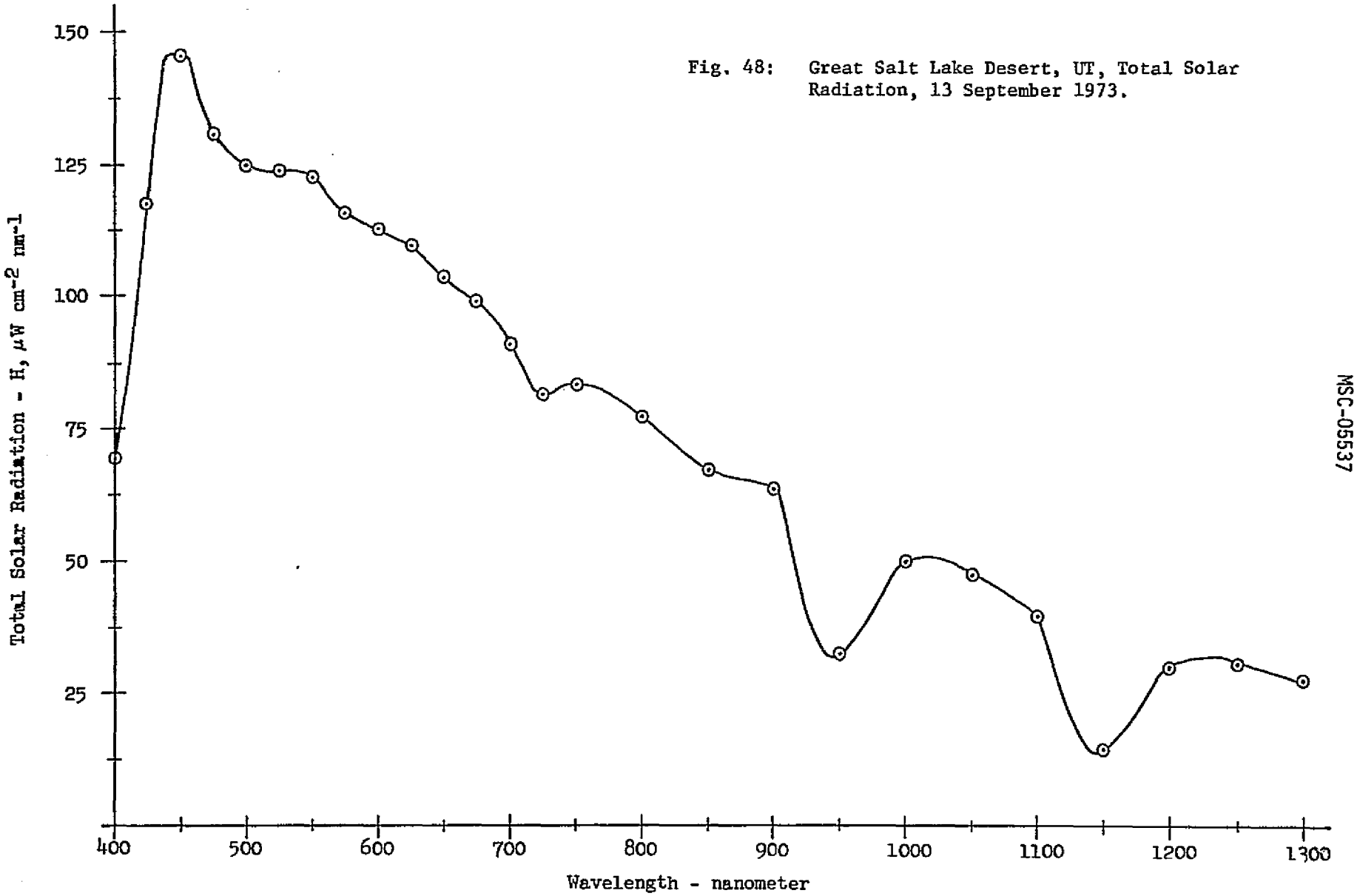

Fig. 48: Great Salt Lake Desert, UT, Total Solar Radiation, 13 September 1973.

Fig. 49: Great Salt Lake Desert, UT, Diffuse Solar Radaition, 13 September 1973.

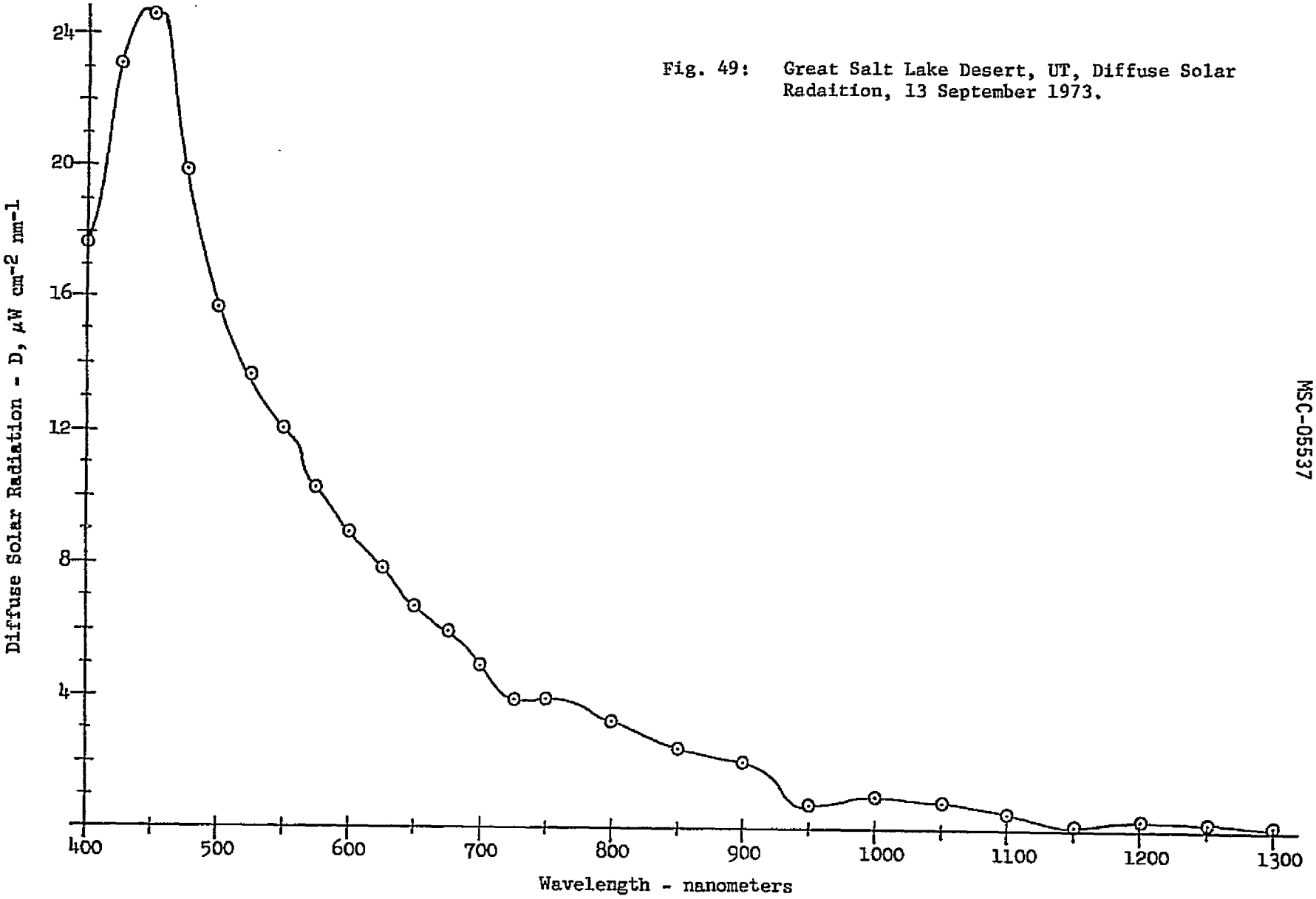

MSC-05537

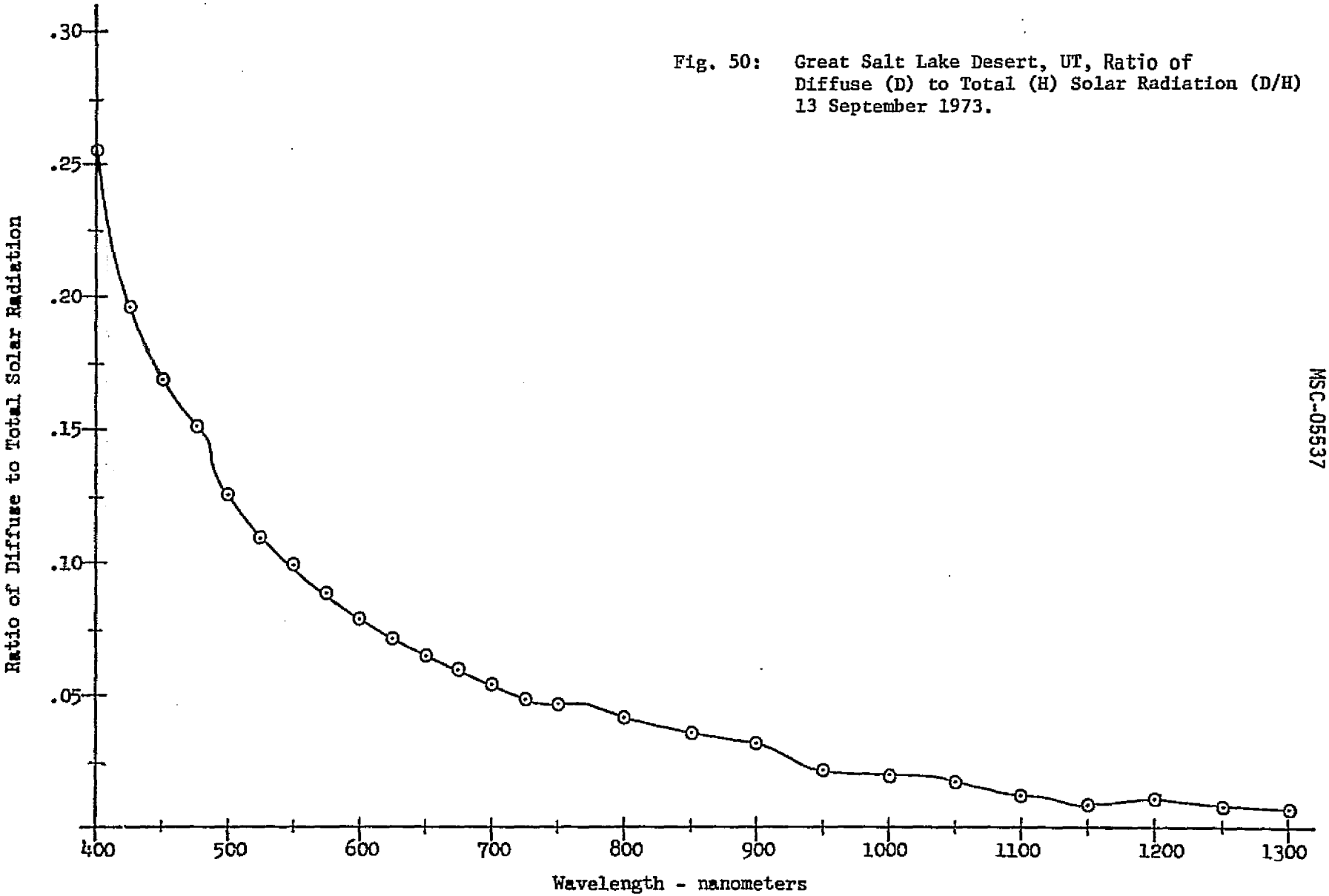

Fig. 50: Great Salt Lake Desert, UT, Ratio of Diffuse (D) to Total (H) Solar Radiation (D/H) 13 September 1973.

MSC-05537

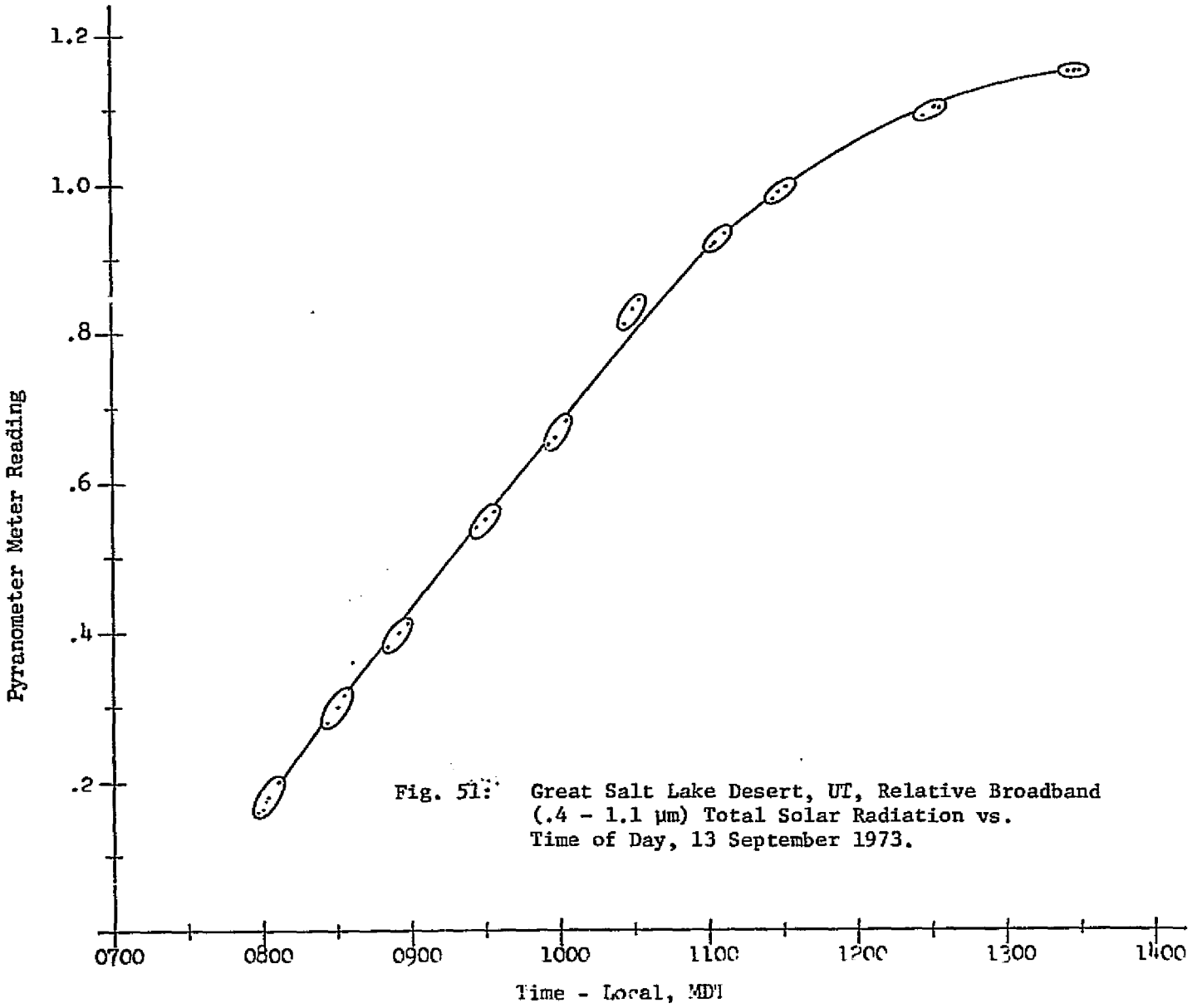

Fig. 51: Great Salt Lake Desert, UT, Relative Broadband (.4 - 1.1 μm) Total Solar Radiation vs. Time of Day, 13 September 1973.

Great Salt Lake Desert (09/13/73) Total and Diffuse Solar Radiation			
Wavelength (nm)	H *	D *	D/H
400	69.23	17.66	.255
425	117.6	23.08	.196
450	145.4	24.56	.169
475	131.1	19.91	.152
500	125.1	15.71	.126
525	124.0	13.66	.110
550	122.9	12.12	.0986
575	116.1	10.30	.0887
600	113.3	8.92	.0787
625	109.4	7.84	.0717
650	103.7	6.72	.0648
675	98.99	5.98	.0604
700	91.55	4.96	.0542
725	82.12	3.90	.0475
750	83.56	3.95	.0473
800	77.43	3.27	.0422
850	67.27	2.43	.0361
900	63.46	2.04	.0321
950	32.60	.722	.0221
1000	50.05	1.00	.0200
1050	47.55	.831	.0175
1100	39.72	.499	.0126
1150	14.64	.135	.0092
1200	29.96	.328	.0109
1250	30.90	.250	.0081
1300	27.44	.192	.0070

* microWatts $(centimeter)^{-2}$ $(nanometer)^{-1}$

Table 14: Great Salt Lake Desert, UT, Total and Diffuse Solar Radiation, 13 September 1973.

is shown in Figure 49 and also listed in Table 14. The ratio of diffuse to total solar radiation is shown in Figure 50 and listed in Table 14. Shown in Figure 51 is the nature of the broadband (.4 to 1.1 μm, 400 to 1100 nm) total solar radiation, discussed in detail in section 3.2.2.3.

3.2.4.4 Atmospheric Optical Depth/Transmittance - The field data, pyrheliometer meter readings vs. air mass used for deriving atmospheric optical depth, described in detail in section 3.2.2.4, are shown in Figures 52 and 53a, 53b, 53c, 53d, and 53e. The resultant optical depths are shown in Figure 54. As with the previous determinations (Figures 35 and 18), excellent agreement is obtained between the I.S.C.O. spectral measurements, the Bendix broadband measurements, and a visual range model of 33.1 Km. Tables 15 and 16 list the optical depths.

3.2.4.5 Target Reflectivity and Radiance at Ground Level - The appropriate normalization data for normalizing target radiances taken at other times than EREP overpass are shown in Figure 55. The technique of normalization is discussed in section 3.2.2.5.

The Bendix R.P.M.I. was used to directly measure radiance at ground level, at a desert site (same as used on 08 August 1973) and at the Bonneville Salt Flats, see Figure 11. The target radiance of the desert site is shown in Figure 56 and the Salt Flats radiance is shown in Figure 57. The ratio of the desert to Salt Flats radiance is shown in Figure 58. As with the wet vs. dry desert target areas measured on 08 August, the highest contrast (lowest ratio) exists in the visible wavelengths. The target radiances are listed in Table 15.

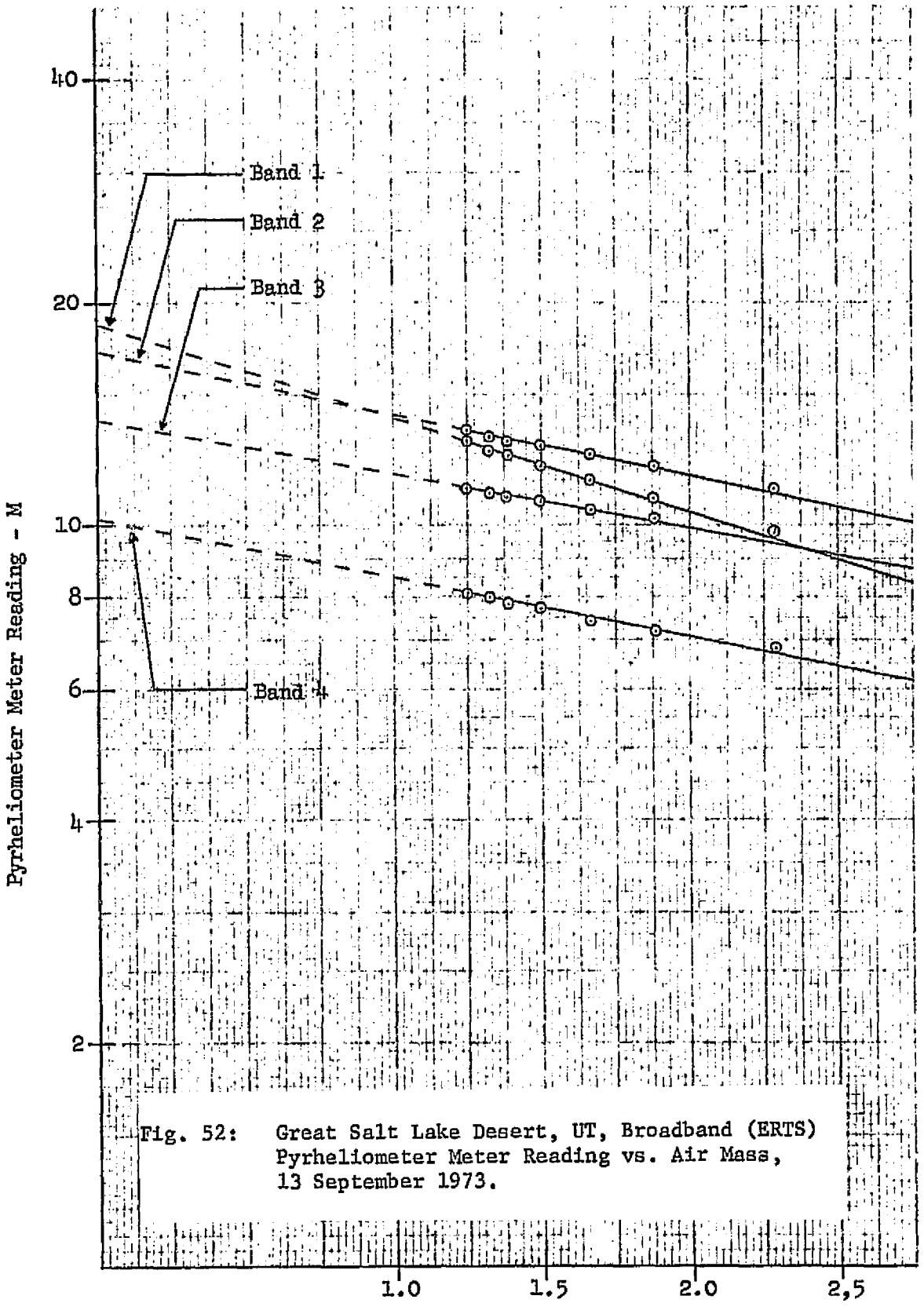

Fig. 52: Great Salt Lake Desert, UT, Broadband (ERTS) Pyrheliometer Meter Reading vs. Air Mass, 13 September 1973.

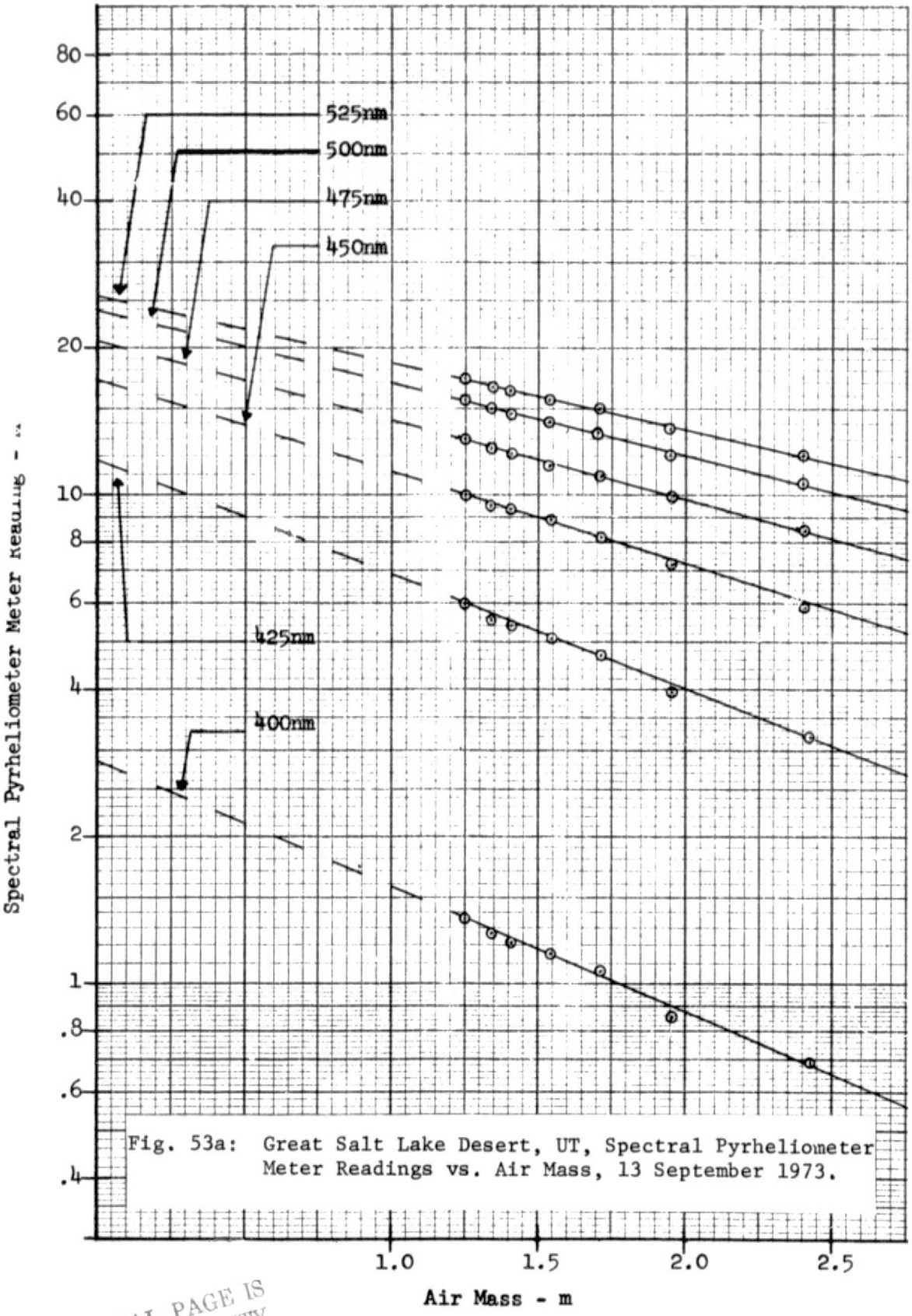

Fig. 53a: Great Salt Lake Desert, UT, Spectral Pyrheliometer Meter Readings vs. Air Mass, 13 September 1973.

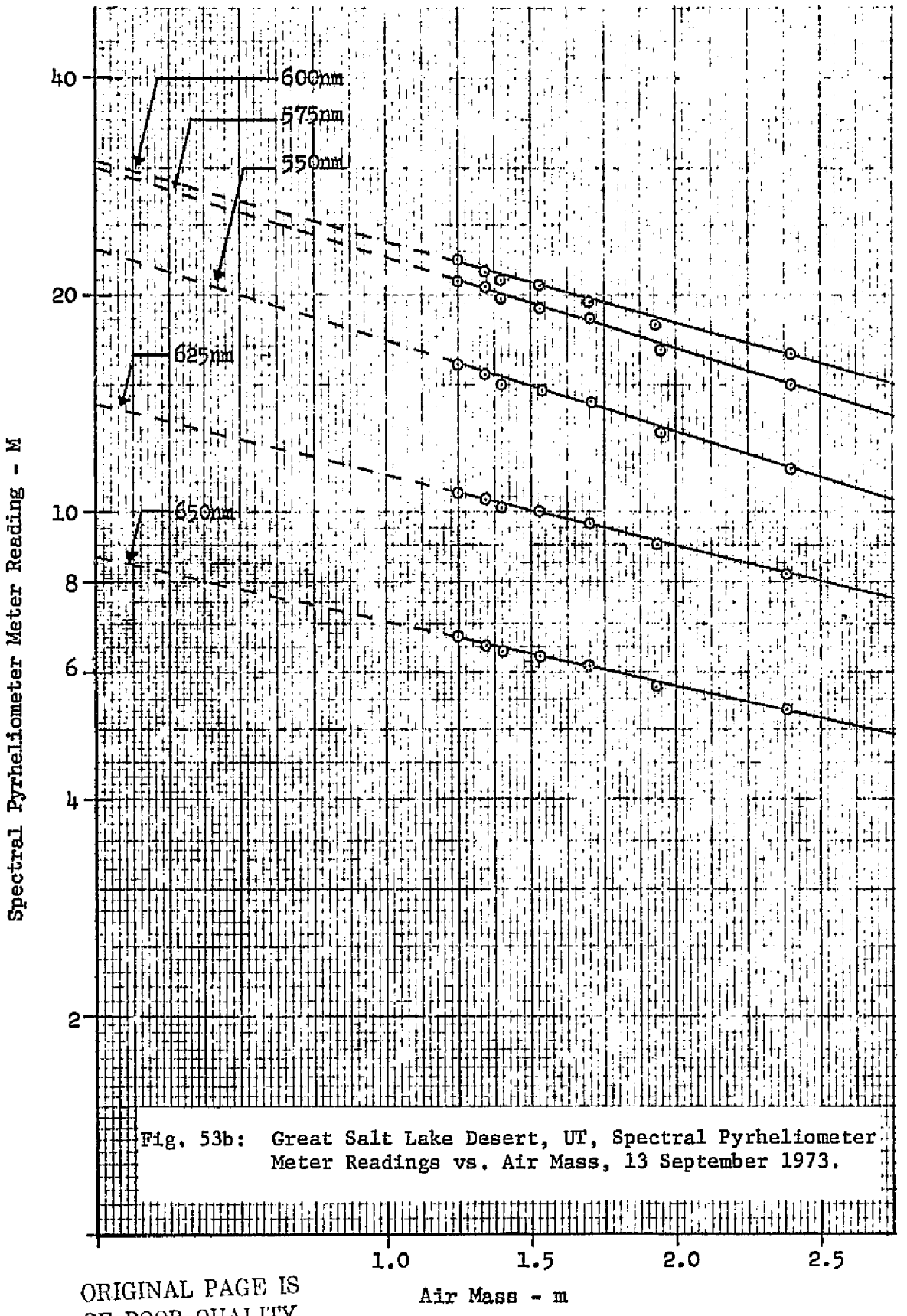

Fig. 53b: Great Salt Lake Desert, UT, Spectral Pyrheliometer Meter Readings vs. Air Mass, 13 September 1973.

Fig. 53c: Great Salt Lake Desert, UT, Spectral Pyrheliometer Meter Readings vs. Air Mass, 13 September 1973.

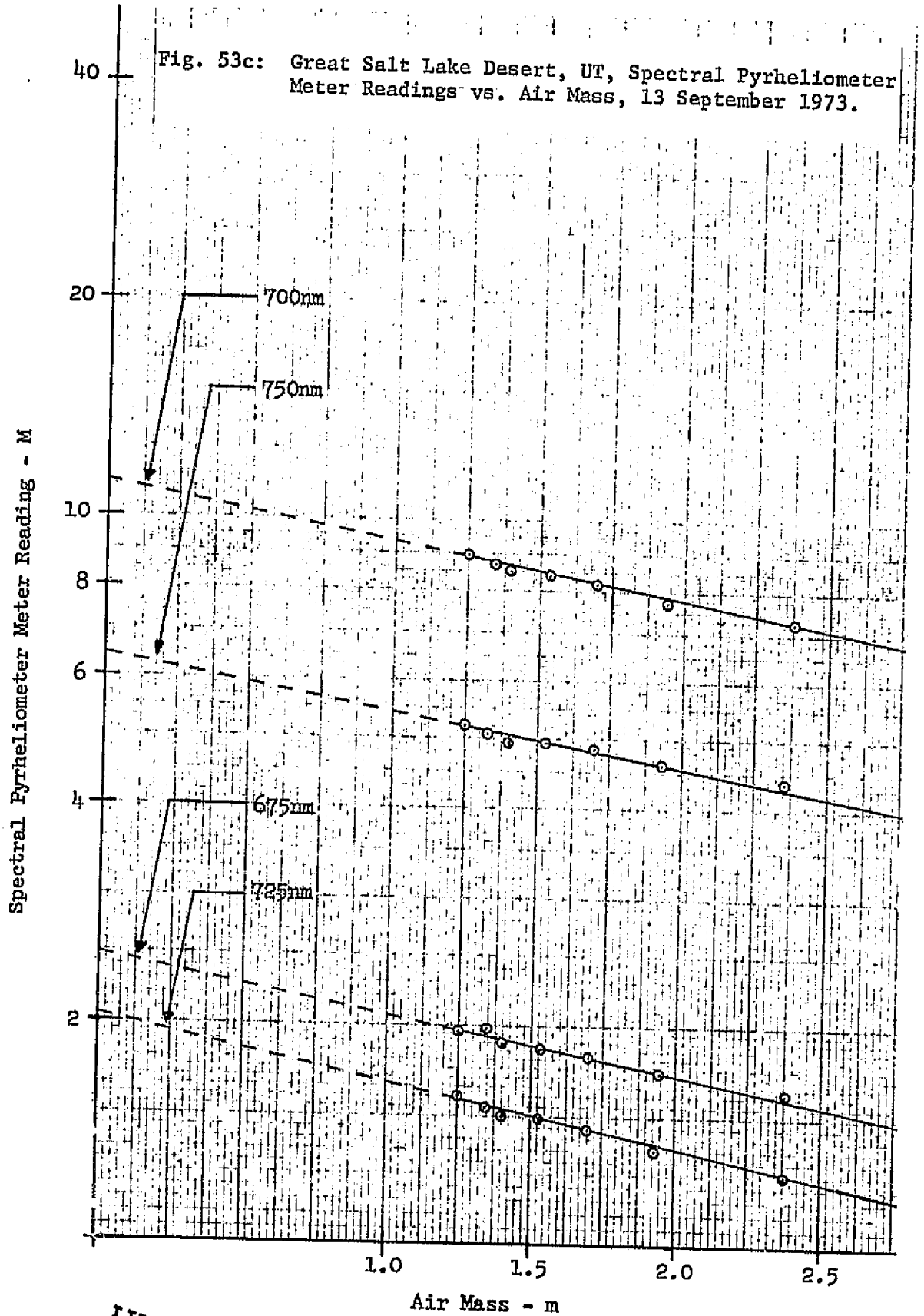

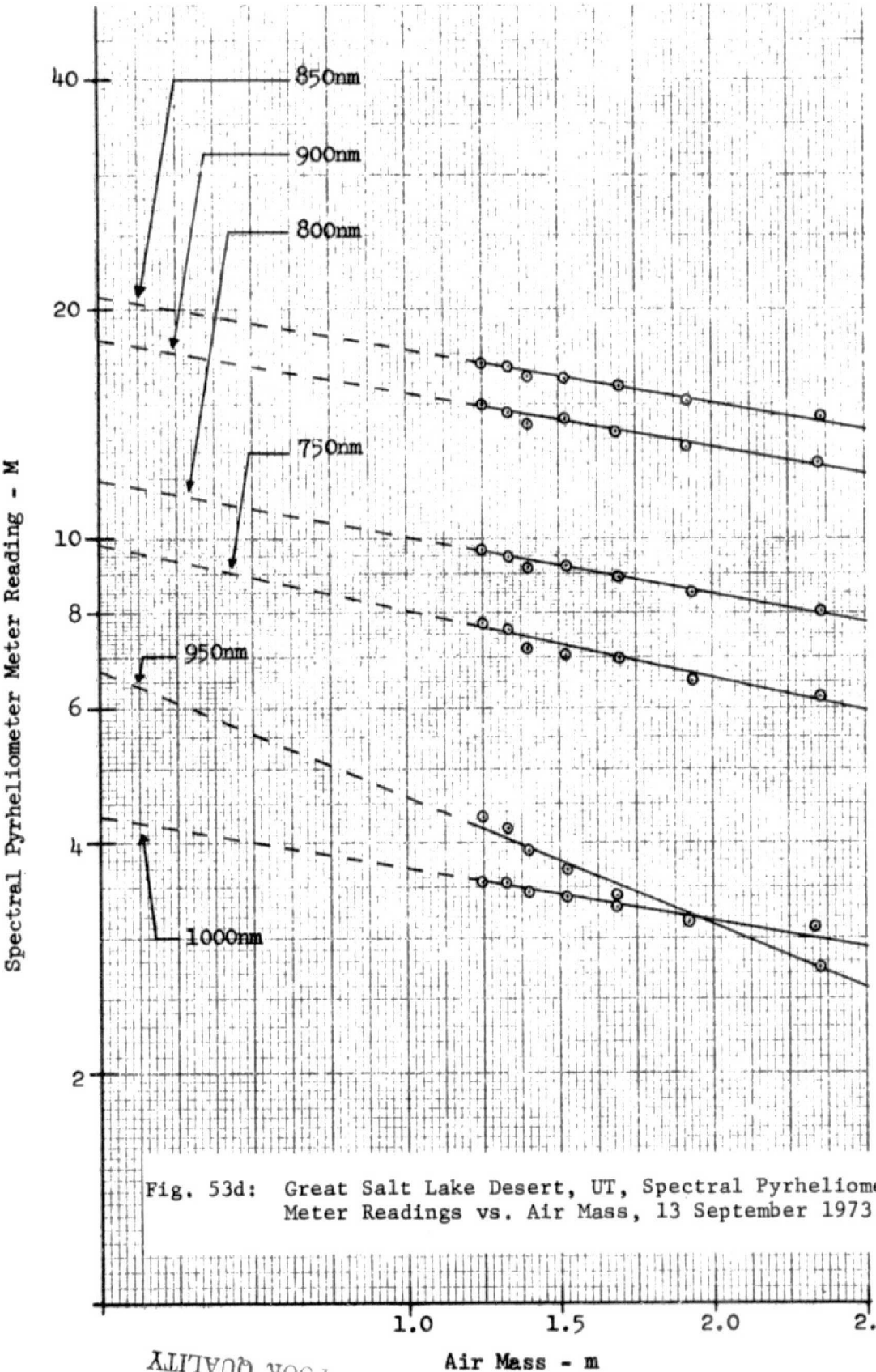

Fig. 53d: Great Salt Lake Desert, UT, Spectral Pyrheliometer Meter Readings vs. Air Mass, 13 September 1973.

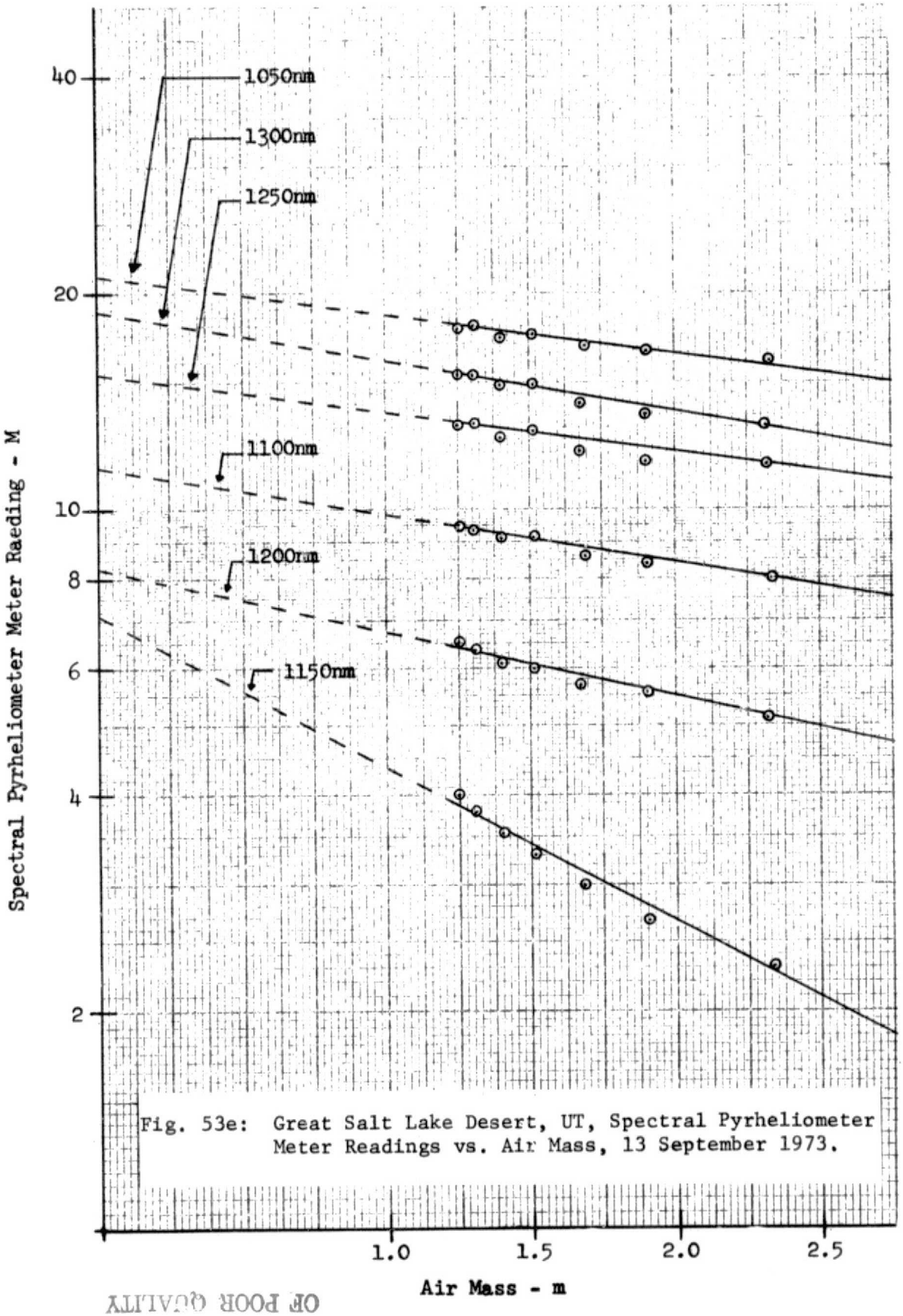

Fig. 53e: Great Salt Lake Desert, UT, Spectral Pyrheliometer Meter Readings vs. Air Mass, 13 September 1973.

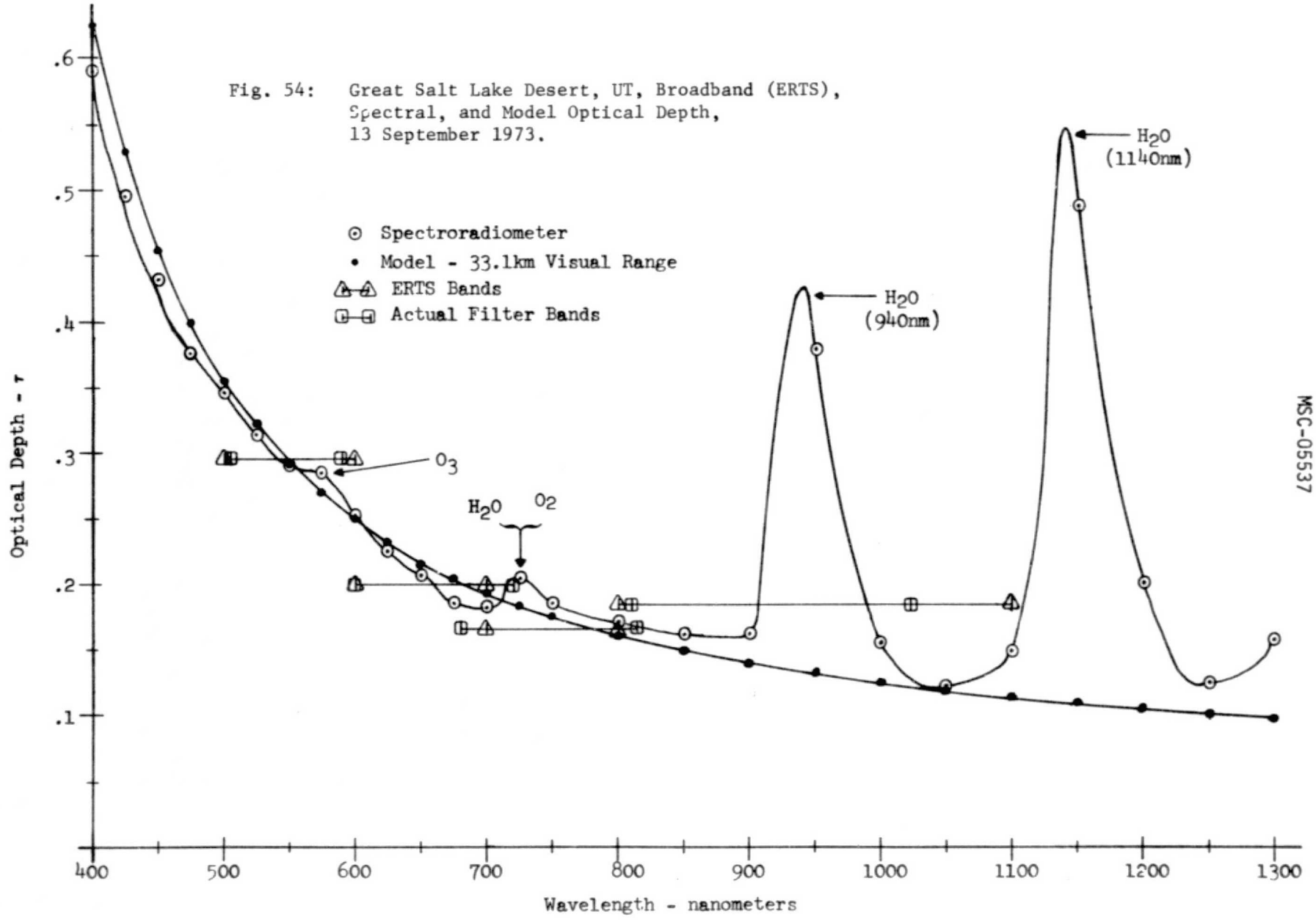

Fig. 54: Great Salt Lake Desert, UT, Broadband (ERTS), Spectral, and Model Optical Depth, 13 September 1973.

MSC-05537

The field data and derivations, as explained in section 3.2.2.5, for the broadband (Bendix R.P.M.I.) target reflectivities are shown in Figures 59 and 60. The resultant target reflectivities are shown in Figure 61. It is interesting to note that the Salt Flats have just the opposite reflectivity dependence with wavelength as compared to the desert area. The desert area measured represented a nominal surface of the area. The wet and dry spots, measured for the 08 August mission were still in existence, but did not make up a very large portion of the general area. If one takes the average reflectance of the wet and dry spots (08 August), one obtains a reflectivity very close to that measured for 13 September; B1-.283 vs. .292, B2-.309 vs. .319, B3-.324 vs. .336, and B4-.340 vs. .340 respectively. Table 15 lists the reflectivities obtained.

Shown in Figure 62 is the desert target reflectivity obtained with the I.S.C.O. Also shown is a comparison with the Bendix derivation; excellent agreement is obtained. The spectral reflectivities are listed in Table 16.

3.2.4.6 Target Radiance at EREP - As previously discussed in sections 3.2.2.6 and 3.2.3.6, the apparent target radiance at EREP can be given as

$$N_s = N_t(g)T + N_a \qquad \text{(Eq. 14)}$$

where all quantities have been previously (secions 3.2.2.6 and 3.2.3.6) defined. For the 13 September mission, an atmospheric visual range of 33.1 Km was derived, see Figure 54, and used in conjunction with the E.R.I.M. computer program in order to calculate N_a (atmospheric path radiance). The results are shown in Figures 63 and 66 and are listed in Tables 15 and 16.

The resultant target radiances are shown in Figures 64 (broadband, Salt Flats), Figure 65 (broadband, desert site), and Figure 66 (spectral, desert). The results are listed in Tables 15 and 16. The values of N_s shown in Table 15 are for a sensor viewing angle of 0° (nadir). The values shown in Table 16 are for a sensor viewing angle of .1° (actual S190A view) and for a sensor viewing angle of 5° (actual S192 view). Also shown in Figure 66 is a comparison of the Bendix derived values with the I.S.C.O. derived values. As can be seen, a good agreement exists spectrally, but a relatively poor agreement exists in terms of radiance. This could be due to the collimator radiance problem and/or the normalization factors used for the Bendix radiance data (Figure 55),or any number of procedural error possibilities when the field data was collected. Because neither set of data (Bendix or I.S.C.O.) can be ruled out on the basis of any known error in either, both derivations are reported.

Fig. 55: Great Salt Lake Desert, UT, Relative Broadband (ERTS) Measurements of Horizontal Direct Solar Radiation vs. Time of Day, 13 September 1973.

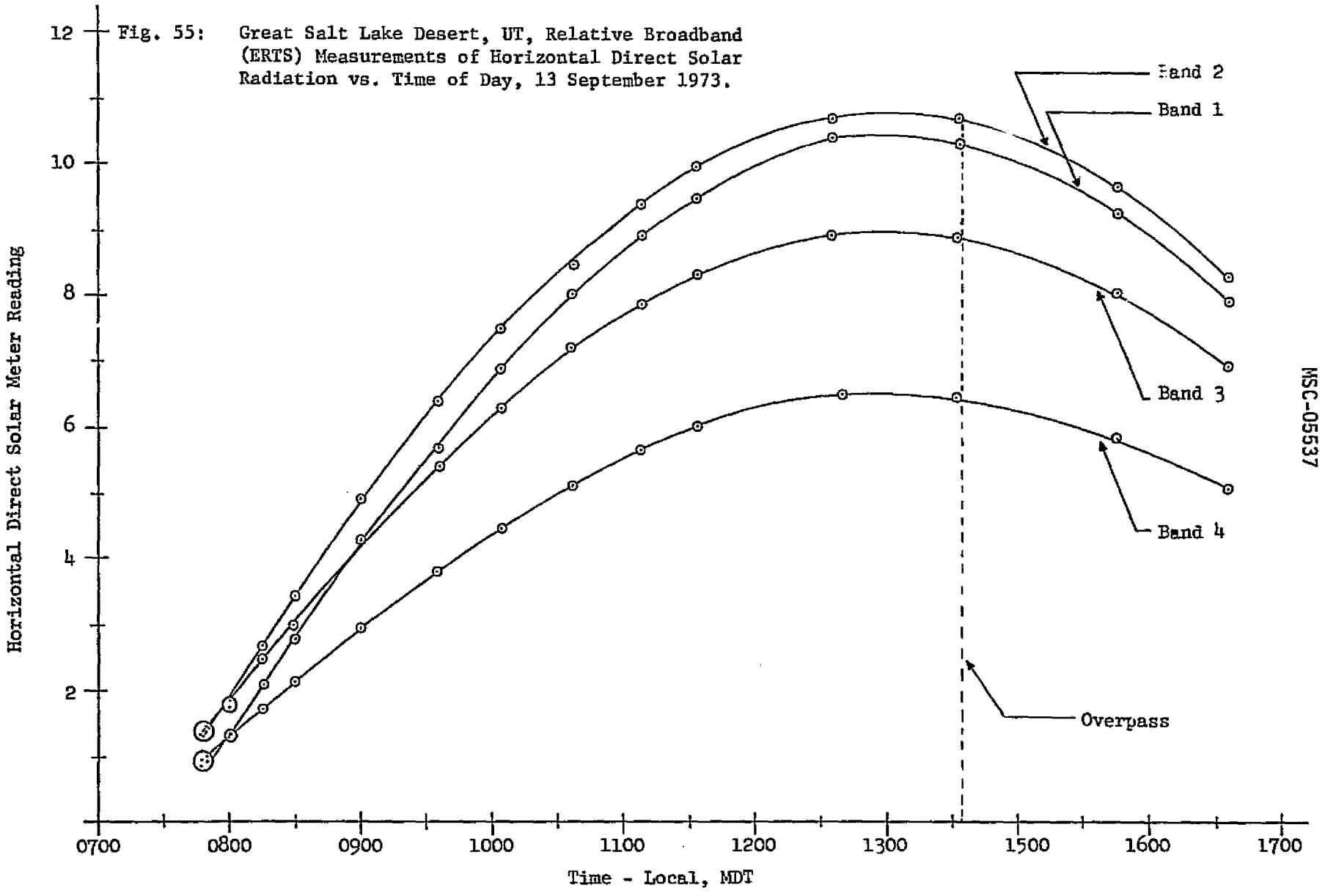

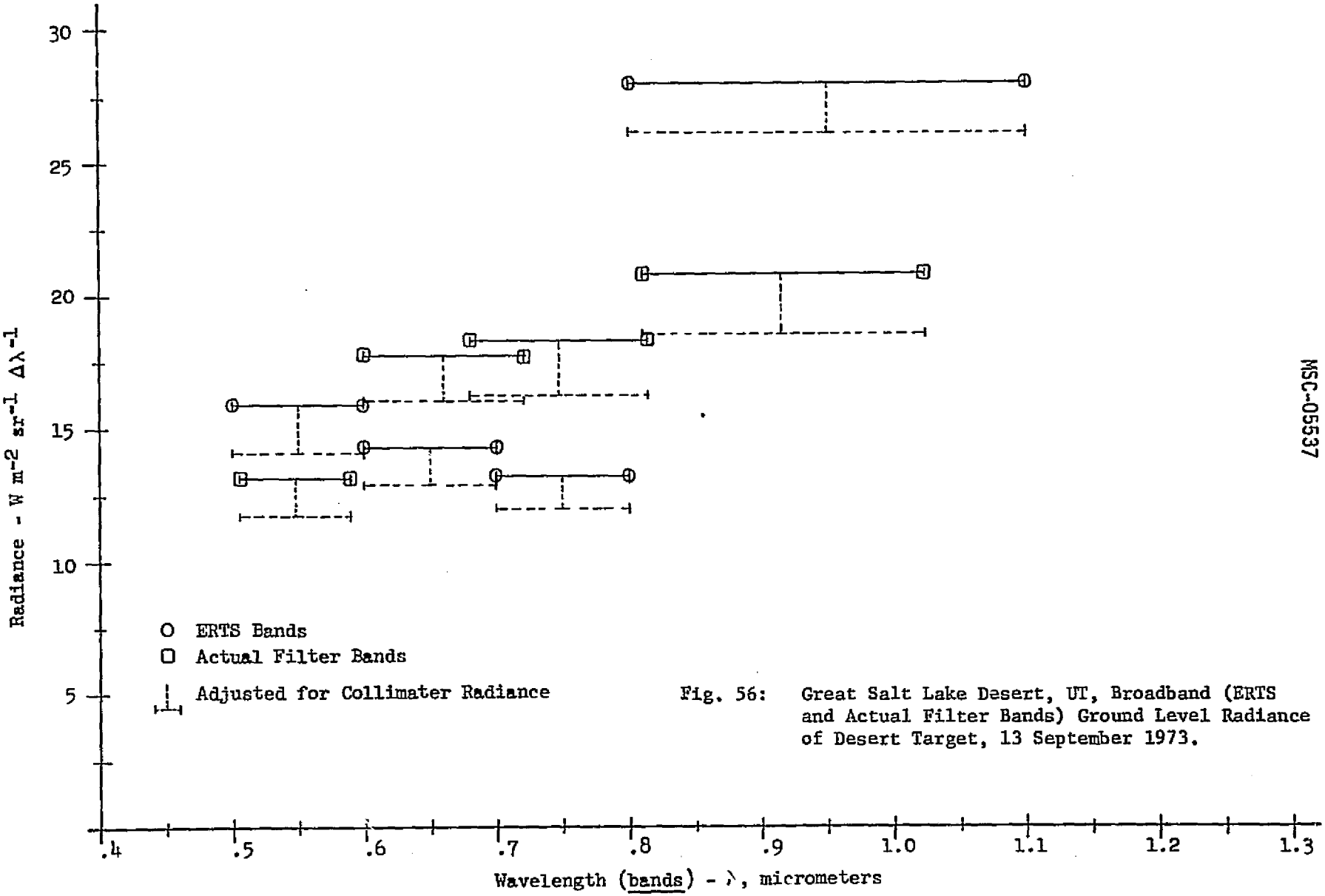

Fig. 56: Great Salt Lake Desert, UT, Broadband (ERTS and Actual Filter Bands) Ground Level Radiance of Desert Target, 13 September 1973.

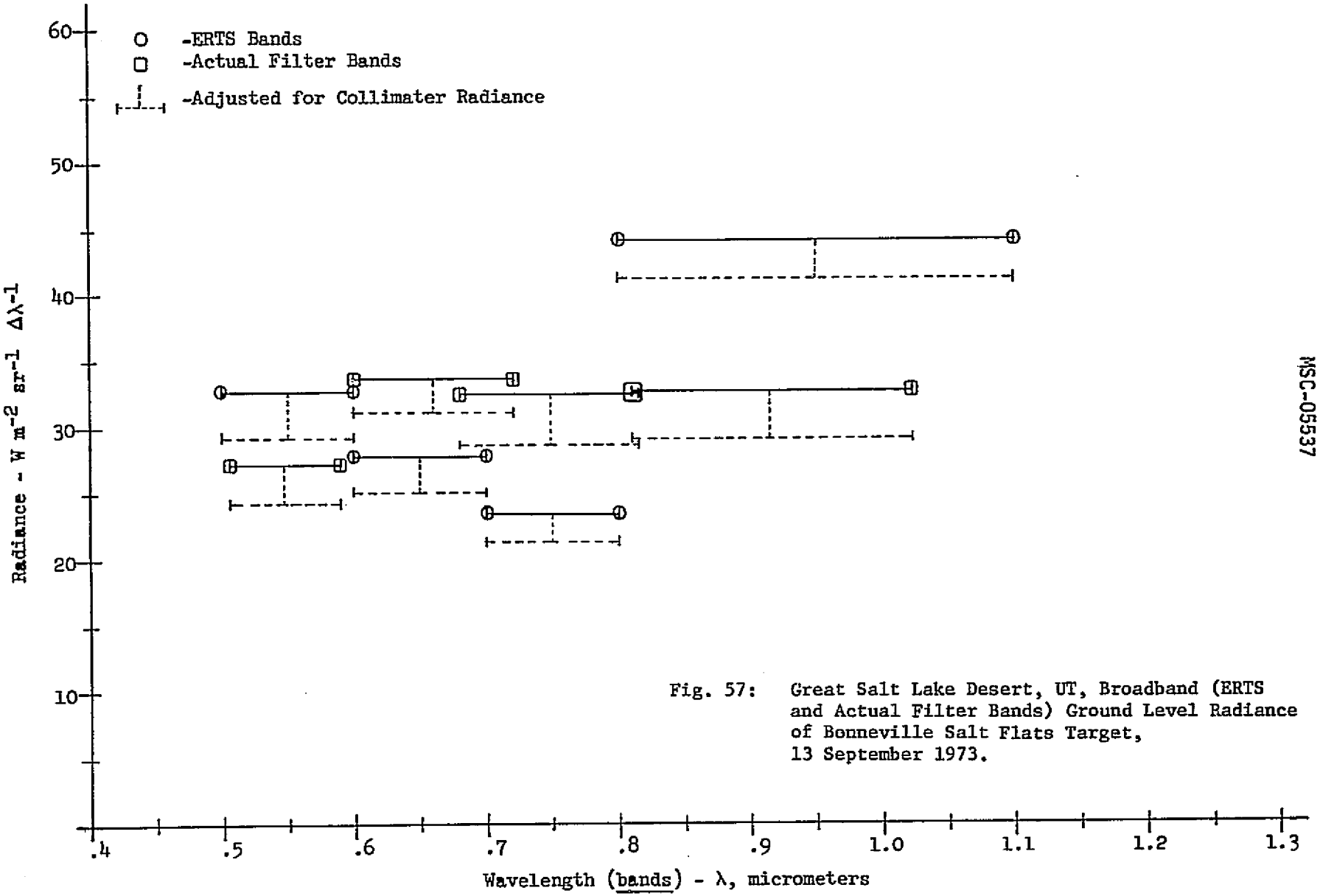

Fig. 57: Great Salt Lake Desert, UT, Broadband (ERTS and Actual Filter Bands) Ground Level Radiance of Bonneville Salt Flats Target, 13 September 1973.

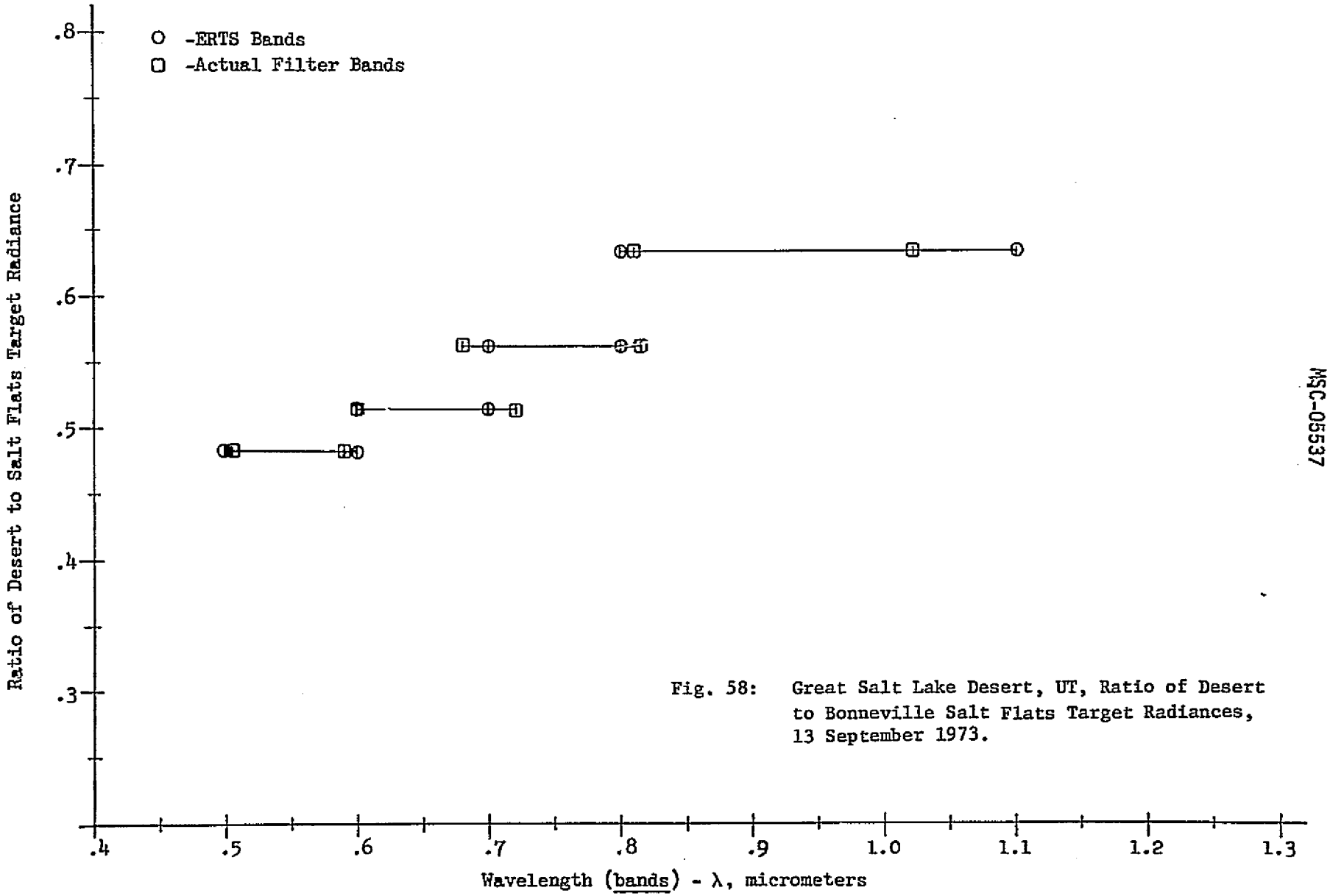

Fig. 58: Great Salt Lake Desert, UT, Ratio of Desert to Bonneville Salt Flats Target Radiances, 13 September 1973.

Fig 59: Great Salt Lake Desert, UT, Determination of Bonneville Salt Flats Reflectivity Using Cards, 13 September 1973.

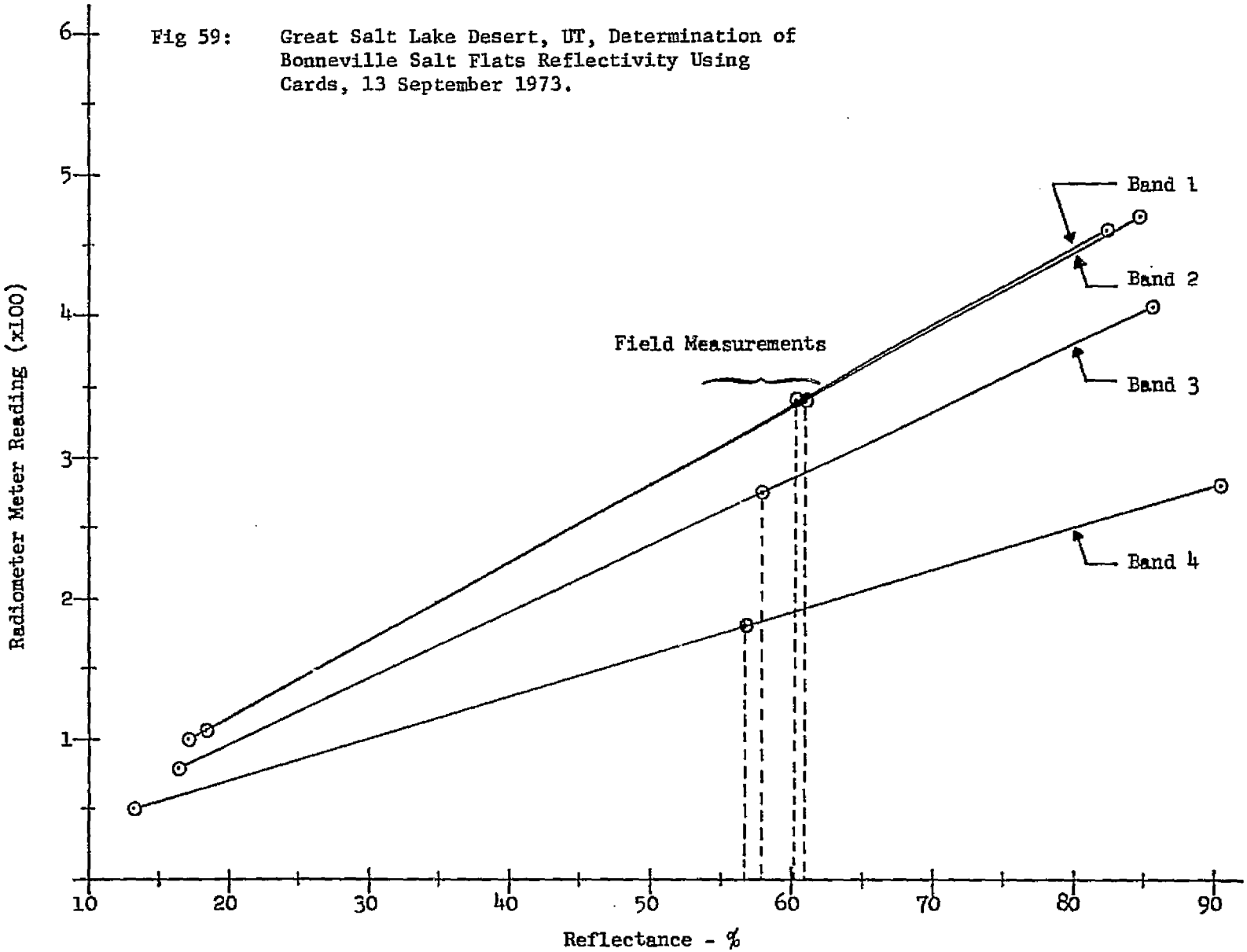

Fig. 60: Great Salt Lake Desert, UT, Determination of Desert Site Reflectivity Using Cards, 13 September 1973.

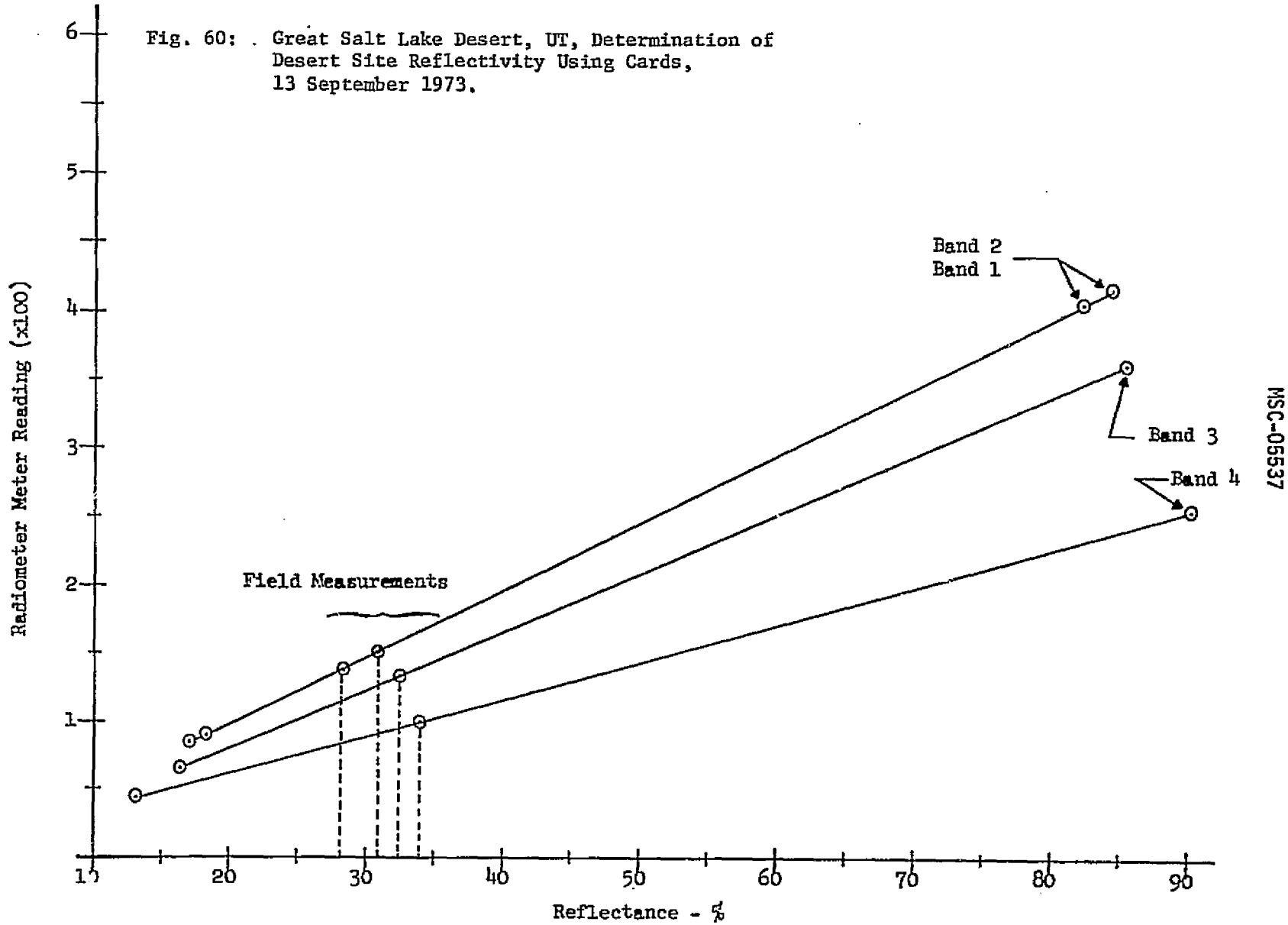

MSC-05537

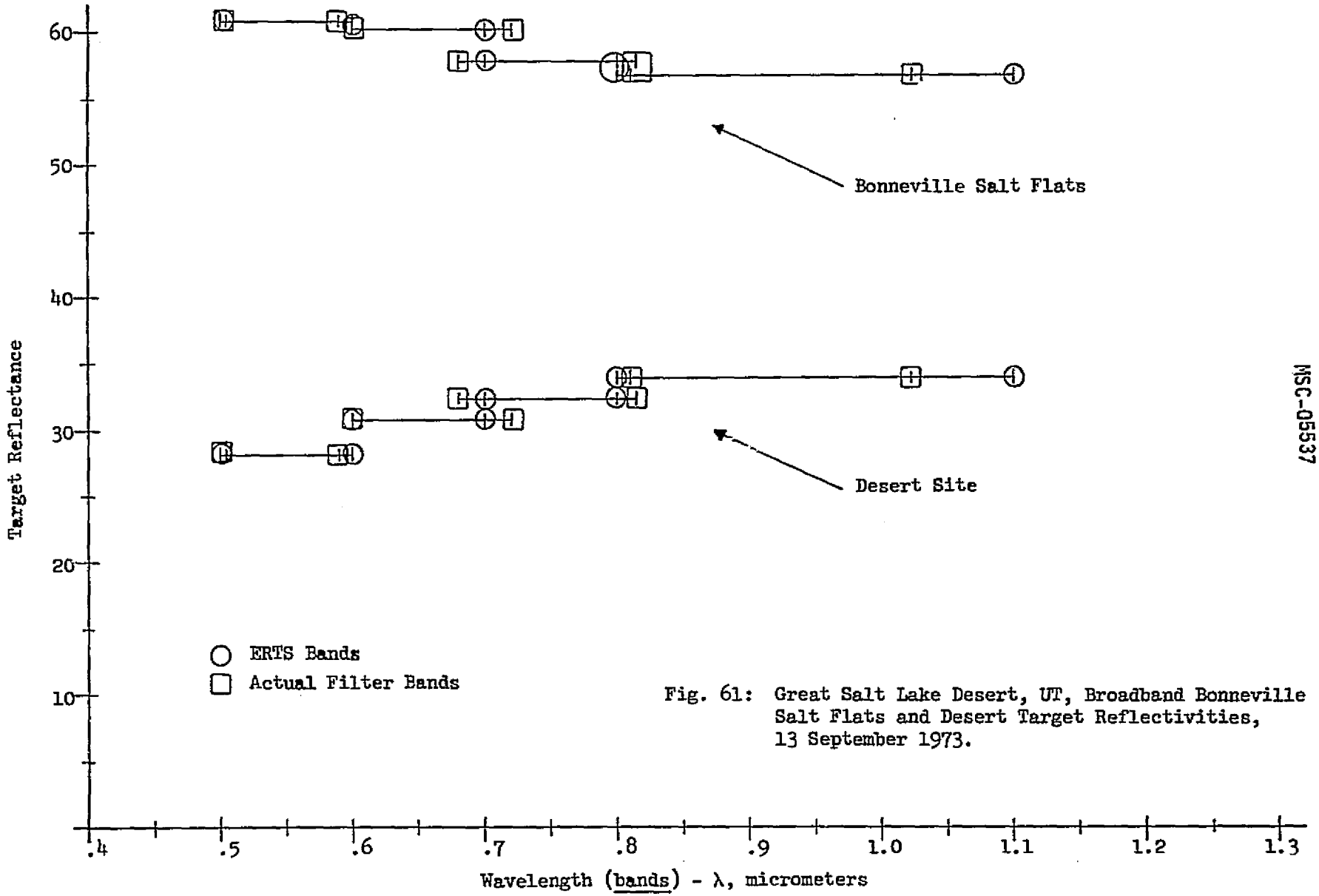

MSC-05537

Fig. 61: Great Salt Lake Desert, UT, Broadband Bonneville Salt Flats and Desert Target Reflectivities, 13 September 1973.

Fig. 62: Great Salt Lake Desert, UT, Spectral Desert Target Reflectivity, 13 September 1973.

MSC-05537

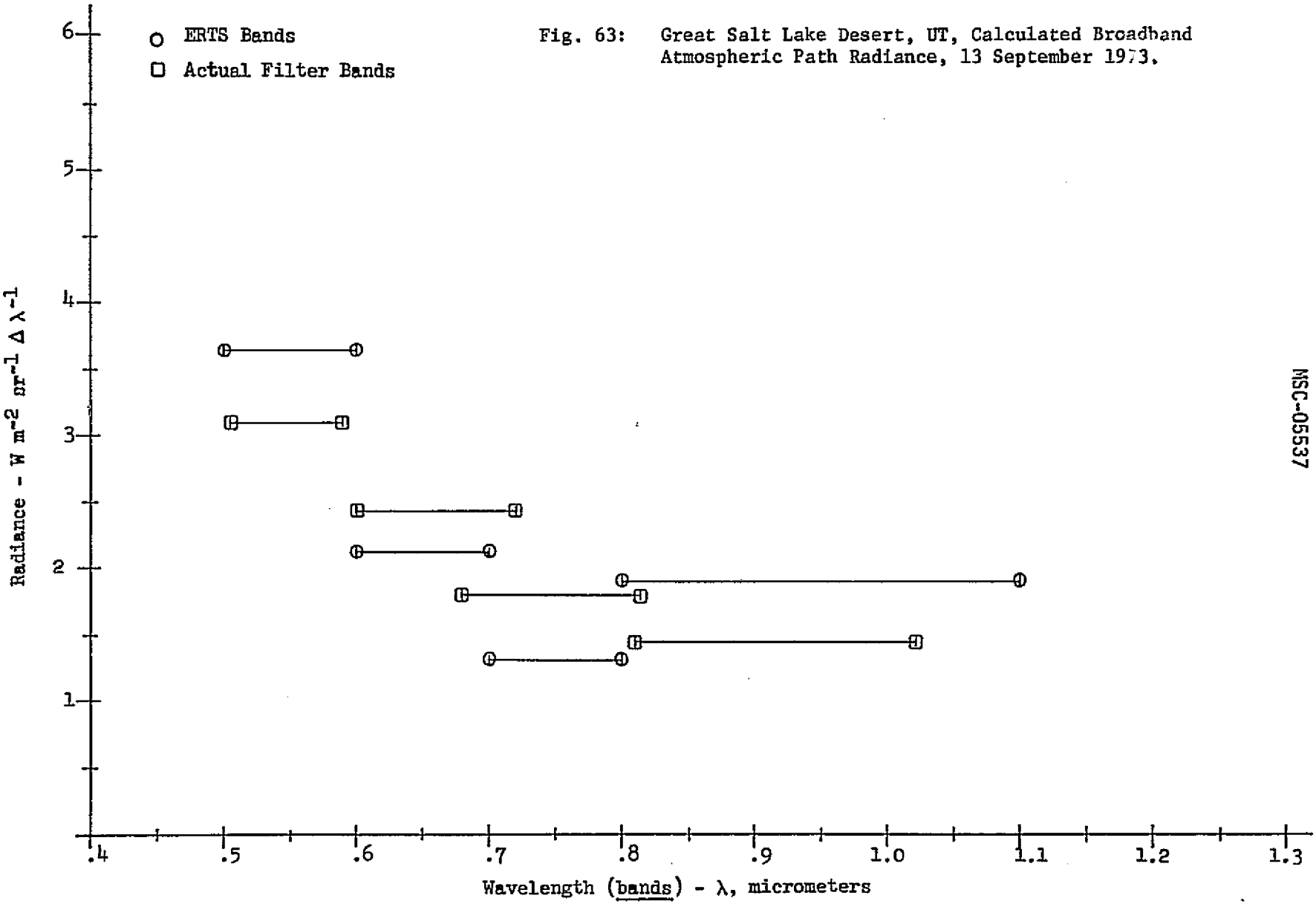

Fig. 63: Great Salt Lake Desert, UT, Calculated Broadband Atmospheric Path Radiance, 13 September 1973.

MSC-05537

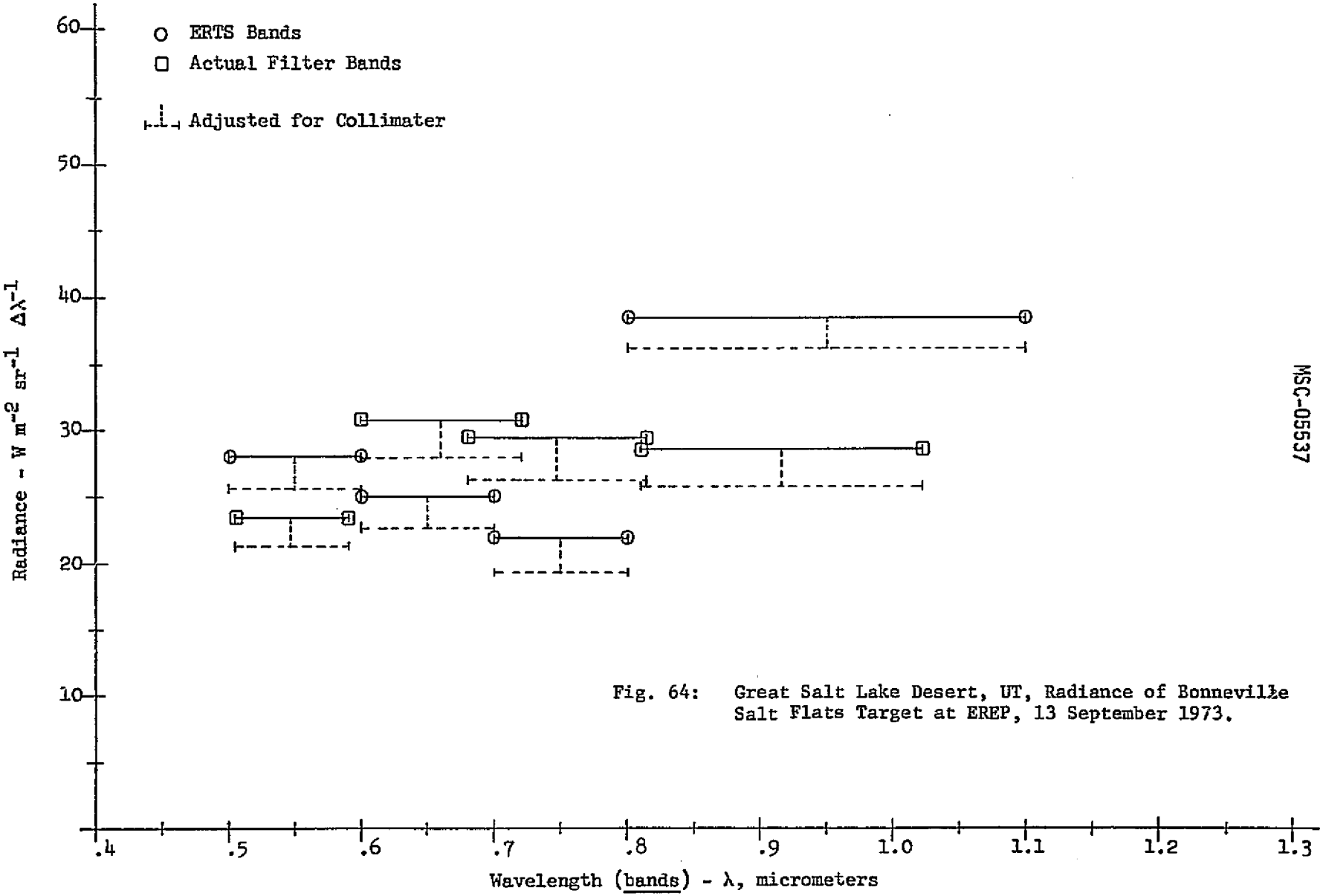

MSC-05537

Fig. 64: Great Salt Lake Desert, UT, Radiance of Bonneville Salt Flats Target at EREP, 13 September 1973.

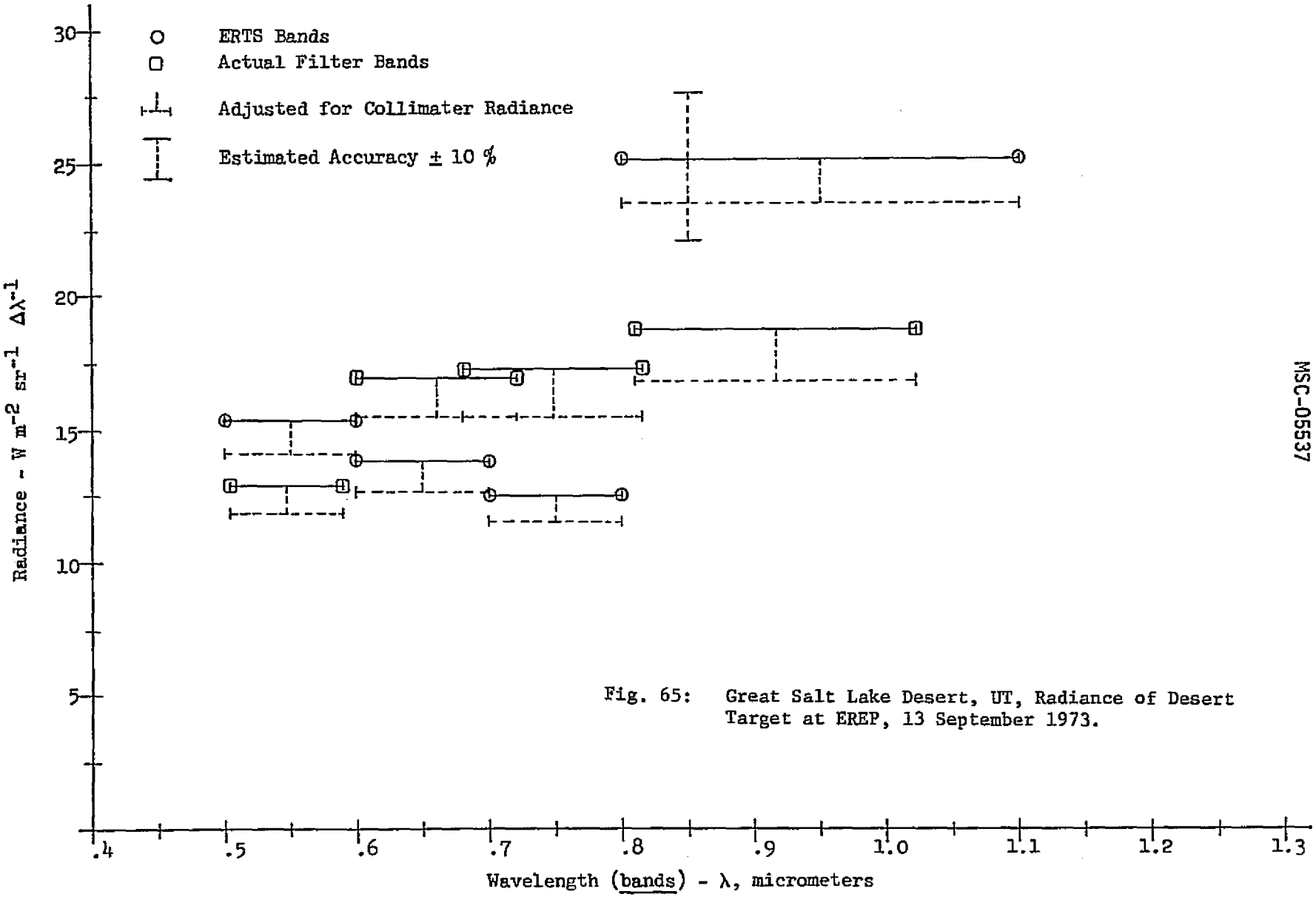

Fig. 65: Great Salt Lake Desert, UT, Radiance of Desert Target at EREP, 13 September 1973.

MSC-05537

Fig. 66: Great Salt Lake Desert, UT, Spectral Atmospheric Path and Desert Target Radiance at EREP, 13 September 1973.

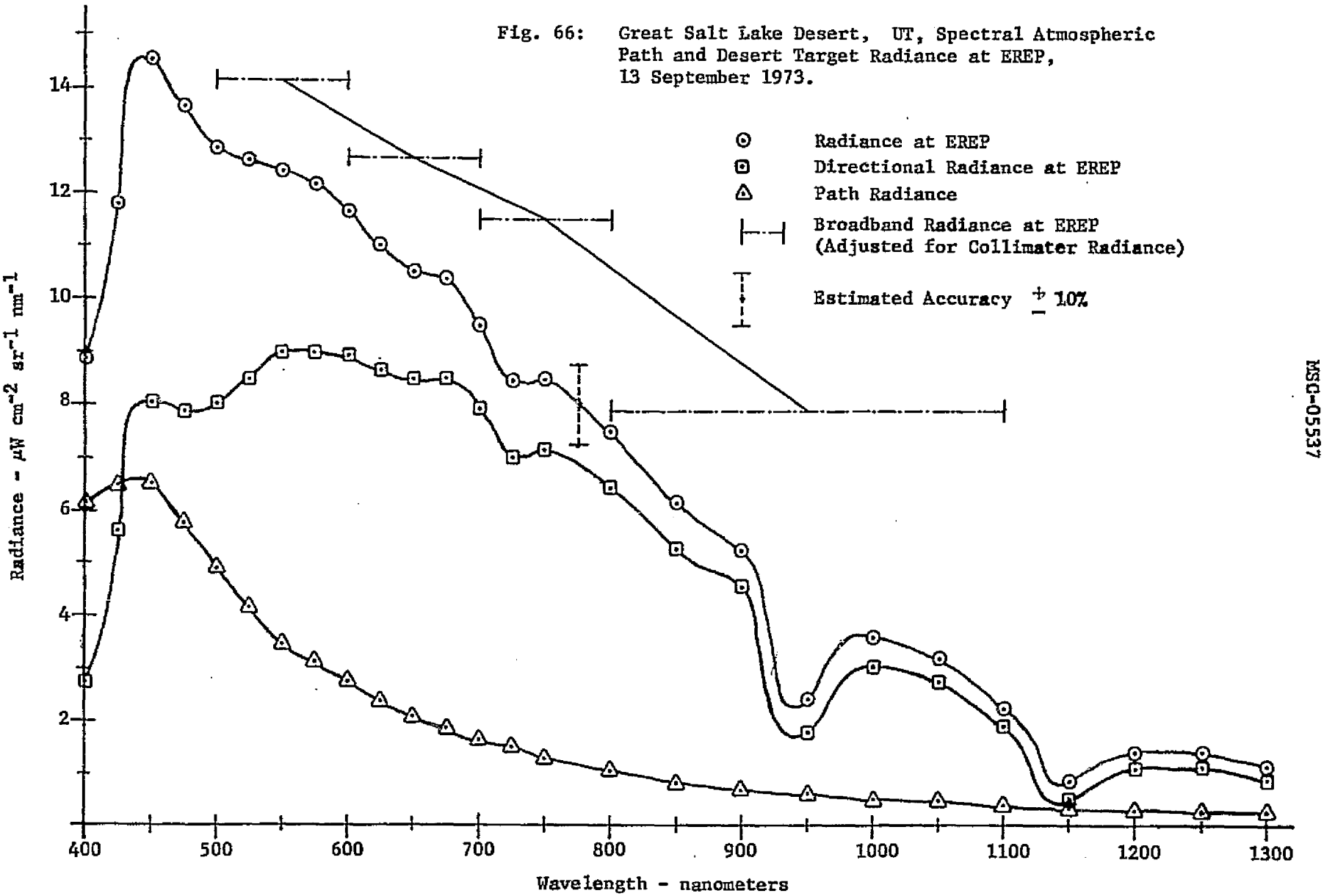

Great Salt Lake Desert (09/13/73) Broadband Atmospheric and Target Radiance											
Band	τ	T	Reflectance (ρ)		$N_t(g)$ *		$N_t(d)$ *		N_a *	N_s *	
			Flats	Deser	Flats	Deser.	Flats	Deser.		Flats	Deser.
B1	.296	.744	60.3	28.3	32.85	15.84	24.44	11.78	3.65	28.09	15.43
B1R					27.26	13.15	20.28	9.78	3.10	23.38	12.88
B2	.200	.819	60.9	30.9	27.89	14.33	22.84	11.74	2.12	24.96	13.86
B2R					34.70	17.82	28.42	14.59	2.43	30.85	17.02
B3	.167	.846	58.0	32.4	23.50	13.23	19.88	11.19	1.31	21.19	12.50
B3R					32.60	18.35	27.58	15.52	1.80	29.38	17.32
B4	.186	.830	56.8	34.0	44.23	28.06	36.71	23.30	1.90	38.61	25.20
B4R					32.80	20.81	27.22	17.27	1.45	28.67	18.72
Adjusted for Collimator Radiance											
B1					29.33	14.14	21.82	10.52		25.47	14.17
B1R					24.34	11.74	18.10	8.73		21.2	11.83
B2					25.13	12.90	20.58	10.56		22.7	12.68
B2R					31.26	16.05	25.60	13.14		28.03	15.57
B3					21.36	12.03	18.07	10.18		19.38	11.49
B3R					28.85	16.24	24.41	13.74		26.21	15.54
B4					41.34	26.22	34.31	21.76		36.21	23.66
B4R					29.28	18.58	24.30	15.42		25.75	16.87

* Watts $(meter)^{-2}$ $\Delta\lambda^{-1}$ $(steradian)^{-1}$

$\Delta\lambda$(micrometers) ⇒ B1 = .500 - .600 B1R = .505 - .590
B2 = .600 - .700 B2R = .600 - .720
B3 = .700 - .800 B3R = .680 - .815
B4 = .800 - 1.10 B4R = .810 - 1.02

T = Transmittance = $e^{-\tau \sec \theta}$

τ = Atmospheric Depth

$N_t(g)$ = Target Radiance at Ground Level

$N_t(d)$ = Target Directional Radiance at EREP = $\frac{\rho HT}{\pi}$

N_a = Atmospheric Path Radiance

N_s = Radiance at EREP = $N_t(d) + N_a$

Table 15: Great Salt Lake Desert, UT, Broadband Atmospheric and Target Radiance, 13 September 1973.

Great Salt Lake Desert (09/13/73) Spectral Atmospheric and Target Radiance										
Wavelength (nm)	τ	T	H*	Reflectance (ρ)	$N_t(d)$**		N_a**		N_s**	
					0.1°	5.0°	0.1°	5.0°	0.1°	5.0°
400	.590	.554	69.23	.223	2.72	2.72	6.16	5.86	8.88	8.58
425	.495	.610	117.6	.247	5.63	5.61	6.47	6.18	12.10	11.80
450	.432	.649	145.4	.268	8.05	8.04	6.51	6.23	14.56	14.27
475	.377	.686	131.1	.275	7.88	7.87	5.79	5.55	13.68	13.42
500	.347	.707	125.1	.285	8.02	8.01	4.84	4.65	12.86	12.66
525	.315	.730	124.0	.293	8.46	8.44	4.16	4.01	12.62	12.45
550	.291	.748	122.9	.306	8.96	8.94	3.46	3.34	12.42	12.28
575	.287	.751	116.1	.323	8.96	8.94	3.17	3.07	12.18	12.01
600	.253	.776	113.3	.318	8.90	8.90	2.76	2.68	11.66	11.58
625	.226	.798	109.4	.312	8.66	8.65	2.38	2.31	11.04	10.96
650	.207	.813	103.7	.316	8.48	8.47	2.07	2.02	10.55	10.49
675	.187	.829	98.99	.327	8.53	8.53	1.84	1.80	10.37	10.33
700	.184	.832	91.55	.326	7.90	7.90	1.62	1.58	9.52	9.48
725	.206	.814	82.12	.328	6.98	6.98	1.46	1.42	8.44	8.40
750	.187	.829	83.56	.325	7.17	7.17	1.29	1.26	8.46	8.43
800	.171	.843	77.43	.309	6.42	6.42	1.04	1.02	7.46	7.40
850	.163	.850	67.27	.291	5.30	5.29	0.83	0.81	6.13	6.10
900	.162	.850	63.46	.265	4.55	4.55	0.67	0.66	5.22	5.21
950	.380	.684	32.60	.251	1.78	1.78	0.61	0.60	2.39	2.38
1000	.157	.855	50.05	.224	3.05	3.05	0.53	0.52	3.58	3.57
1050	.113	.893	47.55	.202	2.73	2.73	0.45	0.44	3.18	3.17
1100	.150	.861	39.72	.168	1.83	1.83	0.37	0.37	2.20	2.20
1150	.506	.603	14.64	.166	0.47	0.47	0.35	0.35	0.82	0.82
1200	.201	.818	29.96	.137	1.07	1.07	0.30	0.30	1.37	1.37
1250	.126	.882	30.90	.128	1.11	1.11	0.27	0.27	1.38	1.38
1300	.159	.853	27.44	.117	0.87	0.87	0.24	0.24	1.11	1.11

* microWatts (centimeter)$^{-2}$ (nanometer)$^{-1}$

** microWatts (centimeter)$^{-2}$ (nanometer)$^{-1}$ (steradian)$^{-1}$

τ = Atmospheric Depth

T = Transmittance = $e^{-\tau \sec\theta}$

H = Total Solar Radiation

$N_t(d)$ = Target Directional Radiance at EREP = $\frac{\rho HT}{\pi}$

N_a = Atmospheric Path Radiance

N_s = Radiance at EREP = $N_t(d) + N_a$

Table 16: Great Salt Lake Desert, UT, Spectral Atmospheric and Target Radiance, 13 September 1973.

APPENDIX

Instrument Calibrations, Analyses
Techniques, and Error Analyses

1. NEAR SURFACE METEOROLOGY

The near surface meteorology measurements were made with a sling psychrometer, dry and wet bulb temperatures - accuracy of ± 1°F; a hand-held cup anemometer - accuracy of ± 2 m.p.h., and an aneroid barometer - accuracy of ± .1 in. of Hg.

2. ATMOSPHERIC TEMPERATURE AND HUMIDITY PROFILES

The atmospheric temperature and humidity profiles were obtained by releasing a Colspan Environmental Systems Co. (Boulder, CO.) radiosonde from a helicopter. Data from a coated bead thermistor (temperature) and a carbon element hygristor (ML-476) were telemetered to a ground receiving station (403 MHZ). The radiosonde descended to the surface on a parachute at approximately 25-26 ft/sec. The data was recorded on two identical strip charts, during the radiosonde descent. To calibrate the radiosonde temperature sensor/recorder, an internal potentiometer (within the ground station) is set just prior to being loaded into the helicopter. This potentiometer adjusts the slope of the current vs. temperature response, which is set according to the measured (mercury thermometer) ambient air temperature. Because the current output of the sensor is linear with respect to temperature, the atmospheric profile temperatures can then be accurately determined, based on the ground-based mercury thermometer calibration. To calibrate the humidity sensor, just prior to being loaded in the helicopter, the hygristor is replaced with a precise 20k ohm resistor. This value of resistance corresponds to a humidity of 33%, an internal potentiometer is then set to correspond to this humidity. Calibration tables relating the outputs of the bead thermistor and hygristor sensors to temperature and humidity are subsequently used to derive the absolute atmospheric temperatures and humidities.

The combined accuracy of the radiosonde telemetry system nd the ground receiving and recording (strip charts) station equals the accuracy of the sensors plus 1.0% of recorder (strip chart) span. The temperature sensor's accuracy is ± .2°C from 0 to 50°C, and ± .4°C from -40 to 0°C. This accuracy combined with the 1.0% of recorder span factor results in a net ± .30°C accuracy of the final data reported. The accuracy of the humidity sensor is ± 5.5% relative humidity (R.H.), above 0°C, and in an operating range of 10 to 100% R.H. This accuracy combined with the 1.0% of recorder span factor, results in a net ± 6% R.H. accuracy of the reported data.

The response times of the sensors combined with the descent rate of the radiosonde, results in a slight error of altitude positioning. The temperature sensor has a response time of 2.5 seconds, resulting in a 62 ft. altitude error, and the humidity sensor has a response time of 1.5 seconds, resulting in a 38 ft. altitude error. In all cases of data analysis, four time constants (10 sec.) were allowed for the temperature sensor to stabilize to ambient air conditions, and two time constants (5 sec.) were allowed for the humidity sensor to stabilize. Any data prior to this, as recorded on the ground station strip charts, were not used/reported. The altitude errors of 62 and 38 ft., mentioned above, are not significant compared to a total drop range (typically 10,000 ft.) of the radiosonde.

The actual altitude of the radiosonde, above sea level, was derived by having a knowledge of the helicopter's altitude when the radiosonde was released, the radiosonde's descent rate (25 - 26 ft./sec.) and the rate of travel of the data strip chart recorders. In addition, the point/time of radiosonde impact with the surface could be detected by a sharp fluctuation in the data. From this print, the known descent rate,and the rate

of travel of the strip chart, were then used to reconstruct the altitude profile.

3. THERMAL BRIGHTNESS TEMPERATURE

The thermal brightness temperatures of the lake waters were measured with a Barnes PRT-5 Radiation Themometer. This instrument senses thermal, blackbody, radiation from 8 to 14 μm; it has a sensitivity range of -20 to +75°C, a field of view of 2°, an accuracy of .5°C, and a stability of better than 1%.

Two methods of calibration were used to calibrate the PRT-5. For temperatures below ambient temperature, a blackbody temperature equivalent was immersed in a dry ice and acetone controlled bath and allowed to stabilize for one-half hour at each temperature measured. The temperature of the bath was monitored by a stem thermometer traceable to the National Bureau of Standards. For ambient and higher temperatures, a blackbody standard, traceable to N.B.S., was allowed to stabilize at given temperatures.

The PRT-5 was simply taken aloft in helicopter in order to make rapid and thorough determinations of the lake waters. The PRT-5 sensor head was pointed directly down (nadir), out of the helicopter's door. The reference blackbody cavity control was continuously monitored in order to assure that no adverse effects on the data occurred.

4. SOLAR RADIATION - DIRECT, TOTAL, DIFFUSE, AND TARGET RADIANCE AT GROUND LEVEL

In order to derive absolute quantities of total and diffuse solar radiation, the I.S.C.O. spectroradiometer and Bendix Model 100 R.P.M.I. were calibrated with standard, tungsten strip bulbs.* Intensity calibration factors, C.F. (I), were derived by comparing the raw outputs of the I.S.C.O. and Bendix, I_r, with that of the

*Traceable to N.B.S. and the National Research Council of Canada.

standard bulb absolute intensity, I_{std}. The desired intensity calibration factor is then

$$C.F.\ (I) = I_{std}/I_r$$

Hence, field data consisting of I_r values can be converted to absolute units by simply multiplying the raw data by the intensity calibration factor. The resultant absolute accuracy is approximately $\pm$ 5% in the 400 to 750 nm region, and $\pm$ 7% in the 750 to 1300 nm region.

For the I.S.C.O., the intensity calibration factor was derived at each wavelength increment (25 nm from 400 to 750 nm, and 50 nm from 750 to 1300 nm) of the wavelength scan. The results are shown in Figure A-1. In addition, because the I.S.C.O. was used to measure total solar radiation, the actual cosine response of the I.S.C.O. diffuser, fiber optics head, was measured. A true cosine response is defined as

$$I_\Theta = I_{\Theta = o} \cos \Theta$$

where I_Θ is the instrument intensity reading when the normal to the diffuser makes an angle of Θ with the source (plane parallel) radiation, and $I_{\Theta = o}$ is the intensity reading when the source radiation is normally incident to the diffuser. The I.S.C.O. diffuser head was positioned at angles of 0°, 10°, 30°, 45°, 60°, and 70° with respect to the standard bulb source, and each intensity reading at each wavelength increment of scan was recorded. A cosine response Correction Factor, C.F. (c), was derived by the following relationship

$$C.F.\ (c) = \frac{I_r\ (\Theta = o) \cos \Theta}{I_r\ (\Theta)}$$

where I_r (Θ = o) is the I.S.C.O. intensity reading when the diffuser is normal to the source, and I_r (Θ) is the actual intensity reading at an angle Θ. Hence, if the diffuser has a true cosine response the C.F. (c) would be equal to unity. The derived cosine response Correction Factors are shown in Figures A-2 and A-3. As can be seen, the diffuser has an excellent cosine response in the visible wavelength region; however, a very significant departure occurs at the longer wavelengths. The raw field data of total solar radiation taken with the I.S.C.O. required correction for this departure. This was done by simply multiplying the raw data by the cosine response Correction Factors, for the specific solar zenith angle that occurred at the time of measurement. Hence, the I.S.C.O. raw field data for total solar radiation was converted to absolute units, I_{abs}, by the following relationship,

$$I_{abs} = I_r * \text{C.F. (I)} * \text{C.F. (c)}$$

The raw field data for diffuse solar radiation was converted to absolute units by the following relationship;

$$I_{abs} = I_r * \text{C.F. (I)}$$

because the diffuse sky radiation has no directional properties (hence, no cosine correction is required).

The wavelength scan of the I.S.C.O. was periodically, both in the field and laboratory, checked with a Schott BG-36 absorption filter. This filter has well defined, by a Beckman DK-2 Spectrophotometer, narrow absorption bands that were used to check the I.S.C.O. wavelength integrity. The wavelength integrity was found to be very good and accurate to approximately $\pm$ 2 nm in the 400 to 750 nm region, and $\pm$ 3 nm in the 750 to 1350 nm region.

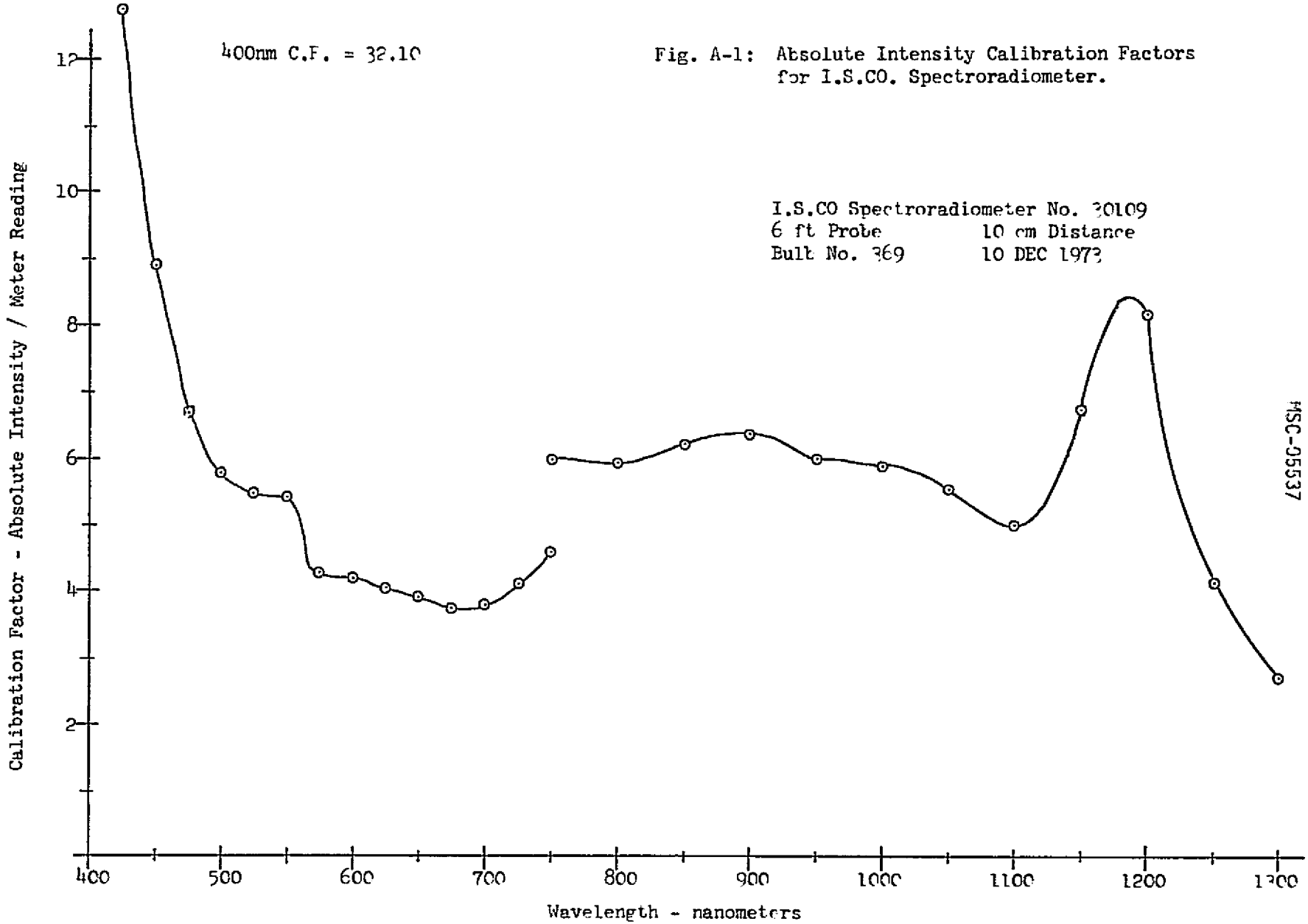

Fig. A-1: Absolute Intensity Calibration Factors for I.S.CO. Spectroradiometer.

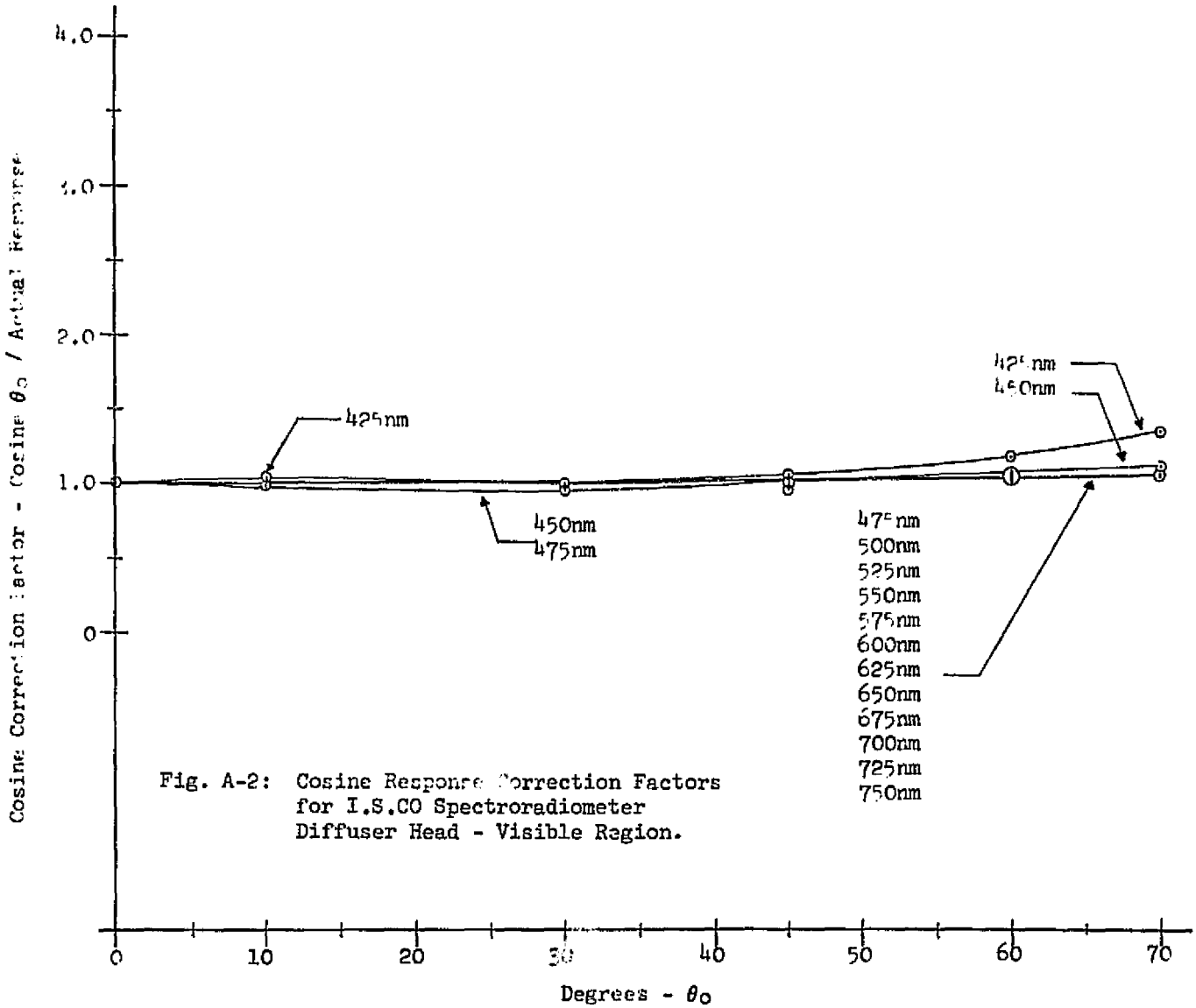

Fig. A-2: Cosine Response Correction Factors for I.S.CO Spectroradiometer Diffuser Head - Visible Region.

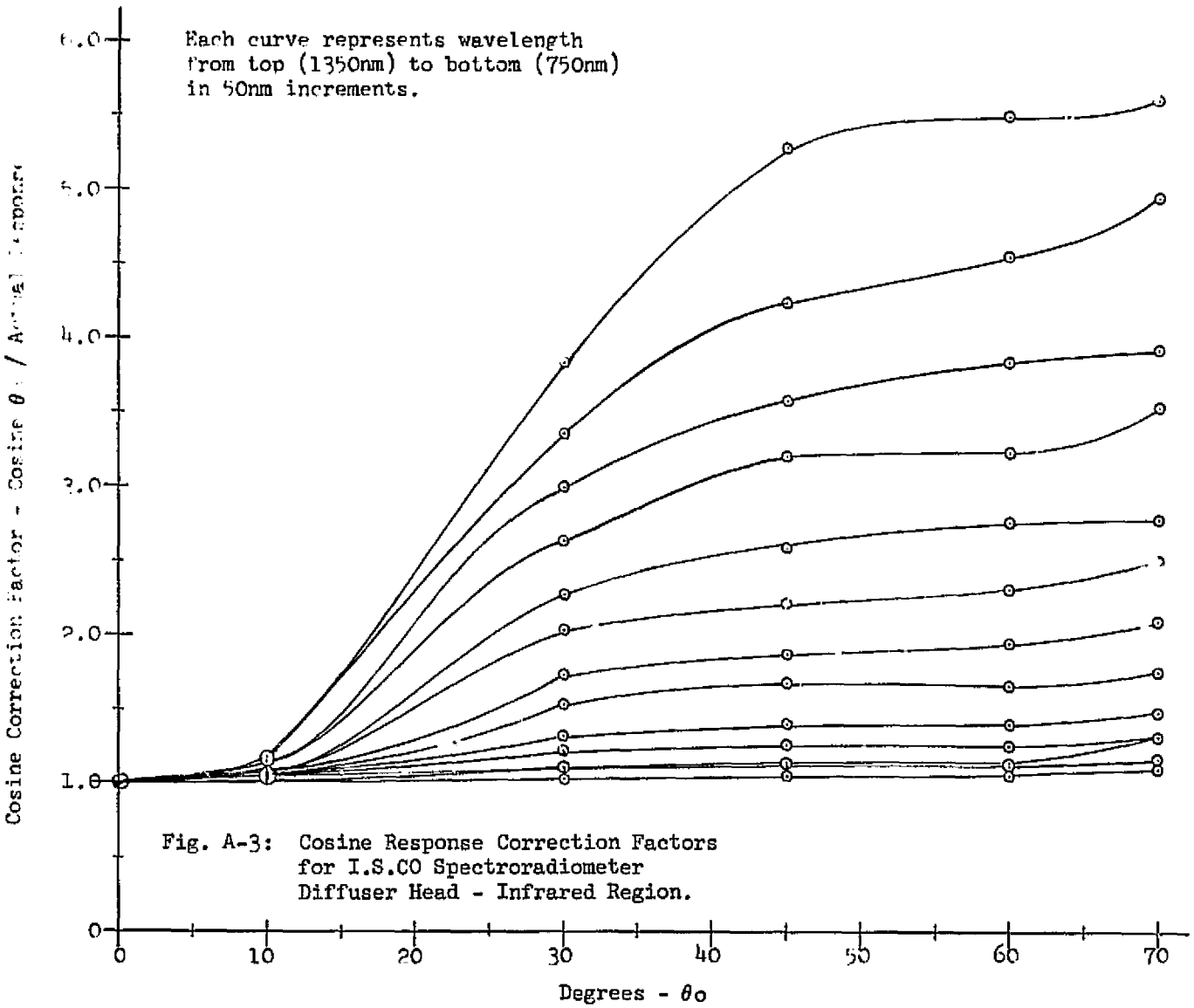

Fig. A-3: Cosine Response Correction Factors for I.S.CO Spectroradiometer Diffuser Head - Infrared Region.

As an independent check for the I.S.C.O. measurements and integrity, a field mission was performed on top of Mt. Evans, CO., 14,000 feet A.S.L. Meter readings at various air mass were obtained and used to derive a meter reading outside of the atmosphere, as described in section 3.2.2.4. This meter reading was then multiplied by the intensity calibration factors derived in the manner described above. This resulted in an absolute measurement of the solar constant. These Mt. Evans, I.S.C.O. measurements for the solar constant were then compared to those reported by M. Thekaekara, "Evaluating the Light from the Sun", Optical Spectral, March, 1972. A mean deviation (over all wavelengths) of less than 5% was obtained, as shown in Figure A-4. Both the I.S.C.O. (No. 30109) used for deriving the total and diffuse solar radiation quantities reported herein, and the I.S.C.O. (No. 17336) used for deriving optical depth, were used. The agreement between the two instruments and with the proposed standard solar constant is considered to be acceptable and within the absolute accuracy, $\pm$ 5% in the 400 to 750 nm region and $\pm$ 7% in the 750 to 1300 nm region, that is associated with the calibration techniques described previously.

The Bendix R.P.M.I. was calibrated for both total, direct, and diffuse measurements, as discussed above, and for target radiance measurements. Calibrations were performed both for the ERTS bands (B1-.500 to .600 μm, B2-.600 to .700 μm, B3-.700 to .800 μm, and B4-.800 to 1.10 μm), and for the actual/real half-bands, as shown in Figure A-5, (B1R-.505 to .590 μm, B2R-.600 to .720 μm, B3R-.680 to .815 μm, and B4R-.810 to 1.02 μm). The calibrations were adjusted for the fact, because of the broadbands, that the calibration source spectrum (standard bulb) is different than that of the solar radiation spectrum. These bulb to solar correction(s) were performed by Bendix. The results are shown in Table A-1.

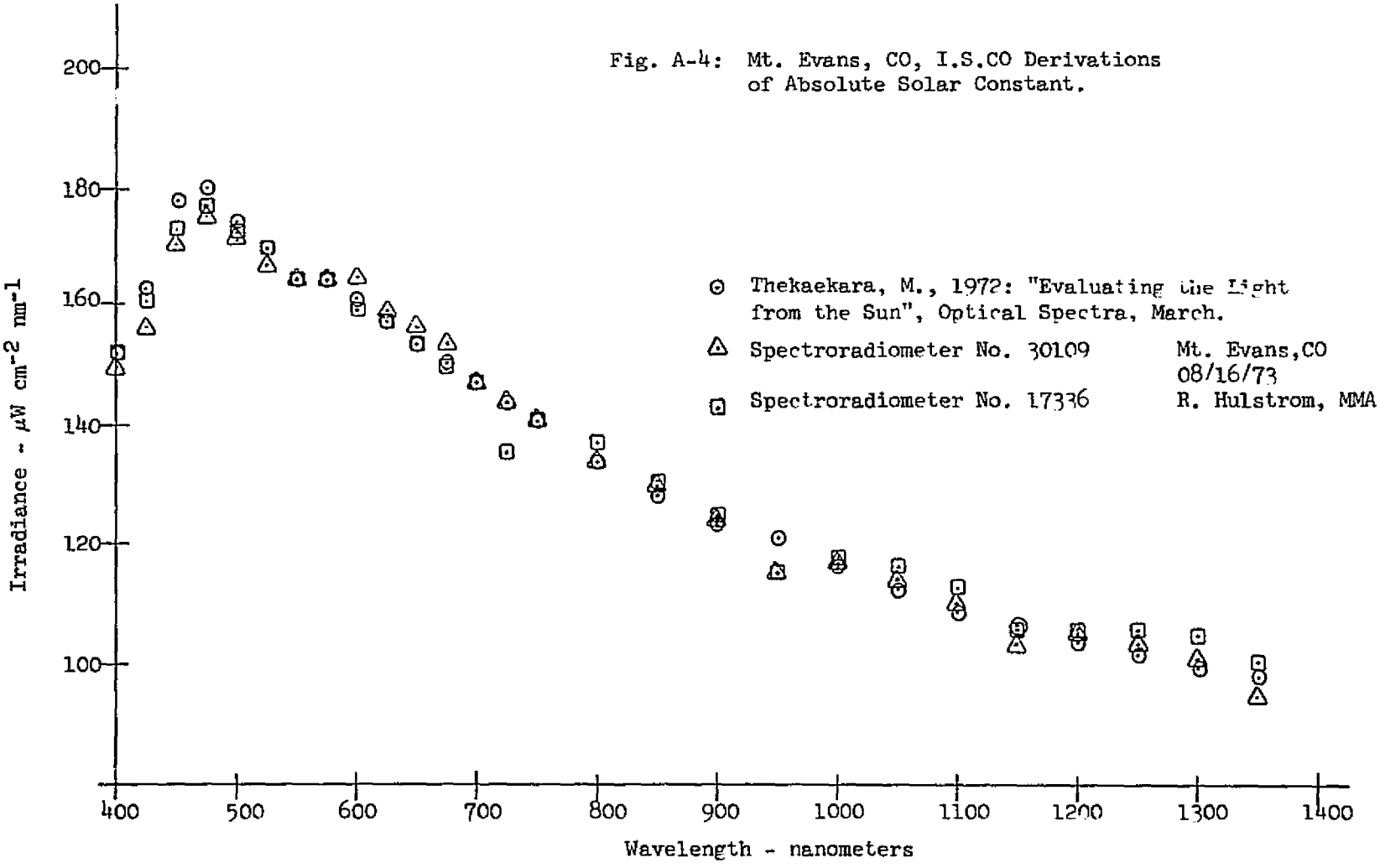

Fig. A-4: Mt. Evans, CO, I.S.CO Derivations of Absolute Solar Constant.

Fig. A-5: Spectral Responses of Bendix R.P.M.I. - Filters and Sensor.

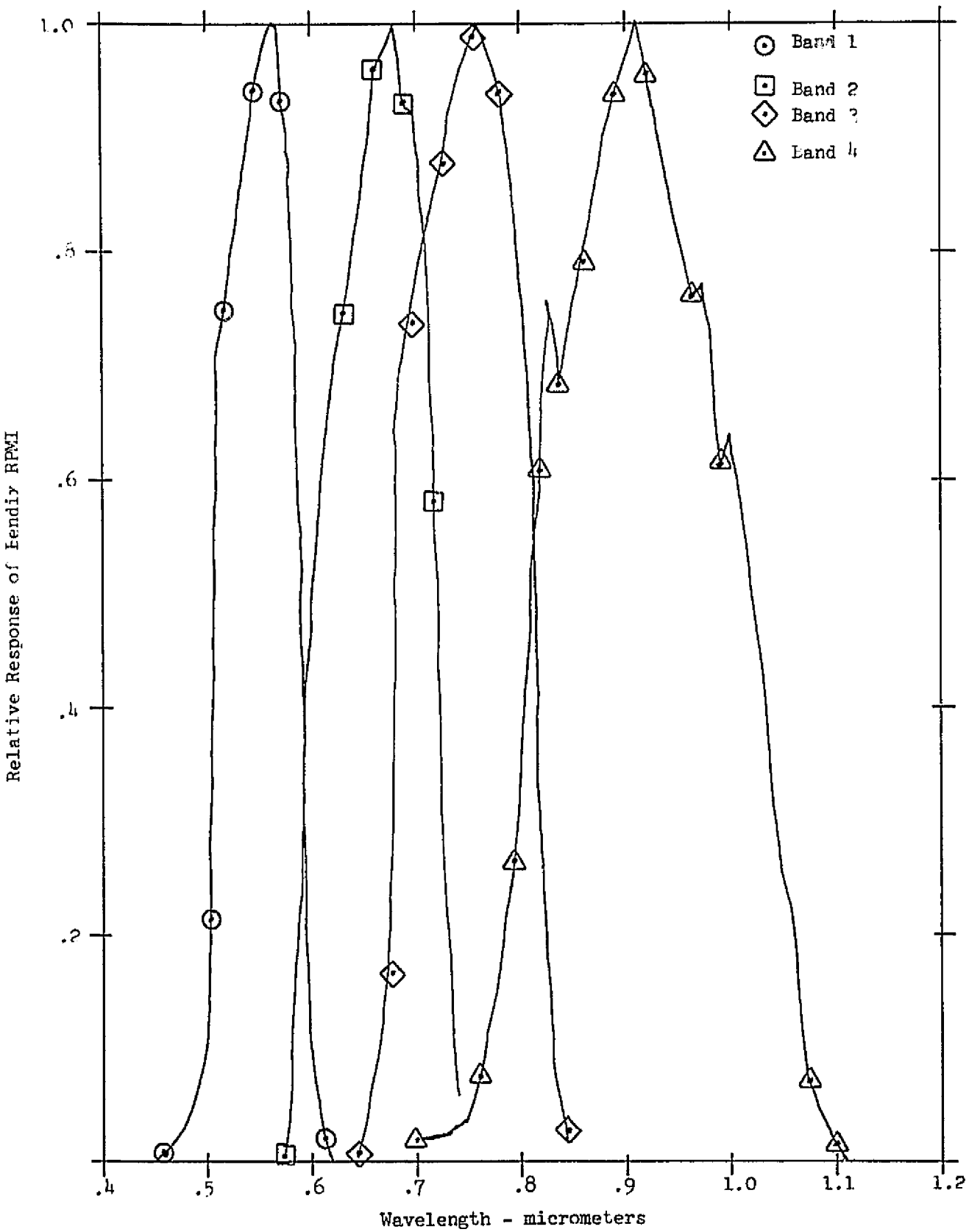

Table A-I

Absolute Calibration Factors of Bendix R.P.M.I .

Band	CF(I) Solar	S*	$CF(I)_{radiance}$
B1	11.52	.970	895
B1R	9.59	.970	743
B2	9.80	.988	758
B2R	12.24	.988	943
B3	10.41	.985	778
B3R	14.01	.985	1079
B4	31.05	.958	2245
B4R	21.96	.958	1665

* Radiant Power Measuring Instrument for ERTS Ground Truth, Operation and Maintenance Manual for PN2373045, Bendix Aerospace Systems Division

The Bendix R.P.M.I. meter readings when multiplied by by $CF(I)_{solar}$ (direct, total, diffuse) result in absolute quantities of watts meter^{-2} $\Delta\lambda^{-1}$, and when multiplied by $CF(I)_{radiance}$ (viewing the target with a 7.0° F.O.V. collimator) results in absolute quantities of watts meter^{-2} steradian^{-1} $\Delta\lambda^{-1}$.

The absolute accuracy of the R.P.M.I. is $\pm$ 5%. In addition, a determination of the solar constant was performed with the R.P.M.I. by Dr. R. Rogers of Bendix, resulting in a + 5.2% (R.P.M.I. value compared to solar constant) agreement for B1, a -.3% agreement for B2, a -.3% agreement for B3, and a +1.2% agreement for B4. In addition, a comparison of Calibration Factors derived by R. Hulstrom of Martin Marietta Aerospace, shown in Table A-I,with those derived by R. Rogers of Bendix Aerospace, indicates an agreement ranging from .5% for B1 to 5% for B4. This is well within the accuracy of the calibration limitations of the methods used.

No cosine response calibration of the Bendix R.P.M.I. was performed because it was not required for analyzing the field data. The R.P.M.I. was used only on the 08 August Great Salt Lake Desert mission to measure total and diffuse solar radiation. The method used to derive the total solar radiation was that of measuring the direct horizontal solar radiation and adding that to the measured diffuse solar. Hence, no cosine response function was involved.

As derived and discussed in detail in section 3.2.2.5, it is suspected that the collimator of the R.P.M.I. introduces additional radiance to the direct measurements of target radiance. This was detected in the comparison, section 3.2.2.5, of the direct field measurements by deducing target radiance from measuring the incident solar radiation and the target's reflectivity. This comparison revealed that the collimator radiance attributed an additional 7-12% radiance. To verify this field measurement finding, a laboratory experiment was conducted. A plane-parallel calibration source of light was viewed with and without the collimator in place. It was found that the collimator inplace readings were 10% higher for B1, 12% higher for B2, 13% higher for B3, and 14% higher for B4. These laboratory derivations are in fair agreement with the field derivations. Therefore, the target radiance values reported throughout the main text of this report were adjusted for collimator radiance. However, it should be kept in mind that the actual magnitude of such an adjustment depends upon the incoming solar radiation conditions and target reflectivity. Due to the fact that most of the targets measured were roughly similar in reflectivities, the collimator radiance adjustments made are thought to be fairly accurate.

5. TARGET RADIANCE AT EREP

The target radiance at EREP, N_s, was determined by

$$N_s = N_t(g)\ T + N_a \qquad \text{(Eq. 14)}$$

where $N_t(g)$ is the target radiance at ground level, T is the atmospheric fractional transmittance, and N_a is the atmospheric path radiance. The target radiance at ground level can further be given by

$$N_t(g) = \frac{H\ \rho}{\pi} \qquad \text{(Eq. 9)}$$

where H is the total amount of solar radiation, and ρ is the target reflectivity.

The accuracy to which the target radiance at ground level is mainly determined by the accuracy to which the total solar radiation was measured. As mentioned previously, this is $\pm$5% in the I.S.C.O. visible and Bendix bands, and $\pm$7% for the I.S.C.O. infrared. The accuracy of the target reflectivity is much less of a factor because it is derived from relative instrument readings. Both the I.S.C.O. and Bendix have $\pm$1% meters and/or strip charts. Taking the worst case then, the accuracy of the target radiance at ground level is approximately $\pm$6% for the I.S.C.O. visible and Bendix bands, and $\pm$8% for the I.S.C.O. infrared region.

The atmospheric transmittance, T, can be given as

$$T = e^{-\tau \sec \Theta} \qquad \text{(Eq. 3)}$$

where τ is the atmospheric optical depth and Θ is the sensor view angle, which was zero or near zero in all cases reported. The I.S.C.O. measurements from Mt. Evans, discussed previously, and comparisons of the Bendix and I.S.C.O. derivations of optical depth, suggest that the atmospheric optical depth measurements

are consistent/accurate to within approximately ± .02 units. The optical depths reported herein ranged from approximately .600 to .100, the optical depth error of ± .02 then becomes equivalent to a ± 2% accuracy for atmospheric transmittance.

Taking the combined errors of the target radiance at ground level and the measurement of atmospheric transmittance, an accuracy of ± 8% for the 400 to 750 nm and a ± 10% for the 750 to 1300 nm region is obtained.

The accuracy/error associated with the atmospheric path radiance is difficult to assess. The use of actual field measurements of atmospheric optical depth and target reflectivity should maximize the accuracy of the computer model calculations of path radiance. A comparison of experimental path radiance measurements with model calculations is shown in Figure A-6. As can be seen, a good agreement exists. However, it is simply impossible to assign a quantitative accuracy to the path radiance derivations. Further research utilizing EREP and ERTS data is required in order to do this. Since the path radiance constitutes a major portion of the radiance derived at EREP (see Figure 46) for the shorter wavelengths, it is this region that has the highest degree of uncertainty. Since the path radiance decreases very rapidly at longer wavelengths, it is this region that has the lowest degree of uncertainty. The accuracy of the radiance derived at EREP in the infrared region (750 to 1300 nm) is approximately equal to the accuracy derived previously - ± 10%.

☆ U.S. GOVERNMENT PRINTING OFFICE: 1974—671-194/ 535